Mads Urang Nilsen

Using AERMOD to predict the dispersion of emissions from the aluminum industry

Master's thesis in Materials Science and Engineering
Supervisor: Kristian Etienne Einarsrud
Co-supervisor: Gabriella Tranell
June 2022

Master's thesis

NTNU
Kunnskap for en bedre verden

Mads Urang Nilsen

Using AERMOD to predict the dispersion of emissions from the aluminum industry

NTNU
Norwegian University of
Science and Technology

Acknowledgments

Abstract

Increased focus on the environmental effects of pollutants has enforced stricter regulations in terms of emission control in the aluminum industry. For this reason, the industry wants to adapt efficient ways of estimating the dispersion of pollutants. Dispersion models, which use various parameters to calculate the dispersion of emissions, are proposed as a part of the solution. In this thesis, EPA's recommended dispersion model for calculating the dispersion of short range emissions (<50 km), AERMOD, has been used.

The goal of this thesis is to provide a first step for aluminum industries to apply dispersion models when evaluating the impact of their emissions. In light of this objective, a walkthrough of how to use AERMOD, and a description of how AERMOD works and its capabilities have been provided. In addition, a modeling case, calculating the dispersion of emissions from Hydro Aluminium Høyanger, have been performed. In this context, the practical considerations for the modeling case have been assessed, and the eventual challenges that may arise using the tool have been uncovered. The modeling case also includes a factorial design experiment to test how different parameters influence the results.

Due to the number of uncertainties of the modeling case, the results could not be deemed representative. The biggest uncertainty was the implemented weather data being acquired from weather stations too far from the plant. Still, the results showed that the tool accounted for many of the fundamental factors influencing the dispersion of emissions, thus implying that the tool can be used for a qualitative assessment of emission dispersion.

The biggest challenge of performing the modeling case, was acquiring applicable and representative data. Establishing efficient routines for acquiring readily implementable-, and representative data would ease the modeling process significantly.

Sammendrag

Økt fokus på de miljøskadelige effektene av utslipp har gitt opphav til strengere krav i sammenheng med utsippskontroll i aluminiumsindustrien. Derfor ønsker industrien å innføre effektive måter å estimere dispersjonen av utslipp. Dispersjonsmodeller, som bruker ulike parametere for å beregne utslipps' dispersjon, er blitt foreslått som en del av løsningen. I denne oppgaven er EPAs anbefalte dispersjonsmodell for evaluering av utslipp over korte rekkevidder (<50 km), AERMOD, blitt brukt.

Målet med oppgaven er å danne et grunnlag for at aluminiumsindustrien kan ta i bruk dispersjonsmodeller når de evaluerer deres utslipps påvirkning på miljøet. For dette formålet, har en gjennomgang av hvordan man bruker AERMOD, hvordan det fungerer og hvilke egenskaper det har, blitt gitt. I tillegg inneholder oppgaven en modelleringscase utført på Hydro Aluminium i Høyanger. I denne sammenheng gjennomgår oppgaven de praktiske betraktningene og utfordringene som kan oppstå ved å gjennomføre en slik case ved bruk av AERMOD. Casen inneholder også et faktorielt eksperiment for å teste innvirkningen forskjellige parametere har på resultatene.

Grunnet de mange usikkerhetsmomentene forbundet med casen, kunne ikke resultatene bli sett på som representative. Den største usikkerheten var at værdataen var hentet fra stasjoner som lå langt unna verket. Likevel viste resultatene at verktøyet tok høyde for mange av de grunnleggende faktorene som påvirker dispersjonen av utslipp, noe som impliserer at verktøyet kan bli brukt for å kvalitativt vurdere utslippenes dispersjon.

Den største utfordringen ved å utføre casen, var å anskaffe representative-, og anvendelige data. Ved å etablere effektive rutiner for å anskaffe implementerbare-, og representative data, vil man forenkle modelleringsprosessen betydelig.

Contents

List of Tables

List of Figures

1 Introduction

The adverse pollutants originating from the aluminum industry has imposed strict regulations in terms of emission control. Pollutants' harm towards health and the environment are mainly governed by the pollutants' characteristics, mass and dispersion. While established routines exist for measuring characteristics and masses, efficient ways of measuring dispersion have traditionally been lacking. Measuring the dispersion of emissions is crucial, as their concentrations dictate their effects on the local environment. Physical measurements of dispersion have been expensive and work-intensive with somewhat lacking results, hence these are rarely performed. This gives rise to the need of more efficient ways of measuring the dispersion of emissions.

To remediate this issue, dispersion modeling has been proposed as a part of the solution. Dispersion models use various data, many of which are readily available, to calculate the dispersion of emissions. These models only need a computer and accurate input data to work, making them significantly cheaper and more convenient than their physical counterparts. The models can also achieve more extensive results, as their results are not constrained by having to travel to the physical areas where measurements are performed.

Still, dispersion modeling is not necessarily a simple task. For accurate results one is dependent on accurate input parameters. Inaccurate inputs will propagate in the model calculations, potentially intensifying these inaccuracies when implemented. Even with accurate inputs, the many factors influencing emission dispersion, and the synergy between these, can cause very complex cases which are hard to accurately describe using algorithms. Dispersion models differ in their approaches to handle these calculations, and it is therefore important to consider if the model chosen can describe the dispersion in a satisfactory manner. Due to the complexity of dispersion modeling, supplementation with physical measurements and continuous evaluations of the modeling approach may be necessary for thorough validation of the results.

The goal of this study is to provide a first step towards aluminum industries adopting dispersion models in their routinely measurements. For this purpose, how dispersion models generally work, and a guide of the AERMOD [6] dispersion model will be given. The challenges of performing a dispersion modeling case, and how to cope with them, will be identified by executing such a case on an aluminum plant located in Høyanger. This modeling case will include a factorial design experiment, testing how various parameters influence the results. The modeling results, in light of the modeling approach, the factorial experiment, and the data that was used, will then be discussed in terms of their validity and correlation with theory. The main findings of

the thesis will finally be summarized in the conclusion.

2 Dispersion modeling

The significance of emissions is mainly dependent on their characteristics, magnitude and dispersion. The characteristics of a specie governs its effect on human health and the environment, and their magnitudes govern their total environmental impact. The dispersion of emissions dictates how concentrated the specie will be at different locations. As a specie's impact scales with its concentration, mapping the dispersion of emissions is crucial for an evaluation of the pollutant's local environmental impact.

The characteristics of emissions can be measured by spectroscopy, while their magnitudes can be measured by a combination of characterization methods and volume flow calculations. Factors that determine the dispersion are for the most part weather conditions, topographical conditions and the properties of the emitted plume[1] [13]. As some of these factors are dynamic, the dispersion of emissions can be expected to vary from day to day, even for static emission processes.

Physical measurements of the emission dispersion can be performed. One method is to place instruments which catch condensed particles in the area of interest [14], another is to measure concentrations of deposited species in moss [15]. These methods are expensive and work-intensive, due to the amount of traveling, equipment and tests performed for a proper analysis. Since the measured emissions are for all the accumulated emissions in the area, one cannot properly trace the emissions to one specific event or emission source. They will also only measure the concentrations at the specific points where the measurements are performed. The dynamic nature of the emission dispersion also makes it hard to estimate dispersion based on previous measurements, implying the need for continuous measurements for thorough concentration mapping.

Due to the inconvenience of using physical measurements, dispersion models are often used. Dispersion models describe the dispersion of emissions using mathematical algorithms [16]. The models use various data relevant for emission dispersion as inputs, which when implemented calculates the emission dispersion. The inputs vary from model to model, but most models rely on using topographical-, meteorological- and plume property data, where the level of detail differs depending on the model. The results of the models will be realized as a grid of concentration data, and the characteristics of these (time-interval, resolution, etc.) can be chosen by the modeler.

---

[1] The fluid mass originating from the emission source.

Dispersion models are already in extensive use, and have for instance been used to map the emission dispersion of industries [17] and the consequences of nuclear accidents [16].

Dispersion models can remediate many of the problems associated with physical measurements. Compared to their physical counterparts, dispersion models can achieve more extensive results without substantial resources. To run the models, all one needs is a computer and input data. As long as these data are available, the models can continually predict the dispersion of emissions, despite the dynamic nature of emission dispersion. The very nature of dispersion modeling also gives the opportunity to predict emission dispersion for future events or potential process changes, giving engineers valuable data for sustainable decision-making. The users choose the emission source they want to evaluate, making the models convenient for mapping the emission contribution from specific sources.

Achieving accurate results by dispersion modeling is far from simple. The models can require a wide range of data about the meteorology, topography, emission characteristics and terrain characteristics of the modeling case. Wrongful input data can easily propagate when implemented, causing rigorous demands to their accuracy. Furthermore, complex conditions of the modeling domain are not accounted for by all models. It is therefore important to find a model which is fit for the modeling case. Identifying complex conditions can be demanding, as it may require expertise across several disciplines. Complicated models accounting for such conditions can be challenging to use, requiring expertise from the user. For these reasons, physical validations and routinely audits of the modeling approach can be necessary for thorough validation of the results.

Considerable amounts of models exist today, but the models can generally be put in to three categories depending on their modeling approaches. These are the Eulerian-, Lagrangian- and Gaussian models, using deterministic-, stochastic- and analytic approaches, respectively [16]. As the model used in this project (AERMOD) is Gaussian [17], the Gaussian models will be described in detail, while the Eulerian- and Lagrangian models will be discussed briefly.

2.1 General theory for dispersion models

Although the approaches differ, all dispersion models are based somehow on solving the atmospheric transport equation (ATE)[16]:

$$\frac{\partial c}{\partial t} = -\vec{v}\nabla c + \nabla K \nabla c + E + R + D \qquad (2.1.1)$$

3

Where c is the concentration, t is the time, $\vec{v}$ is the velocity vector and K is the matrix of turbulent diffusion coefficients. E, R and D are related to sinks and sources of emissions, chemical reactions, and deposition of species, respectively [16].

The innate complexity of Equation 2.1.1 makes it practically unsolvable by a direct analytical approach for most real-life instances [16][2], which is why other methods have to be used. This is especially due to the unpredictable turbulence term. Turbulence is characterized by random motion processes in the form of coherent structures [18]. In practice, the random motion of turbulence makes it very challenging to describe analytically, but the overall contribution of the turbulence can be estimated by e.g., statistical or numerical approaches. The R and D terms of Equation 2.1.1 are usually not dealt with by the core algorithm of the model, but with attached simulations or parameterization [16].

2.2 Eulerian- and Lagrangian models

The Eulerian models aim to solve Equation 2.1.1 on the form $c = c(t, x, y, z)$ by numerically solving second order partial differential equations (PDEs) for a certain coordinate frame, (t, x, y, z), with its corresponding initial- and boundary conditions [19]. The parameters of time and space are regarded as independent [16]. Due to the turbulence and wind velocity varying in space and time, these equations cannot be solved analytically, hence a numerical approach is used [16]. This can be done in several ways, but the most common method is the method of lines [16]. The method of lines involves spatial discretization of the modeling domain by either the finite volume method or finite difference method.

The Lagrangian models address the pollutants as individual particles or volumes of pollutants (i.e., fractions of the total amount of emissions), often referred to as "puffs" [16, 19]. The concentration profile is found by looking at the movement of each particle from the following formula [19]:

$$\frac{d\vec{v'}}{dt} = \vec{g} - k(\vec{v} - \vec{v_a} - \vec{v_t}) \tag{2.2.1}$$

Where $\vec{v'}$ is the particle velocity vector, $\vec{v'_a}$ is the advection vector and $\vec{v'_t}$ is the turbulence vector. $\vec{g}$ is the gravitational acceleration vector, which is the term which takes sedimentation into account. k is a function of the particle's size, density, and

---

[2]Gaussian models solve Equation 2.1.1 analytically, but this is only possible due to the many simplifications prescribed to the Gaussian models. Equation 2.1.1 is therefore not directly solved analytically by the Gaussian approach.

4

viscosity, usually based on Stoke's law [19].

The particle velocity vector will be found by the wind velocity- and direction, while the advection vector will be found by coupling with numerical weather prediction (NWP) models. The turbulence vector is estimated by treating the turbulence as a series of Markov processes, described by the Langevin equation. The terms of the Langevin equation will be parameterized based on characteristics of the atmosphere, namely the Monin-Obukhov length[3] and the height of the planetary boundary layer [16]. For further information, the author refers to [19, 20, 16].

There are also hybrid models, using the advantages of two models for better evaluation of the concentration profile. A common combination is the Eulerian-Lagrangian hybrid, which uses a Lagrangian approach for evaluation of emissions close to the source (where the Eulerian models often have issues) and Eulerian approaches for the far-away emissions (where the Eulerian models are the most accurate).

An honorable mention is the computational fluid dynamics (CFD) model. This model is in many ways comparable to Eulerian models, using solutions of Navier-Stokes equations for accurate descriptions of a system [16]. The model is quite heavy on computational requirements, meaning it is mostly suitable for smaller-scale (<1 km) problems. A hybrid approach utilizing CFD at close range and another model for longer ranges can be a powerful approach.

2.3   Gaussian dispersion models

This chapter is partly based on previous work done by the same author in the project assignment corresponding to this master's degree [21]. Some sections will therefore overlap somewhat.

Gaussian dispersion models have been existing ever since statistical and gradient transport theories were founded back in the early 1920s [22]. Since, the models have been in continuous development, through both empirical and theoretical analysis. This development is more or less still on-going today, resulting in a variety of approaches for Gaussian dispersion models. This section will focus on the classic approach formulated by Briggs in the 1970s [23, 24, 2, 25]. While modern models like AERMOD may deviate somewhat, the overall concept has remained much the same ever since. Thus, this section aims to give the reader some insight in how Gaussian dispersion models treat emission dispersion, and which factors are relevant for this treatment. A

---

[3]The height of the sub-layer of dynamic turbulence [20]

discussion of AERMOD's treatment of plumes will be dealt with in Subsection 2.4.1.

Gaussian dispersion models solve Equation 2.1.1 analytically for a single point source [13], by the Gaussian plume equation [13]:

$$\bar{c}(x, y, z) = \frac{\dot{m}}{2\pi\bar{v}\sigma_y\sigma_z}exp(-\frac{y^2}{2\sigma_y^2}\{exp[-\frac{(z-H)^2}{2\sigma_z^2}] + exp[-\frac{(z+H)^2}{2\sigma_z^2}]\}) \qquad (2.3.1)$$

Where $\bar{c}$ is the concentration at coordinates (x, y, z), giving the position of the point to be considered. $\dot{m}$ is the emission rate [kg/s], $\bar{v}$ is the mean wind speed in the mean wind direction over the time-interval to be considered [m/s], H is the effective height of the release [m], σ_y is the horizontal dispersion coefficient [m] and σ_z is the vertical dispersion coefficient [m]. The σ-terms are functions of the downwind distance, x [m]. The equation is in many ways a simplification and reformulation of Equation 2.1.1, much based on using the Gaussian distribution to describe the dispersion of emissions. Most assumptions tied to using Equation 2.3.1 will be discussed in this section.

Gaussian dispersion models describe the emission dispersion as Gaussian distributed concentration profiles, with standard deviances of σ_z and σ_y. The distribution goes along the plume centerline (see Figure 2.3.1), which is parallel to the mean wind direction, x. The σ-terms account for the effect of turbulence, entrainment and fluctuating wind-directions in the y- and z-directions. The diffusion in the x-direction is assumed to be governed by pure advection, as turbulence is deemed negligible compared to the transport caused by the wind. The σ-terms are functions of x, scaling with the downwind distance, giving the concentration profile the shape of a cone extending from the emission source, as seen in Figure 2.3.1.
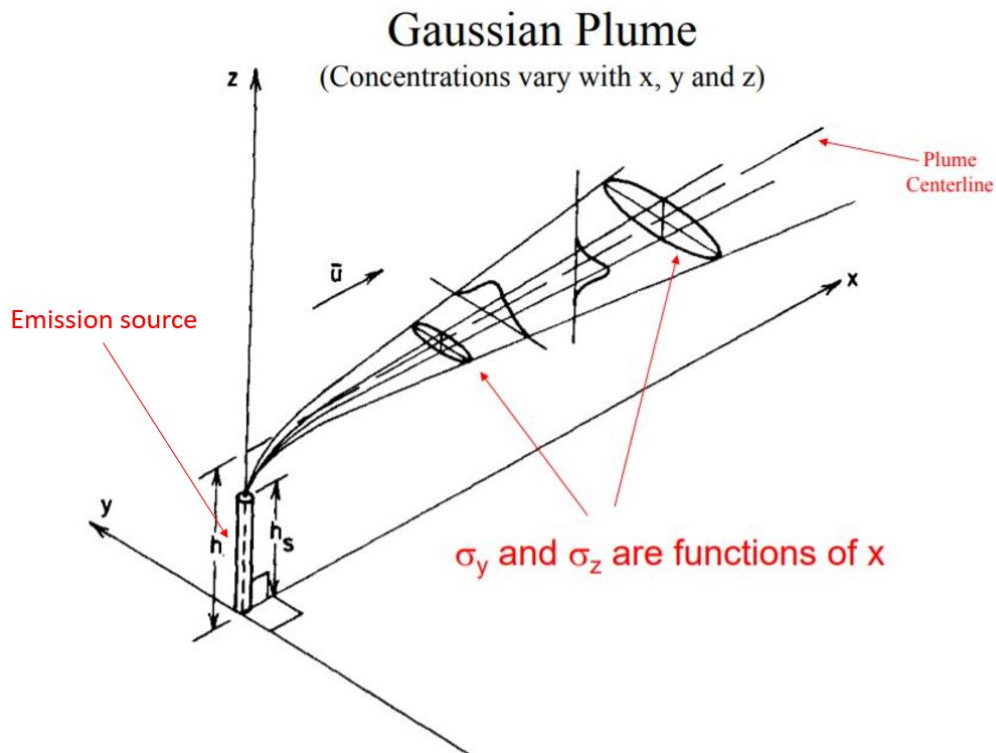
Figure 2.3.1: A Gaussian plume with standard deviances of σ_y and σ_z for the horizontal and vertical directions, respectively. The σ-terms scale with the downwind distance, x, giving the shape of a cone. The mean wind direction is assumed to be constant and parallel to the x-direction. h is the effective height of the plume, while h_s is the height of the stack, which is the point where the plume is released to the atmosphere from the emission source [3].

The σ-terms are, as mentioned, functions of x. These functions are normally found by parameterization. A common approach is to group the plume into a stability class, and then use this to determine the functions of σ_y and σ_z. The stability class is mostly dependent on the weather conditions in the area of the emission source. For this purpose, the Pasquill-Gifford scheme is typically used, found in the table below [1]:

Table 2.3.1: Pasquill-Gifford stability classes based on solar insolation, wind speed and night cloudiness. The classes A-F represent the stability accordingly: A: very unstable, B: moderately unstable, C: slightly unstable, D: neutral, E: slightly stable, F: stable. Table reproduced from [1].

Surface wind speed [m/s]	Day solar insolation			Night cloudiness	
	Strong	Moderate	Slight	Cloudy ($\geqslant 4/8$)	Clear ($\leqslant 3/8$)
< 2	A	A-B	B	E	F
2-3	A-B	B	C	E	F
3-5	B	B-C	C	D	E
5-6	C	C-D	D	D	D
>6	C	D	D	D	D

As stated in Bruce Turner's workbook from 1967, the determination should be done accordingly [1]: "The surface wind speed is measured at 10 m above the ground. Strong day solar insolation corresponds to a clear summer day with sun higher than 60° above the horizon. Moderate day solar insolation corresponds to a summer day with a few broken clouds, or a clear day with the sun being 35-60° above the horizon. The slight day solar insolation corresponds to a fall afternoon, cloudy summer day, or a clear summer day with the sun being 15-35° above the horizon. The night cloudiness is defined as the fraction of sky covered by clouds. For mixed classes (e.g., A-B), the average of their values should be used.". For modern uses, a combination of cloud ceiling height and cloud cover data is used for a more objective assessment of the solar insolation [17].

When the stability class is determined, the functions of the σ-terms can be found from literature. The functions have been determined through extensive empirical studies. Consequently, numerous schemes have been developed for this purpose. Here, Briggs' table from 1973[2, 22] for the determination of σ_y and σ_z, will be showcased:

Table 2.3.2: Formulas for σ_z and σ_y from Briggs based on stability classes for rural and urban conditions for an averaging time of 30 minutes. Table reproduced from [2].

Rural conditions	σ_z	σ_y
A	0.20x	$0.22x(1+0.0001x)^{-0.5}$
B	0.12x	$0.16x(1+0.0001x)^{-0.5}$
C	$0.08x(1+0.0002x)^{-0.5}$	$0.11x(1+0.0001x)^{-0.5}$
D	$0.06x(1+0.0015x)^{-0.5}$	$0.08x(1+0.0001x)^{-0.5}$
E	$0.03x(1+0.0003x)^{-1}$	$0.06x(1+0.0001x)^{-0.5}$
F	$0.01x(1+0.0003x)^{-1}$	$0.04x(1+0.0001x)^{-0.5}$
Urban conditions		
A-B	$0.24x(1+0.001x)^{0.5}$	$0.32x(1+0.0004x)^{-0.5}$
C	$0.20x$	$0.22x(1+0.0004x)^{-0.5}$
D	$0.14x(1+0.0003x)^{-0.5}$	$0.16x(1+0.0004x)^{-0.5}$
E-F	$0.08x(1+0.0015x)^{-0.5}$	$0.11x(1+0.0004x)^{-0.5}$

Where x is in km and the σ-terms are in meters. The values are based on using an averaging time of 30 minutes [2]. Note that this table differs between urban and rural conditions. Emissions in urban environments tend to disperse differently due to topographical effects like building downwash. This is accounted for by the σ-terms having different values for urban conditions.

This approach of describing the plume implicitly states that uniform conditions are assumed for the whole modeling domain, including homogeneous turbulence [13]. This assumption is weak for large-scale modeling, as conditions tend to change from one place to another. Consequently, most Gaussian dispersion models are constricted to a range below 50 km [17]. Through this approach there are also no limits to how far the concentration profile can propagate upwards and horizontally from the emission source [13].

Gaussian dispersion models assume that all emissions are conserved within the plume [13]. This means that there is no deposition, chemical conversion, washout or absorption of emissions, effectively neglecting the R and D terms of Equation 2.1.1. Furthermore, this means that emissions going towards the ground will be reflected back upwards and added to the existing plume [13]. The figure below illustrates the concept:
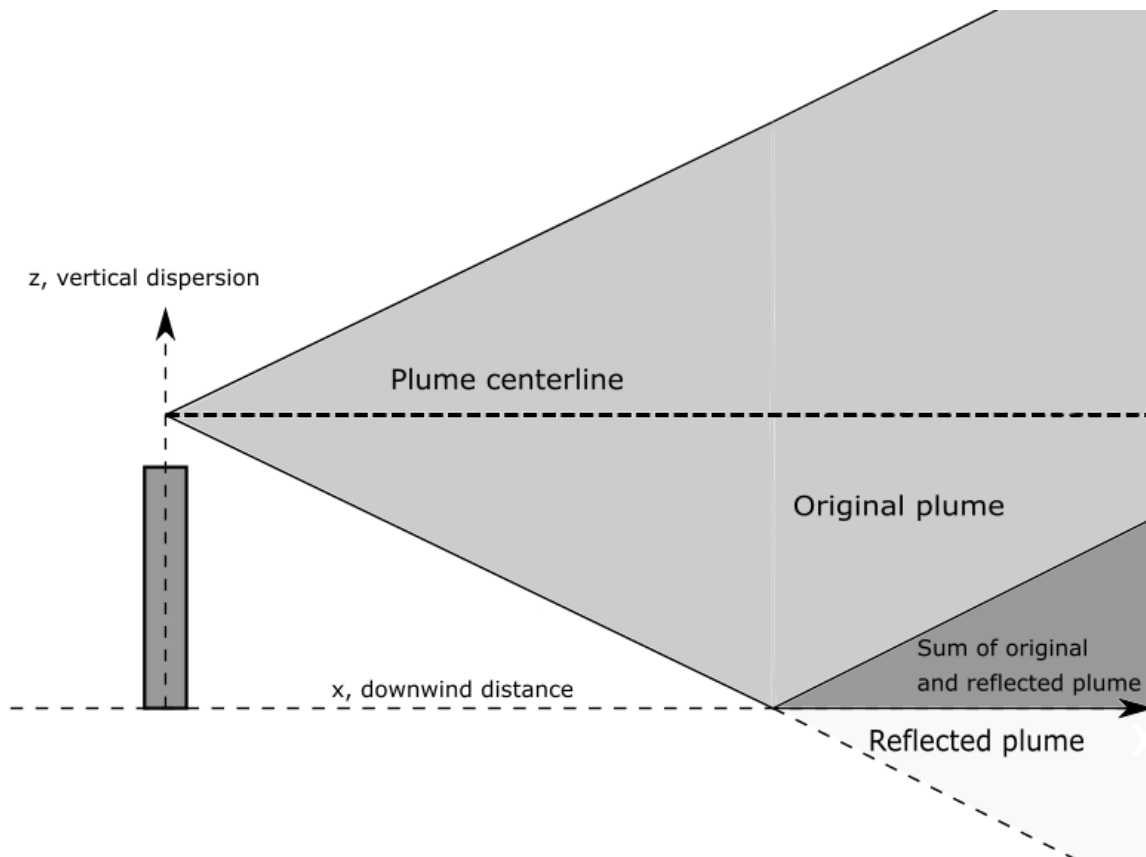
Figure 2.3.2: Illustration of the reflection of plumes.

This effect is accounted for in Equation 2.3.1 in the terms containing σ_z [3, 13]. For a derivation of how this is calculated, the author refers to [13].

The Gaussian dispersion model describes the plume as the average plume obtained after a certain time-interval, rather than an instantaneous plume. This is a prerequisite for the plume to be Gaussian distributed, and is therefore an essential part of the Gaussian dispersion model. The figure below illustrates the plume outlines (to the left) and the corresponding concentration profiles (to the right) of a plume for different averaging times [5]:

Figure 2.3.3: Comparison of time-averaged plume outlines and instantaneous plume outlines (left) with corresponding concentration profiles (right) [5].
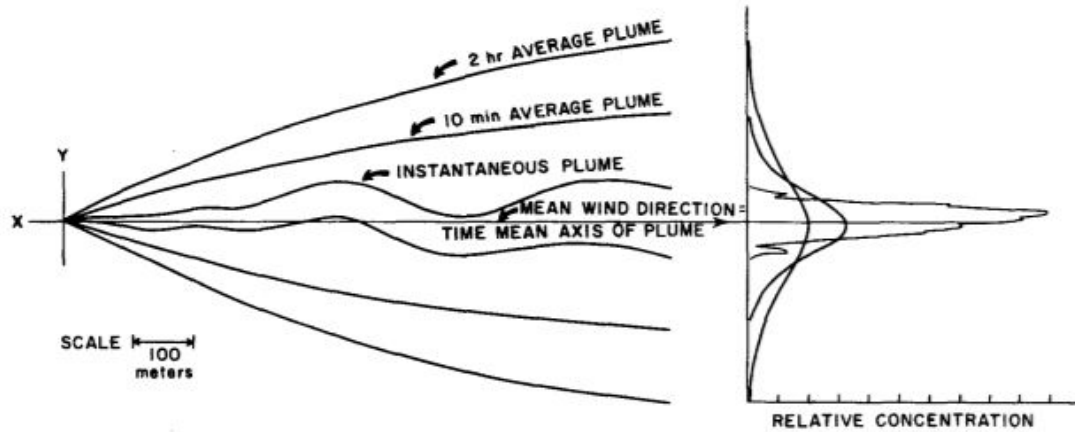
As seen from Figure 2.3.3, the plumes steadily converge towards a Gaussian distribution for longer averaging times. To illustrate, the two pictures below taken at Big Rock Point reactor site in Michigan USA [5] show the difference between a real plume and a Gaussian plume. Figure 2.3.4 is taken with 1/25 seconds of exposure, and illustrates a real plume, while Figure 2.3.5 is taken with 5 minutes of exposure, and illustrates a Gaussian plume. Figure 2.3.5.
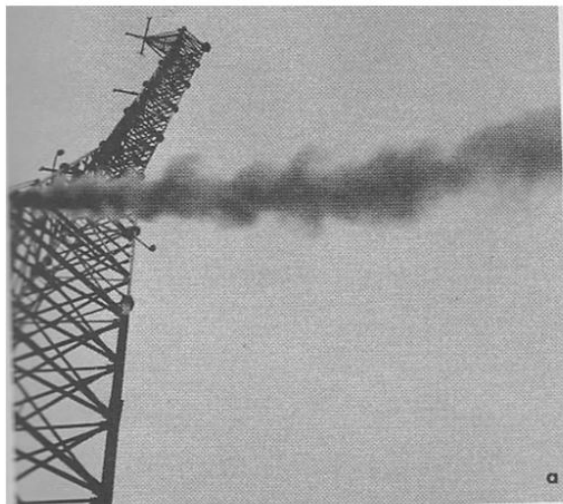
Figure 2.3.4: A continuous emission source captured at 1/25 seconds of exposure at the Big Rock Point reactor site [5].

11

Figure 2.3.5: A continuous emission source captured at 5 minutes of exposure at the Big Rock Point reactor site [5].

The averaging of plumes further requires the assumption that the emission rate in Equation 2.3.1, $\dot{m}$, is constant for the whole averaging period [13]. Commonly the averaging times range between 30 minutes and 2 hours.

Gaussian dispersion models are steady-state models, meaning that they are independent of time inside each time-interval [26]. In practice, this means that the plumes for each time-interval are estimated to instantly arrive at each receptor location when released, thereby not accounting for the travel-time of the plumes. As the conditions of the atmosphere may change during the travel-time of the plume, this puts further constrictions on the use of Gaussian models at larger scales. The steady-state formulation also inhibits the model from "remembering" past plume releases, limiting the model from accounting for causality effects [26].

Note that H in Equation 2.3.1 is termed the "effective height" of the plume release, which is the height from the ground to the plume centerline. After a plume exits the stack, it will initially rise before stabilizing at the plume centerline. It is along the plume centerline the Gaussian distribution is applicable, which is why the effective height is used in Equation 2.3.1. The effective height is the sum of the stack height (h_s) and the plume rise (Δh) [13]:

$$H = h_s + \Delta h \tag{2.3.2}$$

The figure below illustrates the different terms:
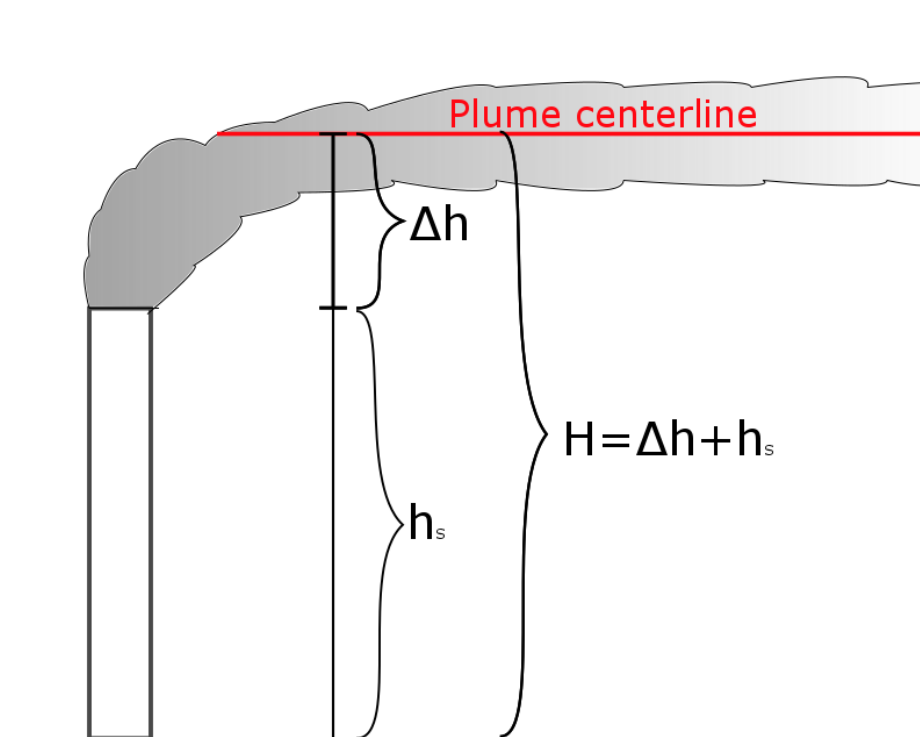
Figure 2.3.6: The figure illustrates the stack height (h_s), plume rise (Δh) and the effective height (H). The stack height is the height of the stack where the plume is released. The plume rise is the height from the stack height until the plume stabilizes, which is at the plume centerline. The effective height of the plume is the sum of the plume rise and the stack height.

The plume rise is how much the plume rises before it stabilizes. This height is termed the plume centerline, as seen in Figure 2.3.6. The plume rises mainly due to two mechanisms; the plume's initial velocity upon entering the atmosphere; and its buoyancy effect due to the plume being warmer than its surroundings [13, 25]. Generally, higher flow rates and higher plume temperatures tend to increase the plume rise. A combination of extensive empirical and theoretical studies have been performed to quantify the value of the plume rise [13, 25, 24]. The details of these will however not be discussed in this thesis. For more on plume rise, the author recommends [13, 25, 24].

The mean wind velocity ($\bar{v}$ in Equation 2.3.1) is a crucial parameter in dispersion modeling, which makes it particularly important to be accurate. Usually, the height where the wind speed is measured is not the same height as the plume centerline. As the wind speed changes in height from the ground, one should take this into account when determining the wind speed which is used Equation 2.3.1. The Environmental

Protection Agency of USA (EPA) has developed a power law for determining the wind speed at different heights [3]:

$$u_z = u_{zref}(\frac{z}{z_{ref}})^p \qquad (2.3.3)$$

Where u_z is the wind speed [m/s] at height z [m], u_{zref} is the wind speed at the point of measurement [m/s] with height z_{ref} [m], and p is the wind profile exponent, which depends on the stability category [-] [21, 3]. The table below shows the different values for p based on stability category:

Table 2.3.3: Values for the wind profile exponent, p, for different stability categories in rural and urban conditions. Table reproduced from [3].

Stability category	Urban	Rural
A	0.15	0.07
B	0.15	0.07
C	0.20	0.10
D	0.25	0.15
E	0.30	0.35
F	0.30	0.55

As with most parameters, there are also other ways of calculating this.

2.4 AERMOD

AERMOD started as a collaborative project between the American Meteorological Society (AMS) and the American EPA in 1991 [27]. Prior to AERMOD, the regulatory dispersion model for short-range emissions was ISC2/ISC3. Outdated algorithms in the ISC-models gave EPA and AMS incentive to develop a new model [27]. The designated task force working with AERMOD was named the AMS/EPA Regulatory Model Improvement Committee (AERMIC) [27]. The overall goal of AERMIC was to create a model which [27]:

- Improved the old ISC3 algorithms with state-of-the-art algorithms where practical.

- Kept the old input/output architecture of ISC3.

- Still had the same capabilities that ISC3 had.

After years of development, the EPA finally proposed AERMOD to replace ISC3 in 2000 [28]. AERMOD was formally fully adopted as the model for regulatory emission

14

assessments in December 2006 [6].

Since AERMOD achieved its status as the recommended tool for short-range regulatory emission assessments, the model has been in extensive use internationally. The popularity of the model stems from it being relatively simple to use in addition to having a decent accuracy and many applications. The large user-base has prompted vast documentation and evaluation of the model, giving the EPA incentive to continuously improve the model.

2.4.1 Model overview

AERMOD is a steady-state Gaussian dispersion model. It does however deviate somewhat from the traditional Gaussian model described in Section 2.3. AERMOD assumes the concentration distribution to be Gaussian in the stable boundary layer (SBL). The convective boundary layer (CBL) is however bi-Gaussian, where the horizontal concentration distribution is Gaussian, while the vertical concentration distribution is described by a bi-Gaussian probability density function [29]. AERMOD also includes additional effects for improved description of the dispersion of emissions in the CBL (see [29], page 17).

AERMOD gives a more comprehensive description of the planetary boundary layer (PBL) than traditional Gaussian models, by combining surface- and mixed layer scaling [29]. AERMOD does this by applying similarity relationships on all available meteorological data to make vertical profiles of the PBL characteristics [29]. This is on the prerequisite that one has the needed meteorological data available. This is only optional, as the model only needs data readily available from national weather service (NWS) stations to run [29].

Despite being a steady-state model, AERMOD can account for vertical inhomogeneities in the atmosphere by "averaging" the actual PBL parameters into "effective" parameters, used to achieve a homogeneous PBL which is equivalent to the real PBL [29]. Essentially, the parameters of the real PBL are converted so that they are represented in the homogeneous PBL.

AERMOD does not distinguish between simple and complex terrain, and accounts for terrain effects by current concepts, in practice meaning the plume either follows and/or impacts the terrain [29]. This effectively liberates the user from defining simple and complex terrain. The terrain effects are designed to be simple to implement, but remain physically realistic.

AERMOD is a three-part integrated model with two modules for pre-processing data, and one computational module which uses this data to calculate the dispersion of emissions, which is AERMOD. The two pre-processing modules are named AERMET and AERMAP.

AERMET takes in meteorological data (e.g., wind speed and -direcion, temperature and cloud cover) and optionally various surface characteristics (see Figure 2.4.1), to calculate PBL parameters which are then passed to AERMOD's internal computational module for meteorological data (called INTERFACE) [29]. The meteorological data is typically gathered from NWS data, while the surface characteristics are provided by the user or an additional module named AERSURFACE [29].

AERMAP is a pre-processing module which both characterizes the terrain and generates receptor grids for AERMOD [29]. The receptor grids are inputs provided by the user, while the terrain data is gathered from digital elevation models (DEM)[4] The terrain data is used to calculate the "terrain-influence height" (h_c) which effectively is a measure of the terrain's effect on the emissions [29]. AERMAP will send the receptor locations and and h_c to AERMOD for further processing.

Other, optional modules are also available. Here, AERSURFACE, AERMINUTE, BPIPPRM and AERPLOT will be discussed briefly. An illustration of the model overview and the data flow is shown in Figure 2.4.1. AERSURFACE, which is already mentioned, has land cover data, gathered from e.g., the national land cover database (NLCD), as inputs [30]. AERSURFACE uses this data to calculate the values of various surface characteristics, such as albedo, Bowen ratio and surface roughness length, which then can be used as inputs in AERMET [30].

---

[4]Database for terrain data.

16
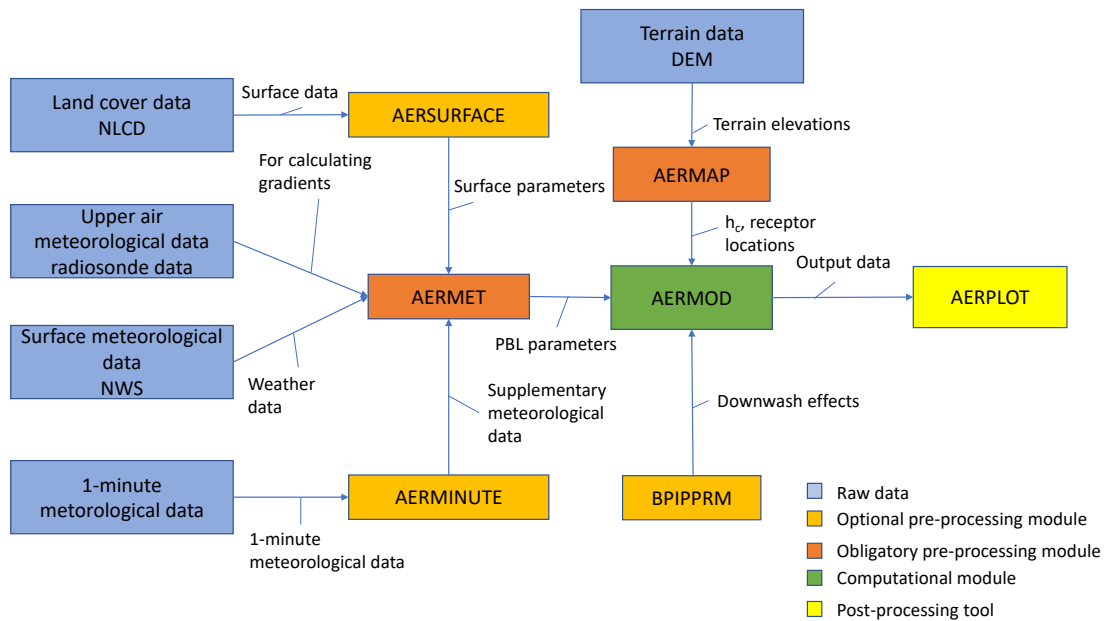
Figure 2.4.1: Model overview and dataflow of AERMOD including the optional modules discussed in this subsection. A more detailed description of some of the data is given in Table 2.4.1.

The table below gives a more detailed description of some of the dataflows in Figure 2.4.1 [29]:

Table 2.4.1: A more detailed description of some of the dataflows given in Figure 2.4.1.

Data from diagram	Typical parameters from categories
Surface data	The characteristics of the surface (e.g., if it is a body of water, a forest, etc.).
Surface parameters	Albedo, Bowen ratio, surface roughness length, etc.
Weather data	Wind speed and -direction, humidity, cloud cover, cloud ceiling height, temperature, etc.
PBL parameters	Friction velocity, Monin-Obukhov length, convective velocity scale, temperature scale, mixing height and surface heat flux.
Output data	Concentration data with corresponding coordinates in accordance with output options.

AERMET takes in hourly measured wind speeds from NWS data. AERMOD has some problems dealing with calm winds and changing wind directions. AERMINUTE is a tool which takes in 1- or 5-minute wind speed data and use the averages of these to supplement otherwise insufficient or missing hourly data gathered from NWS stations [31]. The data acquired from AERMINUTE are then used as inputs to AERMET where needed.

BPIPPRM is a module which calculates the downwash effects caused by buildings in

the modeling domain [32]. The inputs are user-defined and consist of the dimensions and coordinates of the buildings. The module then calculates the downwash effects of these buildings and these are used as inputs in AERMOD.

AERPLOT is a post-processing tool which has the outputs of AERMOD as inputs. AERPLOT is compatible with Google Earth Pro[33], and will readily show the results on Google Earth's map. The showcased results are based on the output options of AERMOD. The results will be showcased as a map with each receptor shown as a point on the map, where one can click on the receptors to get details of the receptor point, see Figure 2.4.2. The data can also be showcased as gradients or contour plots, depending on the user-defined inputs in the AERPLOT output options.
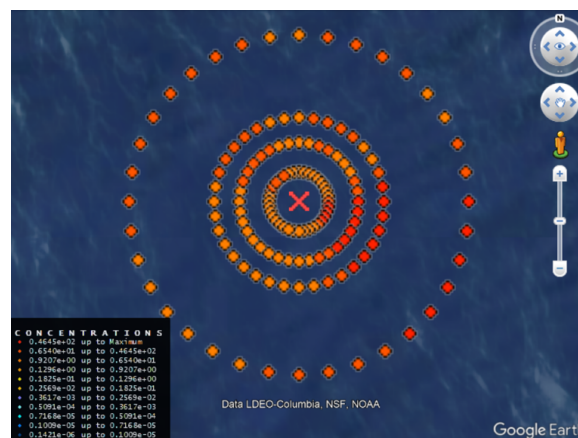
Figure 2.4.2: Outputs from the AERMOD sample run [6] post-processed by AERPLOT.

2.4.2 Overview of features and limitations

This subsection will serve to review AERMOD's features and limitations. This is done both to provide the reader details about the model's capabilities, and to justify the choice of AERMOD for the modeling case.

As AERMOD is a Gaussian dispersion model, it has a range limitation of 50 km [26]. Being fundamentally Gaussian does however make the model simple to use compared to Eulerian and Lagrangian models, as Gaussian models tend to need less data and less knowledge about the characteristics of the atmosphere [26]. It also makes AERMOD require modest computational resources, and the tool can therefore be run on conventional laptops.

A general problem with many Gaussian models is low wind speeds. As Equation 2.3.1

is inversely proportional to the wind speed, the models tend to collapse under these conditions. AERMOD treats the turbulence as non-Gaussian for low wind speeds, meaning results can be achieved even for these conditions [34]. The optional AER-MINUTE module can also help mitigate the problems with low wind speeds in addition to fluctuating wind directions.

Another common weakness with Gaussian models is their inability to account for more than a single point source. AERMOD can treat several emission sources at once, and can trace the impact of each source in addition to their total contribution to the emission concentration [35]. These can be sources of various kinds, as AERMOD can treat point-, open-pit-, volume-, and both buoyant- and non-buoyant line sources [35].

AERMOD has algorithms which can account for wet- and dry deposition [17], although these are not thoroughly verified yet. AERMOD has limited capabilities in dealing with chemical processes. The model can treat simple chemical processes like exponential decay [17].

Due to its efficient treatment of terrain effects, as explained in 2.4.1, AERMOD is recommended for both simple and complex terrain by the EPA [29]. AERMOD can be used for both urban and rural conditions. For urban conditions, population density is used as a metric to measure the effects of the urbanity of the modeling domain. For tall buildings, the BPIPPRM module can be used to account for building downwash effects where these are prominent.

Like the majority of Gaussian models, AERMOD is a steady-state model [6]. In practice, this limits AERMOD's capabilities for unstable conditions and advanced meteorological phenomena. Advanced meteorological phenomena are phenomena like inversions, fumigations and wind circulations caused by steep terrain or the sea. In general these phenomena cause inhomegeneities in the atmosphere, being hard to account for by the model. As an example, comparative studies [36] show that AERMOD has some lacking capabilities in dealing with shoreline fumigation. Still, as mentioned in Subsection 2.4.1, the algorithm AERMOD employs can account for inhomogeneities to a certain degree [29]. The steady state formulation in addition inhibits the model from dealing with causality effects, as the model does not remember past emissions [37].

Despite some lacking capabilities for certain conditions, AERMOD is deemed to be an accurate model where fit [37]. AERMOD has been used in numerous comparative studies, where the model has seen good results despite its relatively simple approach. Some studies and their results are showcased in Table 2.4.2 [21].

Table 2.4.2: Comparative studies done on dispersion models. A simple summary of the conditions is given for each study. The models are given in the order of best performing models (in regards to accuracy) to worst performing models for each study. The performance of the tools is measured by comparing the estimated concentration values of each model with the real (known) values. Note that the results of such studies are highly dependent on the conditions, meaning the results of these are only indicative of a model's performance relative to another.

Study title	Situations modeled	Models eveluated
An evaluation and inter-comparison of AUSPLUME, AERMOD and TAPM for seven field datasets of point source dispersion [36].	Complex terrain/ Flat terrain/ Near-coast/ Urban/ Rural/	TAPM AERMOD AUSPLUME
Evaluation of AERMOD and CALPUFF for predicting ambient concentrations of total suspended particulate matter (TSP) emissions from a quarry in complex terrain [38].	Quarry (complex terrain)	AERMOD CALPUFF
Performance evaluation of AERMOD, CALPUFF and legacy air dispersion models using the Winter Validation Study dataset [39]	Complex terrain, cold conditions	RATCHET CALPUFF ISC2 AERMOD
Comparison of the Complex Terrain Algorithms Incorporated into Two Commonly Used Local-Scale Air Pollution Dispersion Models (ADMS and AERMOD) Using a Hybrid Model [40]	Complex terrain	ADMS AERMOD
Estimating near-road pollutant dispersion: A model inter-comparison [41]	Flat terrain Different meteorological conditions	ADMS/AERMOD RLINE CALINE 3/4
Performance Evaluation of AERMOD and CALPUFF Air Dispersion Models in Industrial Complex Area [42]	SO_2 and NO_x in moderately complex terrain	AERMOD CALPUFF

An advantage with AERMOD is that it is free and easy to install [6]. AERMOD also has a wide user-base, which in combination with the model's comprehensive guides [35, 43, 7] makes the model relatively simple to use and get assistance with. As it is the EPA's recommended regulatory model, the model is under continuous development and evaluation. The model is in addition the recommended regulatory

tool for short-range PM2.5, PM10[5] and SO$_2$ pollution. The model has been used for numerous applications, including modeling the dispersion of emissions at aluminum plants [44, 17].

2.5 How to use AERMOD

This section will present a simple guide on how to use AERMOD. For this purpose, a test case extracted from the AERMOD SCRAM website [6] will be used. The guide will go through and explain the different steps required to model the test case using AERMOD. The reader can follow along by downloading the test case and performing the steps in the manner described in this section. While this will make the reader somewhat familiar with the tool, the author and the EPA still recommends any user that wants to use AERMOD for regulatory purposes to first read AERMOD user's guide [35], AERMET user's guide [7] (at least chapters 1-3) and the AERMAP user's guide [43] (at least chapter 1-2). A reasonable approach is to use these as continuous guidance when performing a modeling case. The guide in this thesis assumes the user to be on a Windows operating system.

The test case of this section will be the Lovett test case found at the AERMOD SCRAM website [6]. The files that are needed to perform the modeling case, are:

- AERMOD executable [6]

- AERMET executable [45]

- AERMAP executable [46]

- AERPLOT executable [46]

- Google Earth Pro software [33]

- Surface meteorological data [45], `14375-88.FSL`

- Upper air meteorological data [45], `14375-88.SAM`

- On-site meteorological data [45], `LVTOSITE.MET`

- Terrain data, `SCRAN-E.DEM` and `HART-W.DEM` [6]

- Hourly emission data [6], `LVTHEMIS.DAT`

- Event data [6], `lovett_evt.DAT`

---

[5]Particulate matter (or dust) with diameters of 2.5 and 10 micrometers, respectively.
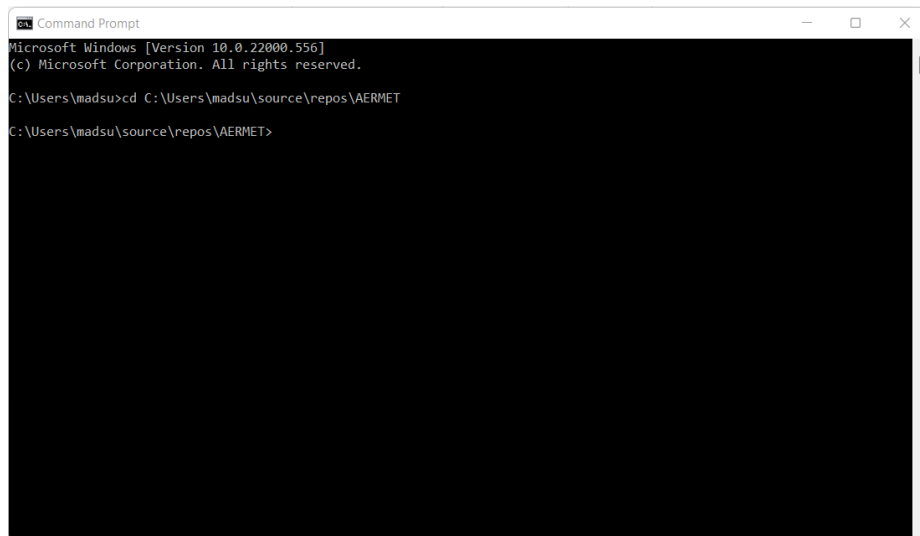
Each file can be downloaded from its respective reference. For the meteorological data, the files are extracted from the AERMET "test cases" zip-file. Inside the zip-file, go to aermet_test_cases_21112 → aermet_def_testcases_21112 → lovett, and find and extract the files from there. The terrain data, hourly emission data and event data can be found from the Lovett zip file found at the SCRAM website [6]. The meteorological data can also be found in the Lovett zip file, although it deviates somewhat from the data found from the AERMET test case due to version difference.

The reader can also choose if it wants to download the input files for each module. The input files for AERMET are found in the same folder as the meteorological files (`LVTSTAG1.INP`, `LVTSTAG2.INP` and `LVTSTAG3.INP`). The AERMAP input file is found in the same folder as the terrain data (`LVTMAP.INP`). The AERMOD input file is named `lovett.INP`, and is found in the "AERMOD test cases" zip file from the AERMOD SCRAM website [6]. To find the input file, go to 21112 aermod_test_cases_21112 → inputs, and the file can be found in this folder. Note that these input files may deviate somewhat from the input files showcased in this tutorial.

2.5.1 General considerations

Running AERMOD with raw data requires the user to firstly pre-process the data by the use of AERMET and AERMAP. The processed data will then be used as input data for AERMOD. As mentioned in Section 2.4.1, AERMET deals with the meterological data, and AERMAP deals with the terrain data. This guide will take the reader through the pre-processing stage using AERMAP and AERMET, the processing stage using AERMOD, and the post-processing stage using AERPLOT.

AERMOD and its modules is run through the command prompt of the computer. To access the command prompt, simply press the "Windows" key and type `cmd`. The command prompt terminal should then pop up as the first alternative. To use any of the executables, one first has to enter the folder of the executable through the command prompt. This is done by typing `cd` followed by the address of the directory of the relevant module. An example is shown in the figure below.
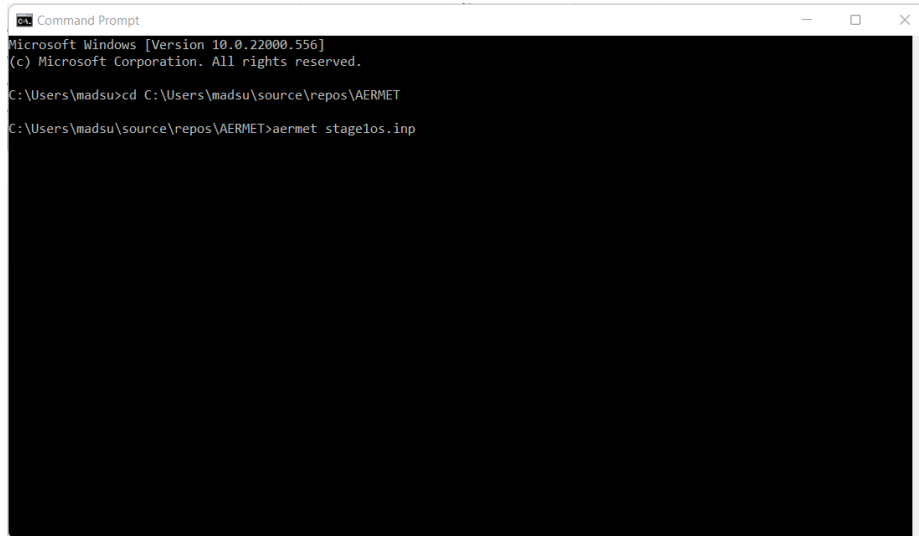
Figure 2.5.1: Example of how to access AERMET in the command prompt.

In the example above, the user has accessed the folder containing the AERMET executable. Each executable should be in their own folder to avoid the executable from reading the wrong files. To run the executable, the user simply has to type the name of the executable to be run (in this case `aermet`) and press enter.

The options of the module to be run is decided through a text file being in the format of `.INP`. If nothing else is specified, the executable will read the input file named `nameofmodule.INP`, where `"nameofmodule"` is the name of the module which is run. If the user wants to run an input file other than the standard input file, the user has to type in the name of the module, the name of the input file the user wants the executable to read, and press enter. An example is shown below for AERMET.

Figure 2.5.2: Example of how to run AERMET with an alternative input file. In this case the input file is named `stage1os.inp`.

In the example the user wants to run `stage1os.INP`. This only works if the input file is in the same folder as the module. If the user includes the directory of the input file, input files from other folders can be accessed. Users are however advised to keep all of the files to be used in the same folder as the executable.

The input files are made by the user, most conveniently done on the "Notepad" app. Experienced users can use tools like Windows Visual Studio [47] to edit and structure the files. All of the modules use the "keyword/parameter approach" [35]. Firstly, the user types in a keyword determining the pathway, where a pathway is a category of keywords. Following the pathway, the keywords inside the category are placed below one another with an indentation (marked either by the spacebar- or tab key), and following these keywords will be the value of each keyword. A new pathway is started whenever a new keyword without an indentation is placed. The figure below illustrates an example of an input file for AERMET.

Figure 2.5.3: Example of an AERMET input file.

Here, *JOB* is the first pathway, which includes the keywords *MESSAGES* and *REPORT*, with values of *lvtstag1.MSG* and *lvtstag1.RPT*, respectively. The syntax rules will not be thoroughly discussed here. The author refers to the user guides for the rules syntax [7, 43, 35]. The keywords and parameters differ from module to module, but generally, the format and syntax remain the same. Keywords and parameters for each module are also summarized in the user guides for the respective modules [7, 43, 35].

2.5.2   AERMET

The pre-processing of the meteorological data is done in three stages, as illustrated in Figure 2.5.4.

25
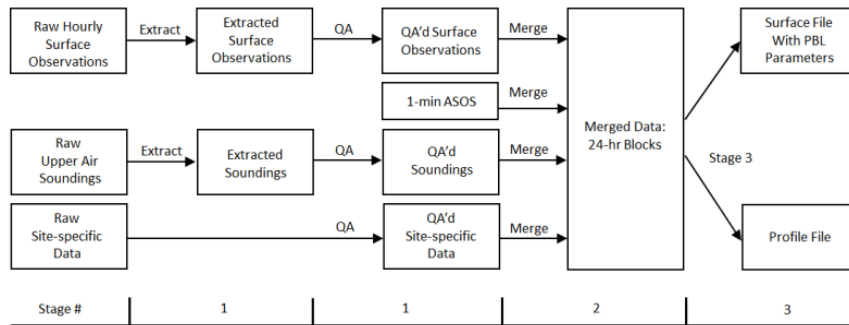
Figure 2.5.4: The process flow of AERMET. The figure comes from the AERMET user's guide [7].

The first stage involves extracting/reformatting and quality assuring (QA) the raw data. In this example there are 3 types of raw data, namely on-site meteorological data, surface data from a NWS-station and upper air radiosonde data. The on-site data is used in combination with the NWS-data. The on-site data is measured on the site of the source, and is therefore deemed as the most representative data. The NWS data is used when the on-site data is lacking, where the limit to when the on-site data is replaced is determined by the user. The upper air data is used to make profiles of the weather conditions of the atmosphere. For the QA of stage 1, an input file containing the following inputs is needed:

```
LVTSTAG1 - Notepad

File    Edit    View

JOB                                     *Pathway which specifies the file names of the job
  MESSAGES lvtstag1.MSG                  *Produces a message file named "lvtstag1.msg"
  REPORT   lvtstag1.RPT                  *Produces a report file named "lvtstag1.rpt"

UPPERAIR                                 *Pathway for determining the options for upper air data
  DATA      14735-88.FSL   FSL           *Name of the file for upper air raw data and its format
  extract   ua14735.iqa                  *Name of the reformatted output file
  location  14735  42.75n  73.80w  5     *Station number, location of the measuring station and the time zone shift
  xdates    88/01/01  88/12/31           *The time period of measurement
  qaout     ua14735.oqa                  *QA output file


SURFACE                                  *Pathway for determining the options for surface data
  DATA      14735-88.SAM   SAMSON        *Name of the file for surface raw data and its format
  EXTRACT   sf14735.iqa                  *Name of the reformatted output file
  location  14735  42.75n  73.80w  0     *Station number, location of the measuring station and the time zone shift
  xdates    88/01/01  88/12/31           *The time period of measurement
  qaout     sf14735.oqa                  *QA output file

ONSITE                                   *Pathway for determining the options for on-site data
  LOCATION Lovett 74.0W 41.3N  0         *Location name, coordinates and time zone shift
  DATA   LVTOSITE.MET                    *Name of the file for on-site raw data
  QAOUT lvtoqa.MET                       *QA output file
  XDATES 88/1/01  88/12/31              *The time period of measurement

  threshold 0.3                          *Threshold value of wind speed
  OSHEIGHTS 10.0 50.0 100.0              *Measurement heights
  READ 1 OSDY OSMO OSYR OSHR OSMN        *Definition of how AERMET should read the on-site raw data
  READ 2 HT01 SA01 SW01 TT01 WD01 WS01
  READ 3 HT02 SA02 SW02 TT02 WD02 WS02
  READ 4 HT03 SA03 SW03 TT03 WD03 WS03

  FORMAT 1 (5(I2,1X))                    *The format of the on-site raw data
  FORMAT 2 (16X,F5.1,1X,F5.1,1X,F7.3,1X,F6.2,1X,F7.2,1x,F7.2)
  FORMAT 3 (16X,F5.1,1X,F5.1,1X,F7.3,1X,F6.2,1X,F7.2,1x,F7.2)
  FORMAT 4 (16X,F5.1,1X,F5.1,1X,F7.3,1X,F6.2,1X,F7.2,1x,F7.2)

  RANGE TT -30 < 40 -99                  *The range of values of temperature to be QA'd
  RANGE SA 0 <= 95  -99                  *The range of values of sigma_y for to be QA'd
  RANGE WS 0 < 50   -999                 *The range of values of wind speed to be QA'd
  RANGE WD 0 <= 360 -999                 *The range of values of wind direction to be QA'd
  AUDIT WS WD SA TT                      *Determining which parameters to QA in addition to the three standard parameters


Ln 1, Col 1                                              80%        Windows (CRLF)        UTF-8
```

Figure 2.5.5: The input file for stage 1 with explanations of each keyword/parameter.

This file contains explanations of each keyword and parameter. When running AER-MET, the explanations need to be omitted from the file. Note that there is one pathway group for each raw data file. The keywords in the *UPPERAIR-* and *SURFACE* pathways are for the most part the same, and fairly self-explanatory. Note, however, the time shifts on the *location* keywords. This shifts the time from the raw data file to correspond to the time zone of the other raw data files. The value is 0 if the time zone is correct.

ONSITE is more complicated, including the *threshold*, *OSHEIGHTS*, *READ*, *FORMAT*, *RANGE* and *AUDIT* keywords. The main reason for this is that on-site data tends to deviate from the standard formats of NWS- and upper air data. The user therefore has to define how AERMET should read the file. The keywords are explained in the list below:

- *threshold*: The minimal wind speed allowed before the wind speed is treated as calm.

- *OSHEIGHTS*: The measurement heights for the on-site raw data.

- *READ*: Defines the parameters of the on-site data so that AERMET knows what the parameters are, and in what order they come. For the definition of the variables, the author refers to appendix B in the AERMET user's guide [7].

- *FORMAT*: The *FORMAT* keyword in combination with the *READ* keyword defines the format of the raw data. For each *READ* keyword, there must be a *FORMAT* keyword. *FORMAT* uses Fortran [48] syntax for defining the format. The author refers to any introductory Fortran manual for learning the language, e.g., this site [49].

- *RANGE*: The range keyword defines which ranges of parameters one will perform the QA on. This is especially useful for on-site raw data, as missing value indicators may differ from AERMET's missing value indicators. Faults in missing value indicators may lead to incorrect calculations. The user can choose the value of the missing value indicator in the last row of the *RANGE* input. AERMET's standard missing value indicators are found in the user guide [7]. For the definition of the variables, the author refers to appendix B in the AERMET user's guide [7].

- *AUDIT*: Enables the user to determine which parameters to be audited in the QA in addition to the automatically audited parameters. The automatically audited parameters vary from which kind of data are used as inputs. For a definition of the variables, the author refers to appendix B in the AERMET user's guide [7].

When the input file is defined, AERMET can be run to finish stage 1. This is done by giving the following command in the command prompt[6]:

```
aermet lvtstag1.INP
```

If the run is successful, the command prompt will start processing all the raw data. The final lines after a successful run should look something like the figure below.

---

[6]Remember that you have to be in the correct folder for it to run. The folder has to contain the raw data files, the input file and the AERMET executable.

Figure 2.5.6: The command prompt at the end of a successful stage 1 run.

A successful run results in 5 output files, one QA file for each of the processed raw data, a message file and a report file. The `.OQA` files are the reformatted and QA'd data which are used for further processing. The message file contains all the errors, warnings, information and QA messages produced by the run. The report file is a categorized summary of the message file. If the executable ran into an error making it unable to run, the following message will be shown:

```
*******************************************************
      *** AERMET Setup Finished UN-successfully ***
*******************************************************
```

This usually happens if something is wrong with the input file. If this happens, it is recommended to check the report file. The command prompt will indicate if the run was successful or not for all stages.

Stage 2 involves merging all QA data into a single file, and replacing missing data from these files with missing value indicators. The stage 2 input file for the example case is showcased in the figure below:

29

```
JOB                              *Pathway which specifies the file names of the job
  MESSAGES  LVTSTAG2.MSG         *Produces a message file named "LVTSTAG2.MSG"
  REPORT    LVTSTAG2.RPT         *Produces a report file named "LVTSTAG2.RPT"

UPPERAIR                         *Pathway determining the options for upper air data
  QAOUT   ua14735.oqa            *The upper air QA data to be merged

SURFACE                          *Pathway for determining the options for the surface data
  QAOUT   sf14735.oqa            *The surface QA data to be merged

ONSITE                           *Pathway for determining the options for the on-site data
  QAOUT   LVTOQA.MET             *The on-site QA data to be merged

MERGE                            *Pathway where the merge options are decided
  OUTPUT MERGE.LVT               *The file name of the merged data
  XDATES 88/1/1  88/12/31        *The time period for the merged data
```

Figure 2.5.7: Stage 2 input file.

This stage is relatively simple. For each of the categories of data, the QA file from stage 1 is given as input as these are the files to be merged. To run stage 2, the following command is given in the command prompt:

`aermet lvtstag2.inp`

The outputs will be the merged file, a report file and a message file.

The stage 3 processing uses the merged file to calculate the boundary layer scaling parameters and creates two output files which are used as inputs for AERMOD. The first output file contains the calculated boundary layer parameters and the observed surface parameters. The second output file contains the calculated profiles[7] of various parameters, like wind speed and temperature. A part of the stage 3 input file for AERMET with explanations is showcased in the figure below.

---

[7]The variation of parameters depending on coordinates.

```
JOB                               *Pathway which specifies the file names of the job
  MESSAGES LVTSTAG3.MSG           *Produces a message file named "LVTSTAG3.MSG"
  REPORT   LVTSTAG3.RPT           *Produces a report file named "LVTSTAG3.RPT"

METPREP                           *Pathway which specifies the options of stage 3 processing
  METHOD    WIND_DIR RANDOM       *Decides how the wind directions are distributed in the general wind direction
  NWS_HGT   WIND 6.1              *The measurement height of the NWS data
  OUTPUT    LOVETT.SFC            *Determines the file name of the surface data
  PROFILE   LOVETT.PFL            *Determines the file name of the profile data
  XDATES    88/1/1    88/12/31    *The time period of measurement
  LOCATION Lovett 74.0W 41.3N  5  *Location name, coordinates and time zone shift for the on-site data
  FREQ_SECT MONTHLY 6             *Indicating the temporal- and directional divisioning for site characteristics
  SECTOR 1  0     35              *Sector 1, being from 0-35 degrees
  SECTOR 2  35    60              *Sector 2, being from 35-60 degrees
  SECTOR 3  60  130               *Sector 3, being from 60-130 degrees
  SECTOR 4  130 175               *Sector 4, being from 130-175 degrees
  SECTOR 5  175 225               *Sector 5, being from 175-225 degrees
  SECTOR 6  225 360               *Sector 6, being from 225-360 degrees
                                  *The site characteristics for each division in the order: month, sector, albedo,
                                   Bowen ratio and surface roughness length

  SITE_CHAR   1   1 0.350  1.150  0.750
  SITE_CHAR   2   1 0.350  1.150  0.750
  SITE_CHAR   3   1 0.350  1.150  0.750
  SITE_CHAR   4   1 0.250  0.550  0.850
  SITE_CHAR   5   1 0.250  0.550  0.850
  SITE_CHAR   6   1 0.120  0.250  1.000
  SITE_CHAR   7   1 0.120  0.250  1.000
  SITE_CHAR   8   1 0.120  0.250  1.000
  SITE_CHAR   9   1 0.200  0.800  0.900
  SITE_CHAR  10   1 0.200  0.800  0.900
  SITE_CHAR  11   1 0.200  0.800  0.900
  SITE_CHAR  12   1 0.350  1.150  0.750
```

Figure 2.5.8: A part of the stage 3 input file.

The whole input file can be downloaded at [45] by following the instructions from Section 2.5.1. The *METHOD* keyword determines different processing options. This example contains one processing option, namely *WIND_DIR RANDOM*. The *WIND_ DIR* keyword determines which precise wind directions to be used in the general wind direction given by the merged data file. As for instance, NWS stations have a 10° accuracy, the *WIND_DIR RANDOM* keyword will make AERMET use a random wind direction inside of the 10° wind direction span. Substitution of on-site data with NWS data is done by including the keyword *METHOD REFLEVEL SUBNWS*. This is not included here, meaning only on-site data will be used. For other options using the *METHOD* keyword, the author refers to the AERMET user's guide [7].

The *FREQ_SECT* keyword determines the division of the temporal- and spatial dimensions of where the user wants to define surface characteristics. The temporal division can be annual, seasonal or monthly. The spatial division is decided by giving the start- and end coordinate (in degrees) of the arc representing the sector. The

31

site characteristics for each temporospatial dimension are given by the *SITE_CHAR* keyword. The parameters are, from left to right: time, space, albedo, Bowen ratio and surface roughness length. Before using this keyword, the user should have some idea of what the different surface characteristic parameters are in the modeling domain. The AERMET user's guide [7] contains tables which can help identify the values of the different parameters. 0° indicates that the direction is north, and every increasing degree goes clockwise from the starting point.

When the input file is ready, the third and final stage will be processed by the command:

```
aermet lvtstag3.inp
```

If run successfully, two output files being used as input files for AERMOD, a message file and a report file will be produced. The two output files being used for AERMOD are the `.SFC`- and `.PFL` files, being the meteorological surface file and meteorological profile file respectively. This is the final step for the AERMET pre-processor.

2.6 AERMAP

The AERMAP pre-processor processes topographical data into an output file with parameters readable for AERMOD, which determine the influence of topographical features in the modeling domain. Optionally, sources and receptors can be added in AERMAP, but these can also be implemented in AERMOD directly.

AERMAP uses DEM- or NED data for topographical data. These should be of DEM- or GeoTiff formats. The data can be extracted from various sites, e.g., Hoyde-data.no for Norway or the MRLC for the USA. Before implementation, the user should make sure that the data is of the correct reference datum. More on this in Subsection 3.2.1.

As with the other modules, the AERMAP options are chosen through an input control file. The control file for this example is shown in the figure below.

```
LVTMAP - Notepad                                                                                    —   □   ×
File   Edit   View                                                                                              ⚙

CO STARTING                              *Control pathway, for selecting pre-processing options
   TITLEONE  AERMAP TEST-1 INPUT FILE    *Keyword determining the title of the project
   TITLETWO  TESTING - LOVETT            *Second title line for project title
   TERRHGTS  PROVIDED                    *Keyword determining whether heights are provided by the user or extracted from DEM/NED data
   RUNORNOT  RUN                         *Keyword determining whether the program should execute a full run or just a diagnostic run
   DATATYPE  DEM1                        *The datatype of the raw input files
   DATAFILE  HART-W.DEM                  *DEM raw data file name
   DATAFILE  SCRAN-E.DEM                 *DEM raw data file name
                                         *DOMAINXY decides the modeling domain in UTM-coordinates
   DOMAINXY  581000.0 4567000.0 18 588000.0 4572000.0 18
                                         *ANCHORXY decides the point of reference for the receptor- and source locations
   ANCHORXY  0.0       0.0      580000 4500000 18 2
CO FINISHED                              *"CO FINISHED" indicates that the options for the CO pathway are finalized

RE STARTING                              *Pathway for determining the receptor options
RE DISCCART         3500.    67750.    242.    *"DISCCART" indicates that the receptor location is given in cartesian coordinates
RE DISCCART         3600.    69700.    320.
RE DISCCART         4520.    69780.    293.
RE DISCCART         5500.    70450.    232.
RE DISCCART         4780.    70700.    323.
RE DISCCART         5110.    70850.    320.
RE DISCCART         5810.    70900.    250.
RE DISCCART         5860.    71340.    168.
RE DISCCART         6250.    71070.    274.
RE DISCCART         6930.    71300.    152.
RE DISCCART         7870.    69130.     27.
RE FINISHED                              *"RE FINISHED" indicates that the options for the RE pathway are finalized

OU STARTING                              *Pathway for determining the output options
OU RECEPTOR  LVTMAP.REC                  *Filename of the output file
OU FINISHED                              *"OU FINISHED" indicates that the options for the OU pathway are finalized

Ln 31, Col 71                                                    100%        Windows (CRLF)        UTF-8
```

Figure 2.6.1: Input file for AERMAP with explanations for each keyword.

For this case, there are two topographical input files, namely `HART-W.DEM` and `SCRAN-E.DEM`. To avoid AERMAP processing all of the data in the files, *DOMAINXY* can be used to define the domain of which the user wants data to be processed. The units can be in longitude/latitude (if *DOMAINLL* is used instead of *DOMAINXY*) or in UTM-coordinates (for *DOMAINXY*). The format (of *DOMAINXY*) is, from left to right: Easting start coordinate, Northing start coordinate, Easting end coordinate, Northing end coordinate and UTM zone for the most north eastern corner of the domain.

The *ANCHORXY* option assigns the reference point for receptor- and source locations in AERMAP. The reference point is assigned in UTM-coordinates, where the two first inputs determine the coordinates of the reference point in the reference space. The coordinates are in this case `0.0` (UTM Easting) and `0.0` (UTM Northing), meaning that the reference point is in origo of the reference space. The next parameters give the coordinates of origo of the reference space relative to the real world. This is given in three parameters, being the UTM Easting coordinate, UTM Northing coordinate and UTM zone, respectively.

The following pathway, *RE*, decides receptor locations. The receptor locations are assigned relative to the reference point defined by *ANCHORXY*. The *DISCCART*

33

keyword denotes that the location is given in cartesian coordinates in meters from origo of the reference space. Three parameters are given to assign the receptor location, namely the x-coordinates, y-coordinates and z-coordinates (in meters), respectively. The user has a variety of options in determining receptor locations. These are described in detail in the AERMAP user's guide [43].

AERMAP is run in much the same manner as of AERMET. Firstly, enter the correct folder containing all the relevant files in the command prompt. Then, execute the following command:

```
aermap LVTMAP.INP
```

A successful run will generate 4 `.OUT` files, and 1 `.REC` file. The `.REC` file will be used as input for AERMOD. This file contains receptor locations and calculated receptor height scales. The `.OUT` files contain various information about the run.

2.7 AERMOD

AERMOD uses the data processed by AERMET and AERMAP, in addition to emission source data and user-defined output options to produce concentration profiles for the modeling domain.

In this example, the output files from AERMAP and AERMET are `LVTMAP.REC`, generated by AERMAP, and `LOVETT.SFC` and `LOVETT.PFL`, generated by AERMET. These should be in the same folder as the AERMOD executable. Alternatively, the user can include the location of the files as inputs when referencing to them in the AERMOD input file. Additionally, a file containing hourly emission data, `LVTHEMIS.DAT`, and an event file, `lovett_evt.INP`, are used as inputs.

The AERMOD input file for the test case is shown in the figure below.

File   Edit   View

```
CO STARTING                                                 *Pathway for selecting the modeling options
   TITLEONE  AERMOD Test Case - Lovett Complex Terrain Study *Title of the model run
   MODELOPT  CONC DFAULT                                     *Keyword determining determining the overall options of the run
   AVERTIME  1 3 24 PERIOD                                   *The averaging periods to be calculated for the run
   POLLUTID  SO2                                             *Keyword denoting the pollutant to be modeled
   RUNORNOT  RUN                                             *Keyword determining whether the program should execute a full run or just a diagnostic run
   EVENTFIL  lovett_evt.inp                                  *File name of file containing event data
   ERRORFIL  LOVETT_ERRORS.OUT                               *Keyword determining the filename of the error output file
CO FINISHED                                                 *"CO FINISHED" denotes that the options for the CO pathway are finalized

SO STARTING                                                 *Pathway for determining the emission source options
   LOCATION  STK4N5  POINT  5510.0   67960.0   1.8           *Location of the emission source
** Point Source       QS      HS     TS     VS    DS
** Parameters:        -----   ----   ----   ----  ---
   SRCPARAM  STK4N5  312.6  145.    382.  23.1  4.5          *Keyword for determining the source parameters
   HOUREMIS  LVTHEMIS.DAT STK4N5                             *The file name of the file containing emission data for source group "STK4N5"
   SRCGROUP  ALL                                             *Keyword determining the grouping of emission sources
SO FINISHED                                                 *"SO FINISHED" denotes that the options for the SO pathway are finalized

RE STARTING                                                 *Pathway for determining the receptor options
   INCLUDED  LVTMAP.rec                                      *File name of the file containing the data generated by AERMAP
RE FINISHED                                                 *"RE FINISHED" denotes that the options for the RE pathway are finalized

ME STARTING                                                 *Pathway for determining the meteorology options
   SURFFILE  LOVETT.SFC                                      *The file name of the file containing the surface data generated by AERMET
   PROFFILE  LOVETT.PFL                                      *The file name of the file containing the profile data generated by AERMET
   SURFDATA  14735 1988 albany                               *Station number, year and location of where the surface data has been extracted
   UAIRDATA  14735 1988  albany                              *Station number, year and location of where the upper air data has been extracted
   SITEDATA  00000 1988 LOVETT                               *Station number, year and location of where the on-site data has been extracted
   STARTEND  88 01 01  88 12 31                              *The time period of meteorological data
   PROFBASE  1.8                                             *The base elevation for the potential temperature profile
ME FINISHED                                                 *"ME FINISHED" denotes that the options for the ME pathway are finalized

OU STARTING                                                 *Pathway for determining the output options
   RECTABLE  ALLAVE FIRST-SECOND                             *Generates a table containing the highest and second highest concentrations for
                                                             each receptor
   MAXTABLE  ALLAVE 400                                      *Generates a table with the 400 highest overall concentration values
   POSTFILE  24 all plot LOVETT_24H.PST                      *Generates an output file suitable for post-processing
   PLOTFILE  period all LOVETTANN.PLT                        *Generates an output file suitable for contour plots
   RANKFILE  1 100 LOVETT1.RNK                               *Generates a file of the top 100 concentration values for the 1-hour averaging periods
   RANKFILE  3 100 LOVETT3.RNK                               *Generates a file of the top 100 concentration values for the 3-hour averaging periods
   RANKFILE  24 100 LOVETT24.RNK                             *Generates a file of the top 100 concentration values for the 24-hour averaging periods
   SUMMFILE  LOVETT.SUM                                      *Generates an output file of high ranked concentration values
   PLOTFILE  1 ALL FIRST LOVETT_01H.PLT                      *Generates an output file suitable for post-processing
   POSTFILE  1 ALL PLOT LOVETT_01H.PST                       *Generates an output file suitable for contour plots
OU FINISHED                                                 *"OU FINISHED" denotes that the options for the OU pathway are finalized
```

Ln 47, Col 1   80%   Windows (CRLF)   UTF-8

Figure 2.7.1: AERMOD input file with explanations for each keyword/parameter.

The *CO* pathway is for determining the overall modeling options. The *MODELOPT* keyword determines the general class of options being used for the run. For this example, the default options are used (indicated by *DFAULT*), measuring the concentration of the pollutant (indicated by *CONC*). The default options denotes that the program will e.g., use elevated terrain algorithms, stack-tip downwash, and certain routines for missing data and calm winds. The default option is recommended for any regulatory assessment by the EPA [35]. For this example, the case includes an event file, `lovett_evt.INP`. Event files can be included to add the influence of specific events, for instance, industry malfunctions causing increased leaking of pollutants for a certain time interval. The event file contains data about the event, and this data will be used in the calculations of the concentration profile.

The *AVERTIME* keyword determines the averaging periods for the model run. In this case, the executable will calculate short-term averages for every 1-, 3-, and 24 hours. The parameter *PERIOD* indicates that an average of the entire data period also will

be calculated. Alternatively, the user can choose to have monthly and/or annual averaging periods, by the *MONTHLY* and *ANNUAL* parameters. The *POLLUTID* keyword contains the pollutant to be modeled. Certain values of the *POLLUTID* keyword can influence the run. This is described in more detail in the AERMOD user's guide [35].

The next pathway is the *SO* pathway, where the user determines the source options. The first keyword, *LOCATION* gives the name, source type and location of the emission source. The location is given in meters (in the order x, y, z) relative to the reference point given by the *ANCHORXY* option in AERMAP. The *SRCPARAM* keyword gives the characteristics of an emission source group (in this case *STK4N5*). The parameters are, in order from left to right: source group name, emission rate [g/s], stack height (above ground, not sea level) [m], stack exit temperature [K], stack exit velocity [m/s] and stack diameter [m]. The next keyword, *HOUREMIS*, extracts emission data from the *LVTHEMIS.DAT* file. From this file, data about the emission rate, stack exit temperature and stack exit velocity is extracted and used for the emission source group specified in the next column (*STK4N5*). When hourly emission data is included, this data will be used in place of the parameters given as input for the *SRCPARAM* keyword. The final keyword of the *SO* pathway, *SRCGROUP*, decides the grouping of emission sources. This allows for separation of sources in output options. For this case, the parameter *ALL* is assigned to the *SRCGROUP* keyword, meaning that all the emission sources are contained in a single group.

The next pathway is the receptor pathway. The receptor options were dealt with by the AERMAP pre-processor, meaning the only input needed here is the `.REC` file produced by AERMAP.

The *ME* pathway deals with the meteorological options for the run. The most important inputs are the meteorological profile- and surface files, which were generated earlier by AERMET. Additionally, information about the location and period of these measurements are included in the next rows. The final keyword is *PROFBASE*, which is the base elevation used for calculating the potential temperature profile. This elevation should correspond with the height of the primary meteorological tower [35].

The last pathway is the *OU* pathway, which decide the output options for the run. The first keyword, *RECTABLE*, generates a table showing the highest and second highest (as indicated by *FIRST-SECOND*) concentration values obtained for all the averaging periods (as indicated by *ALLAVE*). The *MAXTABLE* keyword generates a table containing a table with the highest overall concentration values. *MAXTABLE* takes in averaging period and number of concentration values to be ranked as inputs.

The tables of *RECTABLE* and *MAXTABLE* are displayed in the `.OUT` file.

The *POSTFILE* keyword generates an output file containing raw results convenient for post-processing. *POSTFILE* takes in, from left to right, averaging period, receptor group, format and output file name. *PLOTFILE* generates files specifically made for creating contour plots with graphical post-processing software. *PLOTFILE* takes in the averaging period, receptor group and file name. The *RANKFILE* keyword generates output files ranking the top concentration values. *RANKFILE* takes in the averaging period, the number of concentrations to be ranked and the output file name as inputs. *SUMMFILE* generates a file containing a summary of the run and the highest concentration values.

Before running AERMOD, make sure that all the necessary files discussed earlier are at the correct location. Also, make sure none of the output files to be generated during the run are already in the folder of AERMOD, as this can cause problems. Then, when the input file is ready, type this in the command prompt and press enter:

```
aermod lovett.inp
```

If setup correctly, the command prompt will indicate that the program is running. After a successful run, output files corresponding to that of the output options will be generated. Additionally, an error file and a general output file, showing a summary of the run and its options, will be generated.

2.7.1 AERPLOT

After AERMOD has calculated the concentration values, it is time to review the results. This is most conveniently done graphically, which is why AERPLOT has been developed. AERPLOT takes the `.PLT` or `.PST` files generated by AERMOD as inputs, and showcases the results in Google Earth Pro.

AERPLOT should be in the same folder as AERMOD, as it uses the AERMOD input file and one of the `.PLT` or `.PST` files produced by AERMOD as inputs. The program is run on the command prompt and has an input text file for adjusting the options of the run, much like the other executables. The main difference between AERPLOT and the other modules, is in the format of the input file.

The input file is named `aerplot.INP`, and contains instructions and adjustable keywords for the users to insert their inputs. From the input file, the user can choose the files to be post-processed, how these results should be displayed, and the location of

the modeling domain.

In this example, the data from the `LOVETTANN.PLT` file will be displayed using AER-PLOT. To do this, one has to enter the input file of AERPLOT. From there, the user has to find the keyword `PlotFileName`, and type:

```
PlotFileName=lovettann.plt
```

This makes AERPLOT recognize `lovettann.PLT` as the file to be post-processed. Just beneath the `PlotFileName` variable, there is a keyword called `SourceDisplayInputFileName`. This keyword takes in the AERMOD input file of the run to be post-processed. Next step is therefore to type in the name of the AERMOD input file used for the AERMOD run:

```
SourceDisplayInputFileName=lovett.inp
```

Now, AERPLOT knows which data to post-process, but it does not know the location of the modeling domain. To give the correct coordinates, the user should find the reference point, earlier defined by the *ANCHORXY* keyword. These coordinates can for instance be found in the `LVTMAP.REC` file. The coordinates of the reference point are inputs for the `easting`, `northing` and `utmZone` keywords, found near the top of the AERPLOT input file. The inputs for the location options should look like this:

```
easting=580000
northing=4500000
utmZone=18
inNorthernHemisphere=true
```

The `inNorthernHemisphere` keyword is assigned the value `true`, as the location of the modeling domain is on the northern hemisphere. When this is done, AERPLOT is ready to run. This is simply done by typing `AERPLOT` and pressing enter in the command prompt. As earlier, the user needs to be in the correct directory in the command prompt, this being the directory containing AERPLOT and the necessary files for plotting.

When run, the command prompt will display a summary of the options of the run and Google Earth Pro will be opened. In the Google Earth Pro interface, the receptors will be shown, being color coded as an indicator of their concentration values, see Figure 2.7.2. If the user clicks on the receptor points, information about the receptor will pop up.
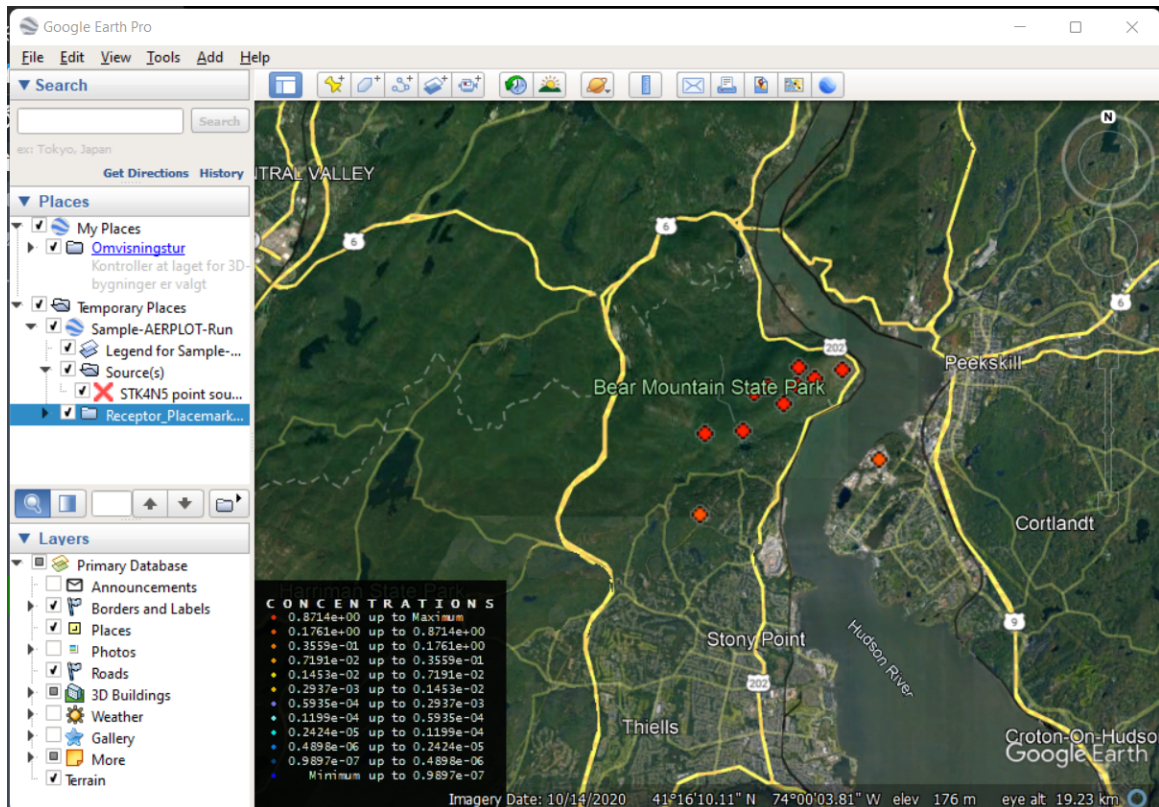
Figure 2.7.2: Post-processed results from AERPLOT for the Lovett test case.

Note that the emission source is misplaced when put into AERPLOT. This may be caused by the source location being unaffected by the location options input into AERPLOT. A possible fix is to manually change the location of the source in Google Earth. This is done by right-clicking the source in the "Places" tab in Google Earth, and pressing `Properties`. From there, the user can manually assign a new location for the source.

The user has a wide variety of post-processing options. In addition to the receptor points shown earlier, the options in the AERPLOT input file allows for showing contours and gradients as well. In addition, all the files of the types `.PST` and `.PLT` can be displayed, giving the user many options for post-processing.

3 Modeling the emissions of Hydro Aluminium Høyanger

The aluminum industry has for long been under strict supervision in terms of emission release. In Norway, several measures are done to keep the emissions to a minimum. The implementation of dry- and wet scrubbers has been an efficient way of dealing with most emissions, but some emissions still escape the scrubbers during operational routines. The resulting emissions to air are routinely measured, both in masses and characteristics, but the dispersion of these are rarely quantified. In context of increased awareness of the harms of the escaped pollutants, governments are enforcing stricter regulations in emission control and -monitoring. It is therefore of interest to be able to quantify the dispersion of the emissions, in addition to their masses and characteristics.

In this thesis, the dispersion of emissions from Hydro Aluminium Høyanger throughout 2021 will be modeled by the use of AERMOD. This modeling case will include a factorial design experiment, testing the influence of changing certain parameters of the modeling case. As dispersion modeling is heavily dependent on the conditions of the modeling domain, these will be described in the first section. Also, a walkthrough of how the applied data was acquired and reformatted, followed by the modeling approach, will be given. The results will be showcased after the modeling approach, and these will be discussed in terms of their validity and correlation with theory.

3.1 Case description

The challenges of dispersion modeling are highly circumstantial, as aspects like the atmospheric properties, plume characteristics, and location-dependent factors all influence the modeling results. The nature of these aspects decide how challenging the modeling case will be in regards of getting representative results. In general, conditions like low wind speeds, steep terrain and complex meteorological phenomena can be problematic to model accurately. In other words, the conditions of the modeling case are detrimental for the expected accuracy of the results. To give the reader insight in the complexity of the case in this thesis, this section will detail the modeling conditions of the plant and how AERMOD can remedy these conditions. How the modeling cases are performed, is explained in Section 3.3.

Hydro Aluminium Høyanger is located in Høyanger, which is in a fjord on the west side of Norway. The location is shown in the figure below.
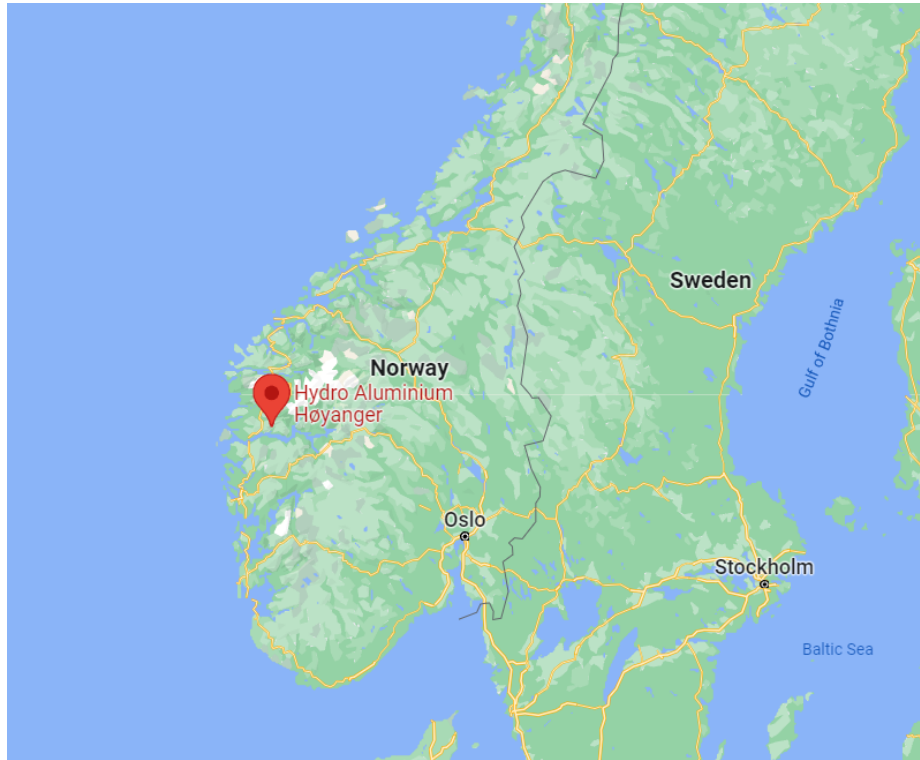
Figure 3.1.1: Hydro Aluminium Høyanger's location. The picture taken from Google Maps [8].

The plant is located at the coast of Høyanger, see Figure 3.1.2. The figure includes the placement of objects deemed relevant for the modeling case.

Figure 3.1.2: Close-up picture of Hydro Aluminium Høyanger [9]. The figure includes the placement of the rooftop pipes of hall A and B, the wet- and dry scrubber and the silos.

All Norwegian aluminum plants contain wet- and dry scrubbers which essentially clean most of the off-gases coming from the pots. The dry scrubbers have emissions to air, while the wet scrubbers have emissions to air and to the ocean. The pipes of hall A and hall B are placed on the top of the roof of the electrolysis halls. These are from here on out referred to as "rooftop pipes". The emissions that escape the cleaning process are emitted through these rooftop pipes and pollute the atmosphere. Most of these emissions are generated by operational routines like anode changes and metal tapping [44]. For this modeling case, the emissions that originate from the electrolysis, these being emitted from the dry- and wet scrubber and rooftop pipes, will be accounted for. In other words, the rooftop pipes, the dry scrubber and the wet scrubber will be the emission sources. The plant as a whole has other emission sources as well, for instance the anode rodding- and butt cleaning facilities. These emissions do not stem from the electrolysis, and will be omitted from this case.

There are 18 rooftop pipes, 9 for hall A and 9 for hall B. Operational routines for hall A and B are deemed identical, meaning there will not be any differentiation between these in the modeling case. The schematic below shows the dimensions of the halls and the dimensions of the pipes.
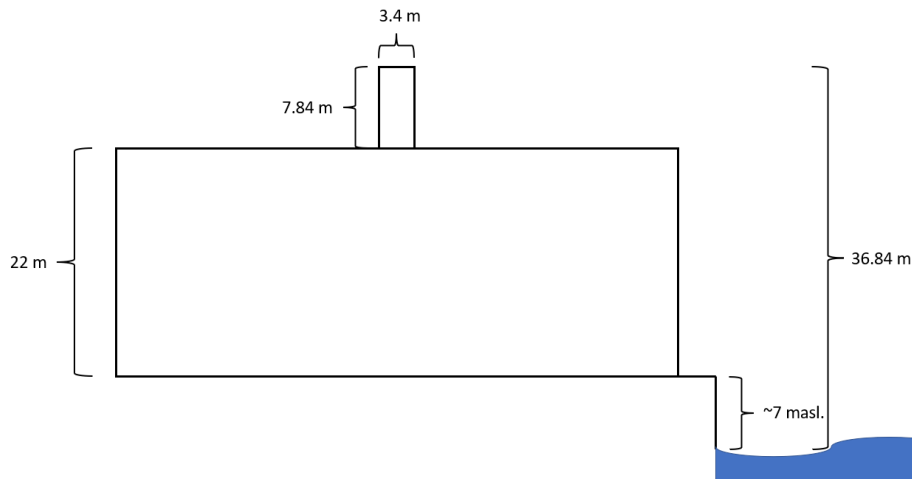
Figure 3.1.3: A schematic of the halls and rooftop pipes. The hall is assumed to be about 7 meters above sea level. The dimensions are extracted from [10].

The dimensions from Figure 3.1.3 give the rooftop pipes an approximate height of 36.84 meters above sea level, 29.84 meters above ground, and a diameter of 3.4 meters [10]. The dimensions of the wet- and dry scrubber are for the most part unknown. The wet scrubber has an inside diameter of about 4.5 meters [50], and the height is assumed to be 56.8 meters above sea level. The dry scrubber is assumed to be 46.8 meters above sea level, with an assumed diameter of 4 meters.

The dimensions and locations of the emission sources are used as inputs in AERMOD. Additional source characteristics, i.e., the stack exit temperature, stack exit velocity and emission rate are also important. The emission rate is continually measured, while the stack exit temperature and -velocity are estimated using previous measurements. The data, and how it was obtained, are given in Subsection 3.2.3.

In addition to being emission sources, the dry- and wet scrubber, in addition to the silos, are the most prominent buildings in the area, eligible to cause building downwash effects. Their placements are shown in Figure 3.1.2. The figures below show close-up pictures of the silos, dry scrubber and wet scrubber, respectively. The pictures are taken from the roof of the electrolysis halls.

43

Figure 3.1.4: Silos at Hydro Aluminium Høyanger.

Figure 3.1.5: The dry scrubber of Hydro Aluminium Høyanger.

Figure 3.1.6: The wet scrubber of Hydro Aluminium Høyanger.

The dimensions and locations of these buildings can be used as input in BPIPPRM or AERMOD to account for building downwash effects. As both the dry scrubber and wet scrubber are relatively small, and the silos are on a lower level than the emission sources, the building downwash effects caused by these are deemed to be minor. As the area is populated, other buildings are present as well. These are however less prominent, and will be deemed insignificant in regards of building downwash effects.

The following figures show the surrounding landscape of the aluminum plant in Høyanger. The pictures are taken in different directions from the roof of the plant, where the rooftop pipes of the electrolysis halls are located. Following the pictures is a figure showing a topographical map of the area.

Figure 3.1.7: North-east side of the plant.

Figure 3.1.8: East side of the plant.

Figure 3.1.9: South-east side of the plant.

Figure 3.1.10: South-west side of the plant.

Figure 3.1.11: West side of the plant.
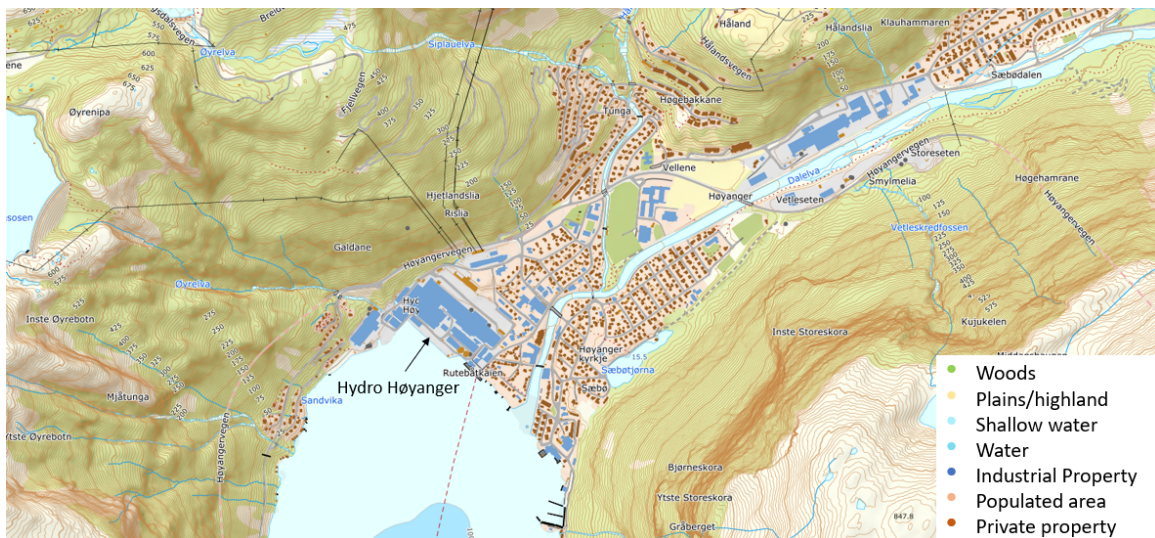
Figure 3.1.12: A topographical map of Høyanger [11]. The numbers indicate the height of the terrain in meters. The map includes a legend explaining the different surface characteristics.

The terrain is significantly steep, which can cause emissions to be "trapped" inside of the fjords. This can cause significant emission concentrations at the hillsides. More detailed topographical data is gathered from DEM/GeoTiff files from e.g., Hoydedata.no [51]. The DEM/GeoTiff files are used as inputs for AERMAP which will account for the topographical effects.

The map in Figure 3.1.12 includes surface characteristics, which is used to determine the surface parameters of the area. For this purpose, a circle with a 2 km radius is drawn surrounding the plant. The circle is divided into arcs representing different surface characteristics, see Figure 3.1.13.
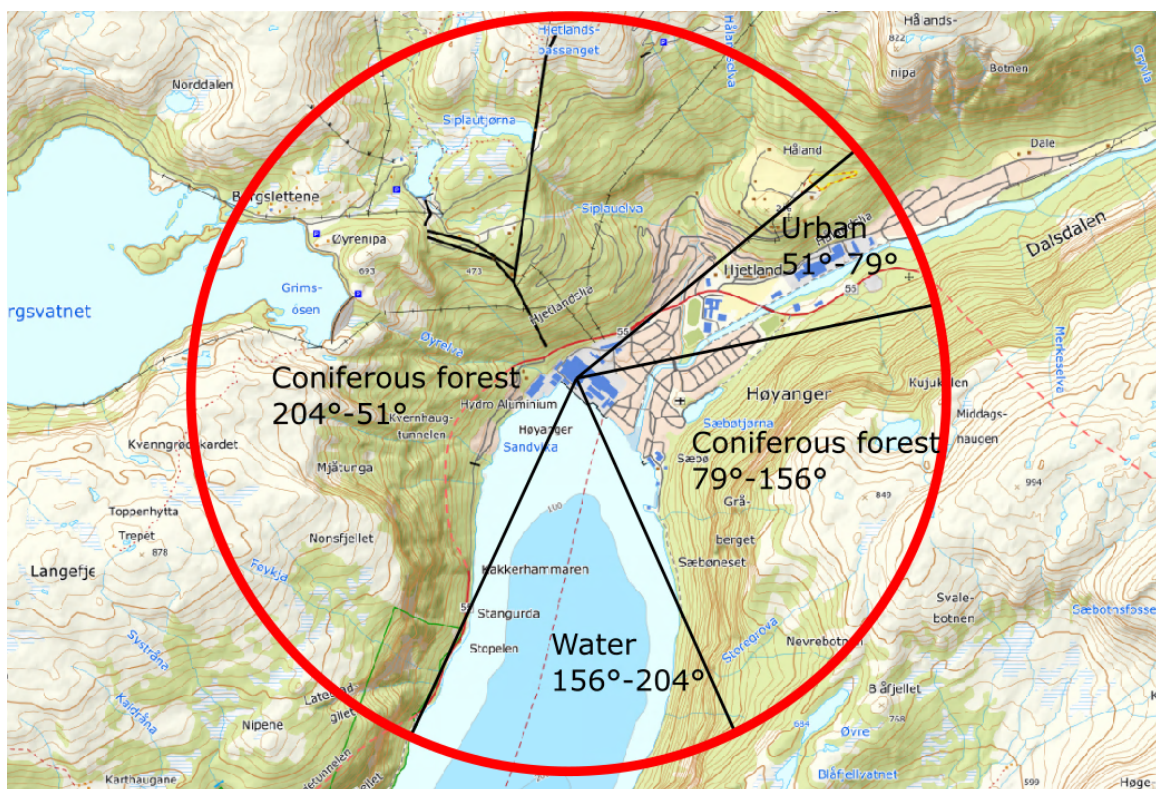
Figure 3.1.13: Division of zones based on surface characteristics in a 2 km radius of the emission source. North is 0°, increasing with every degree going clockwise. This corresponds to the coordinate system used to determine surface characteristics in AERMET. The map is extracted from Norgeskart.no [11].

For each of the surface characteristics, the surface parameters can be determined from tables found in the AERMET user's guide [7]. These surface parameters will be inputs in AERMET. The coordinate system in Figure 3.1.13 corresponds to the

48

coordinate system used to determine sections in AERMET. The surface characteristics also influence the deposition properties of the pollutants, which will be explained later in the section.

Populated areas tend to experience a higher temperature than their surroundings. This is due to man-made structures like pavements and buildings absorbing more heat from the sun than non-urban landscapes [52]. Additionally, urban areas have several heat-generating activities, enhancing the effect [52]. The phenomena is referred to as the "urban heat island" effect.

As Høyanger is a fairly small town, with a population below 4000 citizens [53], the urban heat island effect is deemed to be small. The town is however somewhat industrial for its size, which may indicate a prominent effect relative to its size. AERMOD can estimate urban heat island effects by using the population of the modeling domain as input [35].

The pollutants that will be modeled are gaseous SO_2 and HF, and dust. Differentiating between the pollutants can be important if these have different behaviors when entering the atmosphere, as this behavior further influences the dispersion of the pollutants.

The movement of pollutants in the atmosphere is governed by transport, diffusion and deposition [54]. Additionally, chemical reactions can indirectly influence the movement of pollutants. Transport is dependent on wind speed- and direction, while diffusion is dependent on local turbulence [54]. In other words, both of these mechanisms are independent of the pollutant. Deposition and chemical reactions, however, differs from pollutant to pollutant.

Deposition is a general term for mechanisms that makes the pollutant flow to the ground. Commonly, the term is divided into dry- and wet deposition. Dry deposition involves species traveling to the ground and depositing due to gravitational settling and their affinity to the surface [55]. Wet deposition is when pollutants deposit onto water and wash out during precipitation, and is mainly dependent on the pollutant's solubility in water.

The deposition mechanisms of HF are fairly hard to determine. On one hand, the gas has infinite solubility in water [56], but it seems that the gas' ability to deposit in atmospheric water is low in practice [56]. Studies have found that the depositing of HF requires a significant amount of water, and moreover that vapor-aerosol clouds produced by HF-releases may inhibit the depositing of HF [56]. Additionally, the

49

depositing is limited by the acidity of the droplets, essentially making HF compete against other (wet) depositing gases, like SO_2 [56]. HF's susceptibility to dry deposition is relatively large compared to other gases [56]. HF is considered as chemically inert for low concentrations (<10ppmv) [56].

Tabulated values of surface resistance from parametric studies [57] indicate that SO_2 has relatively little susceptibility to dry deposition, although this is largely dependent on the humidity of the surface [58]. SO_2, being highly soluble in water, is susceptible to wet deposition. SO_2 can be considered chemically inert for low concentrations (<10ppmv) [17], but is fairly reactive for higher concentrations [59, 60]. The pollutant is known to react to higher order sulfur oxides which can contribute to particulate matter pollution [60].

For particulate matter, dry deposition is heavily dependent on the size distribution and density of the agglomerate [57, 61]. This is since these properties determine the weight of the individual particles, and heavier particles more easily flow towards the ground. Particulate matter is susceptible to wet deposition, as it tends to get caught by precipitation and thus travel towards the surface. This effect is also dependent on the size distribution and density of the agglomerate. Measured particle size distribution of the particulate matter at Høyanger from 2010 is shown in the table below [4]:

Table 3.1.1: Measured particle size distribution at Hydro Høyanger from 2010 [4].

Particle sizes [μm]	0-1	1-10.9	10.9-21.2	21.2-33.5	33.5-48.5	48.5-66.1	66.1-100
Fraction	0.013	0.087	0.15	0.25	0.25	0.15	0.1

AERMOD calculates the rate of dry- and wet deposition for gaseous species by inclusion of the specie's diffusivity in air, diffusivity in water, cuticular resistance to uptake by lipids in individual leaves and Henry's law constants [35]. Wet deposition calculations can require one or more of the following surface weather data; the precipitation rate; precipitation code; relative humidity; surface pressure; and cloud cover [35]. Additionally, AERMOD can account for the substances' affinity to the surface, if the user has defined the surface characteristics [35, 57]. The user can choose to adjust the surface characteristics from one time-interval to another, to account for seasonal variations [35]. For HF, the algorithm considers the pollutant to be heavily governed by wet deposition [57], despite its wet depositing behavior in practice being fairly unknown. Generally, the gas deposition algorithms have not been thoroughly verified, and are therefore not regulatory options for AERMOD [35].

The dry- and wet deposition of particulate matter can be accounted for by two methods, depending on the size distribution of the agglomerate, and if this distribution is known. The user can include particle densities and size distributions for deposition calculations. For particulate matter, the deposition algorithms are regulatory options. The deposition calculations for both gaseous and particulate species are mainly based on data from the deposition parameterizations collected by Wesely et. al. [57].

Capabilities for modeling chemical reactions is limited in AERMOD. The model is able to account for exponential decay [17, 35]. For SO_2, the model can include a 4-hour half life to account for chemical reactions.

Weather characteristics is a fundamental factor for the properties of the atmosphere, also making it a detrimental factor for determining the dispersion of emissions. Most important is the wind, as this is the main mechanism for carrying the pollutants. The fjord landscape surrounding the plant can be expected to in part limit the wind-directions experienced at the plant. Therefore, the wind-directions are expected to be mostly in the southern- or northwestern directions of the plant. The annual average wind speed is reported to be about 7.0 m/s 50 meters above sea level [62].

In January until mid-March, the average temperatures are below 0° C, being around -3° C for most of these months [63]. The temperatures are generally stable throughout the day for these months [64]. The average temperatures steadily increase from March, until reaching the summer (June-August) temperatures , which average at about 14° C [63]. The temperature variances from night and day and from day to day increases towards the warmer months, having an about 10° C difference between night and day in the summer. The temperature steadily decreases from August, and starts falling below 0° C in December [63].

The area is high in precipitation, having rainy days for about half of the year [63]. Due to the high amount of precipitation and cold weather, snow can be expected, especially from December until march [64]. Snowy days can also occur in April and May [64], due to the cold nights.

In short, the weather is generally cold and windy, with much precipitation and high variances between night and day towards- and during the summer. During summer days, the sun heating up the surface of the area can cause large temperature gradients when the colder nights arrive, which can cause complexities for the modeling case. Windy environments are generally welcomed when performing a modeling case, as strong wind conditions are generally more stable than calm wind conditions [13].

The amount of precipitation has a high influence on the wet deposition mechanisms of the pollutants, especially when it snows. The high amount of precipitation also indirectly influences the dry deposition of pollutants, as some pollutants, like SO_2, have a higher affinity to humid surfaces [58].

AERMET takes in hourly weather characteristics for calculations of PBL parameters. These calculations can be quite extensive, accounting for most of the weather characteristics involved. This is however limited to the data the modeler is able to acquire and the weather data formats which are used for the modeling case. This will be discussed further in Subsection 3.2.2.

3.2   Data acquisition

AERMOD is most convenient for cases situated in the USA, as the tool relies on American formats and conventions for the topographical- and meteorological raw data. AERMOD's formats are mainly based on the typical formats issued by the governmental instances of USA, so that American users may implement this data directly.

This can pose a challenge for cases located outside of the USA, as other governments may have different formats and conventions for this data. If the formats of the relevant government are not compatible with AERMOD, this requires the user to reformat its raw data to formats compatible with the tool. The AERMOD user's guides provide detailed information about how to acquire data relevant for cases in USA. However, for cases outside of the USA, the sources of raw data may not be obvious for the user.

This section will show how the data for this case was acquired and reformatted, so that future users can learn to do the same. The origin of the emission data will also be included in this section.

3.2.1   Terrain data

Terrain data for Høyanger is readily available at Hoydedata.no. The user can search for the location where it wants to acquire data from in the search tab at the top of the web page. From here, the user can choose the area to download data from in the "Download" tab to the left. The approximate area where raw data was acquired from is shown in Figure 3.2.1.
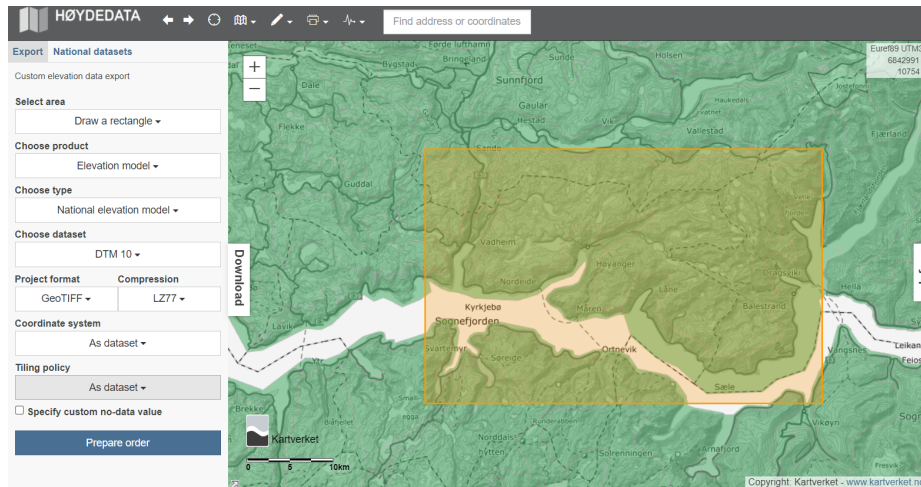
Figure 3.2.1: The approximate area where raw data was acquired from at Hoydedata.no. The figure also shows the options that were chosen for acquiring the data.

When acquiring data, it is important that it is in the right format. AERMAP accepts `.DEM` and GeoTiff (`.TIF`) files, and both of these can be found at Hoydedata. However, the files acquired from Hoydedata have an incompatible reference datum, meaning AERMAP won't accept these data directly. The reference datum is the convention for projecting the coordinates of the spheroid earth to a squared domain. The reference datum for the files acquired from Hoydedata is mainly EPSG 25833. To convert these files to a compatible reference datum, e.g., EPSG 4326 (also known as WGS84), the user has to use a reformatting tool. This is most conveniently done on GeoTiff files, which are acquired by choosing the options shown in Figure 3.2.1.

The GeoTiff file used in this case was converted by using QGIS [65], which is an open source software for analyzing, editing and viewing geospatial data. To convert the file, first open the file to be converted from the browser menu in QGIS, as seen in the figure below:
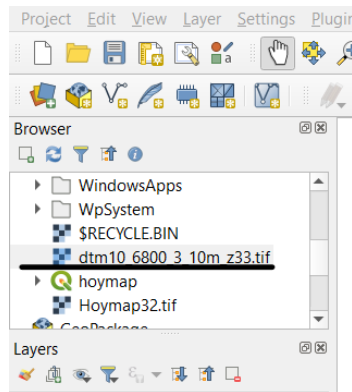
Figure 3.2.2: How to choose the file to be converted using QGIS.

When the file is open, one can see the unconverted image. To convert the image, go to `Raster` (found in the toolbar at the top)-> `Projections -> Warp (Reproject)....` A window containing reprojecting options will then pop up. The options chosen for converting the file in this modeling case are showcased in the figure below.
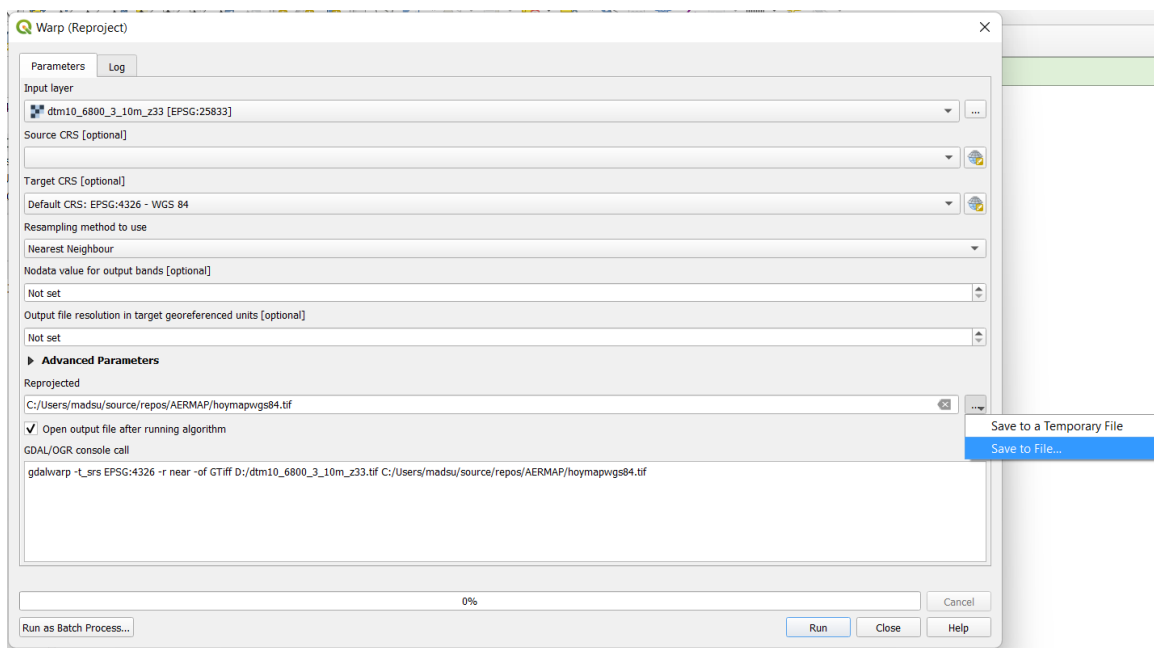
Figure 3.2.3: Options for converting a file to WGS84 using QGIS.

Make sure to change `Target CRS` to the wanted datum (in this case WGS84). Then, choose `Save to File` under the `Reprojected` options. Choose the file name and location of the converted GeoTiff file to be used by AERMAP. The remaining options

can be set to their default settings. Now, click run, and the converted file will be saved to the location chosen by the user after a short rendering time. The file is then ready for input into AERMAP.

3.2.2 Weather data

The weather data was acquired from Seklima.no [12]. Here, raw data from different weather stations can be acquired. For this case, the wind speed, wind direction, cloud ceiling height, temperature and cloud cover were acquired for all hours of 2021. This data originates from two weather stations, where the cloud ceiling height was acquired from Fana, and the remaining parameters were acquired from Flesland. Both of the Weather stations are located in Bergen, see Figure 3.2.4.

Figure 3.2.4: Locations of the weather stations where the raw data were gathered from (in blue) and the location of Høyanger (in red) [11].

The weather stations are about 112 km away from Høyanger. These stations were used

since the nearby stations of Høyanger were lacking the data needed for AERMET. Ideally, one would use on-site data gathered at the location of the plant. Alternatively, one could use modeled weather data, which is calculated weather data based on data gathered from nearby weather stations. In Norway, this data is stored at Thredds.met.no. Acquiring this data requires the user to use e.g., Python to extract the correct data. The Norwegian Meteorological Institute claimed that this could be a difficult and time-consuming process [66], and recommended to use raw data instead. Hence, raw data from Flesland and Fana was used as an example.

The raw data are given as Excel-files. AERMET does not accept these files as input data, so these need to be converted to another format. AERMET accepts a number of formats, but finding documentation on how these formats are structured, and which units they apply, can be challenging. After communicating with the EPA, a document explaining the different formats was given. This documentation can be found here, in appendix A [67]. This document was given to the author after all modeling cases were already performed. Up until then, the only format that there was found enough documentation on was the SCRAM format. The SCRAM format is essentially a reduced form of the more extensive CD-144 format [7]. This format only takes in wind speed and -directions, cloud ceiling heights, total cloud cover, opaque cloud cover and dry bulb temperature as parameters [67]. Parameters that are omitted from this format, like pressure, amount of precipitation and precipitation code, can be important for representative results. Thus, using more extensive formats, like SAMSON or CD-144, is recommended.

The reformatting process was done with a combination of formatting tools in Excel and Python scripts. Python was used to split and reformat the temporal values, while Excel was used for most of the remaining reformatting and unit conversions. The best way to reformat the data, is probably by using the "pandas" [68] package in Python, but this was not used in this case. The reformatted data was pasted into a notepad file, where the file was saved as a `.DAT` file. An excerpt of the final product is shown in Figure 3.2.5.
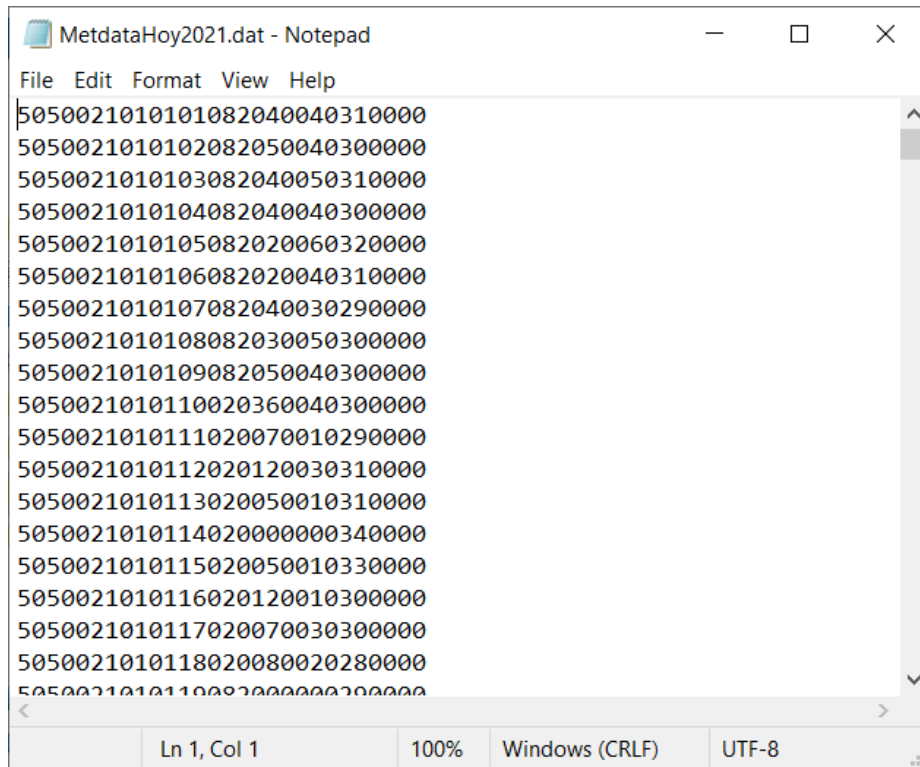
Figure 3.2.5: Excerpt of the SCRAM file used as surface raw data in AERMET.

The upper air radiosonde data were extracted from the NOAA/ESRL Radiosonde Database [69]. From there, the user can choose the time interval and location of the station from which the upper air data can be retrieved. For this modeling case, upper air data for all hours of 2021 were gathered through the Ny-Ålesund station located at Svalbard, 1915 km away from Høyanger. Other radiosonde stations are located closer to the plant, but these lacked data for 2021 through the database. The station did not provide data for June, July and August, meaning the modeling case did not include upper air data for these months. The data were also lacking some values for certain time-intervals, especially the wind speed and -directions for some elevations. The upper air data were readily implemented into AERMET in the FSL [70] format.

Upper air data can alternatively be extracted from The Norwegian Meteorological Institute's database [66], which seems to contain data from radiosonde stations located closer to the plant. This requires the user to extract the data in the same manner as for the surface data provided by Thredds.

3.2.3 Source data

For source data, the locations, elevations and stack diameters of the sources are needed. Additionally, the emission data, being the emission rate [g/s], stack exit temperature [K] and stack exit velocity [m/s] are needed. The data used for this case were based on data given by the industry.

The diameters and height above ground for the rooftop pipes were found from reports delivered by the industry [10]. The height of the ground relative to sea level was estimated to 7 meters. The diameter of the wet scrubber was found from a report delivered by the industry [50], while the elevation was estimated to be 20 meters above the rooftop pipes. The dry scrubber's diameter was estimated to 4.0 meters, while its elevation was estimated to be 10 meters above the rooftop pipes.

The emission rates are routinely measured, although somewhat sporadically for some measurements. For this case, some of the measurements were taken during abnormal circumstances. These are not necessarily representative for the emissions that actually go out of the plant. To remedy with these abnormalities, the average emission rate [g/s] for the whole modeling period was used as input for each pollutant, rather than hourly emission rates.

Measurements in the dry- and wet scrubber included the temperatures of the samples. These temperatures were averaged for the whole modeling period and was used as input for stack exit temperature for the wet- and dry scrubber. The temperature is not routinely measured in the rooftop pipes. Thus, a previously measured value from 2011 was used [10].

The normal volumetric flow rates of the rooftop pipes, wet scrubber and dry scrubber are routinely measured. The normal volumetric flow rate is a conversion of the actual volumetric flow rate. The normal volumetric flow rate is what the actual volumetric flow rate would be if it was under standard conditions. Standard conditions mean that there is a pressure of 1 atm ($1.013 \cdot 10^5$ Pa) and a temperature of 273.15° K[8]. The relationship between the normal volumetric flow rate and the volumetric flow rate can be found by use of the ideal gas law:

$$PV = nRT \rightarrow \dot{V} \cdot \frac{P}{T} = \dot{V}' \cdot \frac{1.013 \cdot 10^5}{273.15} \tag{3.2.1}$$

Where T is the temperature [K], V is the volume [m³], n is the amount of molecules [mol], R is the ideal gas constant (=8.314 J/(K·mol)), P is the pressure [Pa], $\dot{V}$ is

---

[8]The definitions of the standard conditions may vary.

the volumetric flow rate [m³/s] and $\dot{V}'$ is the normal volumetric flow rate [m³/s]. The equation assumes ideal gas law to be applicable. n and R are equal for both conditions.

For the calculation of the stack exit velocities, the normal flow rate was assumed to be equal to the volumetric flow rate. The stack exit velocities for the wet- and dry scrubber were estimated by dividing the normal flow rates by the area of the stacks:

$$\dot{V}' \approx \dot{V}$$
$$\dot{V} = v_{exit} \cdot A' \rightarrow v_{exit} = \frac{\dot{V}}{A'}$$

(3.2.2)

Where v_{exit} is the stack exit velocity [m/s] and A' is the area of the stack [m²]. This approach was used for finding the stack exit velocities of the wet- and dry scrubber. The stack exit velocity used for the rooftop pipes were found from a report by Håkon Skistad [10].

A summary of the data used for finding the necessary parameters for modeling and their uncertainties are shown in the table below. The standard deviations were found by using statistical tools provided by Excel.

Table 3.2.1: Summary of the averaged raw data and their uncertainties. * Indicates that the uncertainties are measurement uncertainties.

	Wet scrubber	Dry scrubber	Rooftop pipes
Normal flow rate [m³/h]	318145±6.50%	254430±7.55%	-
Temperature [K]	295.64±0.89%	358.14±3.17%	313.6±1.0K^*
Stack exit velocity [m/s]	-	-	5.3±3.96%
Emission rates [g/s]	Wet scrubber	Dry scrubber	Rooftop pipes
SO$_2$	1.760±5.61%	9.485±56.58%	0.100±40.89%
HF	0.008±62.05%	0.202±96.19%	0.910±282.87%
Particulate HF	-	0.012±293.06%	0.602±305.5%
Dust	-	0.026±328.52%	2.015±285.55%

All values, except for the temperature and the stack exit velocity of the rooftop pipes are averaged values for the whole year of 2021. The value and uncertainty of the stack exit velocity of the rooftop pipes is given by Håkon Skistad in his report [10]. The temperature and uncertainty of the rooftop pipes was found from the same report, where the uncertainty is a measurement uncertainty. The remaining uncertainties are standard deviations of the averaged raw data. The data of particulate matter consisted of particulate HF and general particulate matter. These data were added

together to represent all particulate matter for the model runs. Note that the standard deviations are exceedingly high for some of the emission rates. This is mainly due to some values referred to as "extra measurement" in the data sets, which generally were much higher than the regular measurements. This will be discussed further in Section 3.5.

The particle size distributions were based on measurements performed in July 2010 at Hydro Aluminium Høyanger [4] (see Table 3.1.1). This data did not include particle densities, so this was estimated to 1 g/cm^3, which has been used in earlier model experiments [71].

3.3   Modeling approach

There are several ways of approaching a modeling case. Varieties can occur in which data are used, and how these data are treated before they are implemented. Additionally, AERMOD offers a wide selection of options to choose from. Some options are not yet verified by the EPA. The options that are verified are called regulatory options.

This thesis contains three regulatory runs, one for each of the pollutants. Furthermore, the thesis includes a factorial design experiment, which contains some options that are non-regulatory. This section will describe the approaches for each of these model runs.

3.3.1   Regulatory modeling cases

Regulatory runs for the dispersion of the gaseous SO$_2$- and HF emissions in addition to the dispersion of particulate matter were performed for the whole year of 2021. The runs being "regulatory" implies that only regulatory options, these being verified by the EPA, were used. The overall treatment of the plumes for the regulatory runs are corresponding to the descriptions given in Section 2.4.1 and Section 2.3. These runs did not include any of the optional pre-processors. The runs being regulatory excludes e.g., calculations of deposition for the gaseous substances, as these options are not regulatory. Dry deposition calculations were included for particulate matter.

For source characteristics, the location (including the elevation), stack exit velocity of pollutants, stack exit temperature and stack diameter were included. Their values are shown in the tables below[9]:

---

[9]The stack exit velocity for the dry scrubber was calculated based on an area of 12.39 m^2. In reality this area should be 12.57 m^2, as this is the area of a 4 meter diameter circle. This means that the actual stack exit velocity of the dry scrubber should have been 5.6 m/s and not 5.7 m/s (<2 % difference). The significance of this is deemed negligible compared to other uncertainties.

Table 3.3.1: Values of source characteristics which are shared between pollutants. The stack elevations are relative to sea level, their elevations relative to the ground are assumed to be 7 meters lower. * Indicates that the given value is undocumented, and therefore estimated.

Source	Stack elevation [m]	Stack diameter [m]	Stack exit velocity [m/s]	Exit temperature [K]
Rooftop pipes	36.8	3.4	5.3±3.96%	313.6±1°K
Dry scrubber	46.8*	4.0*	5.7*±7.55%	358.1±3.17%
Wet scrubber	56.8*	4.5	5.6±6.50%	295.6±0.89%

Table 3.3.2: The emission rates of the sources for the different species. * The data used for emission rates of particulate matter is a combination of data for particulate HF and general particulate matter. The standard deviations for these data are found in Table 3.2.1.

Emission rates [g/s]			
Source	SO_2	HF	Particulate matter
Rooftop pipes	0.100±40.89%	0.910±282.87%	2.62*
Dry scrubber	9.485±56.58%	0.202±96.19%	0.040*
Wet scrubber	1.760±5.61%	0.008±62.05%	Not provided

All values were based on averaged data for the whole year of 2021. Each emission source was described as a point source, one accounting for all of the rooftop pipes on the roof of the electrolysis, one for the dry scrubber and one for the wet scrubber. The rooftop pipes were approximated to a single source, as these were in close proximity to each other. No options for urban sources were included. Half-life decay of the pollutants was not accounted for. For particulate matter, data about the size distribution (those shown in Table 3.1.1) were included for deposition calculations.

The surface weather data included wind direction, wind speed, cloud ceiling height, temperature and cloud cover. Surface characteristics for calculations of the albedo, Bowen ratio and surface roughness length for the modeling domain (corresponding to the surface domains in Figure 3.1.13) were included. The values of these parameters were estimated through the parameterization described in chapter 4.7.8 in the AERMET user's guide [7].

Upper air data was extracted for all months except for June, July and August. The data were lacking some values for certain elevations and time-intervals, where wind speeds- and directions were the most lacking parameters.

Topographical data on a 10 meter resolution were used for calculating terrain influences and receptor heights. The receptors were placed at circles 50-, 100-, 200-, 500-

and 1000 meters away from the "rooftop pipes" emission source. Each circle contained 36 receptor points, one for each 10° of the circle. The results will be showcased as a plot of these receptors on a map of Høyanger, each receptor showing the average concentration at the receptor throughout the year.

3.3.2   Factorial design experiments

To study the influence of changing parameters and modeling approach for the case, a factorial design experiment [72, 73] was performed for each pollutant. This study gives insight in how parameters interact with each other, as well as how they individually affect the results of the modeling.

Two main results will emerge from such a study, these being effects and interactions. An effect is how changing a single parameter will affect the results of the study. An interaction is a measure of how the parameters' effects change when several parameters are coupled together.

Typically, the parameters have several levels of values. Here, each parameter, being A, B, C and D, will have two values. These will be referred to as their standard values, and their non-standard values. The results of the studies will be given as y, where the subscript of y denotes which parameters are turned to their non-standard values. For instance, y_A is the result of the study where parameter A (and only A) is turned to its non-standard value, and y_{AB} is the result of the study where both A and B are turned to their non-standard values. The calculated effects of turning parameters A, B, C, and D to their non-standard values are given as A, B, C and D, respectively. The interactions between parameters are given as a coupling of the parameters to be evaluated. For instance, AB will be the calculated interaction between parameters A and B.

Calculations of effects and interactions were done by comparison with a standard case. Here, the standard case will be the case where all parameters are turned to their standard values, being the case most comparable to the regulatory run. The standard case is denoted by "-".

Prior to finding the effects and interactions, all results are divided by the result of the standard case to normalize the results. Thus, all effects and interactions found will be a relative fraction compared to the standard case. For instance, a value of 0.9 for the calculated effect or interaction indicates that the given effect or interaction causes a 90 % increase of the results compared to the standard case. Correspondingly, a calculated value of -0.9 indicates that the effect or interaction causes a 90 % decrease of the results compared to the standard case.

The effect of turning a single parameter to its non-standard value, in this case A, is found by the difference between the result of the case where A is turned to its non-standard value, and the result of the standard case:

$$A = y'_A - y'_-$$ (3.3.1)

Where A is the calculated effect of turning parameter A to its non-standard value, y'_A is the normalized result gained when parameter A is turned to its non-standard value, and y'_- is the normalized result of the standard case. As y'_- is normalized by dividing by itself, its value is equal to unity.

The interactions are a measure of how two or more parameters interact with one another, excluding the parameters' individual effects. To find the value of an interaction, each individual effect of the parameters involved, in addition to the normalized standard case, are subtracted from the result of the case where all the involved parameters are turned to their non-standard values. In Equation 3.3.2, the interaction between A and B are found.

$$AB = y'_{AB} - y'_- - A - B$$ (3.3.2)

Where AB is the calculated interaction between parameters A and B, and y'_{AB} is the normalized result of the case where A and B are turned to their non-standard values. A is the effect of turning A to its non-standard value and B is the effect of turning B to its non-standard value. The effects A and B are found by the approach described in Equation 3.3.1. The interaction AB will then be a measure of how the effects A and B change when both are turned to their non-standard values.

The interactions between more than two parameters is found in the same manner. For instance, the interaction between parameters A, B, C and D is found by:

$$ABCD = y'_{ABCD} - y'_- - A - B - C - D$$ (3.3.3)

Where $ABCD$ is the calculated interaction between the effects A, B, C and D. y'_{ABCD} is the normalized result of the run where A, B, C and D are turned to their non-standard values, and C and D are the effects of turning parameters C and D to their non-standard values, respectively.

The effects and interactions of the factorial runs were calculated through a Python script. Other methodologies also exist (see e.g., [72] pages 178-179). This methodology was chosen as it seemed to be one of the more convenient ways of interpreting the results of the experiment.

For the gaseous species, the experiment tested for the inclusion of dry deposition, the influence of weather conditions (for different months), elevated sources and increased diameters, see Table 3.3.3. As deposition of particulate matter is regarded as regulatory, all runs of particulate matter included dry deposition. Therefore, the factorial experiment for particulate matter tested for decreased particle sizes instead of dry deposition being active or not, see Table 3.3.4. Everything else, including the raw data used to perform these runs, was the same as for the regulatory runs for all pollutants.

Table 3.3.3: The parameters that were studied for the gaseous pollutants. "-" indicates conditions corresponding to the standard case, while "+" indicates the non-standard conditions.

A		B	
Dry deposition included	+	Weather January-February	+
No dry deposition	-	Weather May-April	-
C		D	
Elevated sources	+	Increased diameters	+
Standard source heights	-	Standard diameters	-

Table 3.3.4: The parameters that were studied for particulate matter. "-" indicates conditions corresponding to the standard case, while "+" indicates the non-standard conditions.

A		B	
Decreased particle sizes	+	Weather January-February	+
Standard size distribution	-	Weather May-April	-
C		D	
Elevated sources	+	Increased diameters	+
Standard source heights	-	Standard diameters	-

The "-" in the tables indicates the condition corresponding to the standard case. "+" indicates the condition where the parameter is turned to a non-standard value. The standard and non-standard values for source elevation and pipe diameters are showcased in Table 3.3.5. The values of the size distribution for the standard and non-standard conditions are shown in Table 3.3.6.

Table 3.3.5: Values for source elevations and pipe diameters for standard and non-standard conditions.

	Standard [m]	Non-standard [m]
Source elevation rooftop pipes	36.8	46.8
Source elevation dry scrubber	46.8	56.8
Source elevation wet scrubber	56.8	66.8
Stack diameter rooftop pipes	3.4	5.1
Stack diameter dry scrubber	4.0	6.0
Stack diameter wet scrubber	4.5	6.75

Table 3.3.6: Size distributions for the standard and non-standard cases.

Standard values							
Particle sizes [μm]	0-1	1-10.9	10.9-21.2	21.2-33.5	33.5-48.5	48.5-66.1	66.1-100
Fraction	0.013	0.087	0.15	0.25	0.25	0.15	0.1
Decreased particle sizes							
Particle sizes [μm]	0-1	1-2.5	2.5-5	5-7.5	7.5-10	10-15	15-20
Fraction	0.0013	0.087	0.15	0.25	0.25	0.15	0.1

For the elevated sources, all sources were elevated by 10 meters. For the increased diameters, all diameters were multiplied by 1.5. The particle sizes were arbitrarily decreased, following no particular pattern.

For the dry deposition calculations, the surface characteristics for the surrounding landscape were defined in accordance to the guidance given by the AERMOD user guide [35]. Diffusivities in air, diffusivities in water, cuticular resistances to uptake by lipids in individual leaves, and Henry's law constants were defined for the gaseous pollutants in correspondence to values from parameterization schemes [57]. For the particulate pollutants, the particle size distributions and particle densities were defined. The particle density was estimated to 1 g/cm^3[10].

For the factorial design experiment, four receptors' average concentration values throughout the modeling period were investigated. The receptors are named I, II, III and IV, and their locations are shown in Figure 3.3.1.

---

[10]This value has been used in earlier experiments [71].

Figure 3.3.1: Receptor locations for the factorial experiment. The distances are given in meters from the "rooftop pipes" emission source [11].

Each receptor represents different conditions. Receptor I shows how the model conditions affect the concentration values for hillside receptors in forested terrains. Receptor II shows how the model conditions affect the relatively flat, urban environments. III and IV are at the sea floor, where III is close to the plant and IV is far from the plant. As these have the same surface characteristics and heights, these are useful for illustrating the dispersion of the pollutants.

3.4 Results

The results of the modeling cases are divided into results of the regulatory runs and the results of the factorial design experiment. The regulatory runs are presented as plotted results of the average concentration values for the whole modeling period. The factorial design experiment results are showcased as tabulated values. These tables show the normalized results and the results of the factorial experiment calculations, containing values of the parameter effects and interactions between parameters.

3.4.1 Results regulatory runs

All the results are showcased as receptor points projected onto a map of Høyanger, giving their obtained average concentration values for 2021. The receptors are color-coded, where their values are indicated by the legend in the lower left corner. The results are presented in four figures for each pollutant. The first three figures show the results from different perspectives, while the last figure shows the location and

66

value of the highest valued receptor. All concentrations are given in $\mu g/\text{m}^3$.

The results from the regulatory run of SO_2 are shown in the figures below.
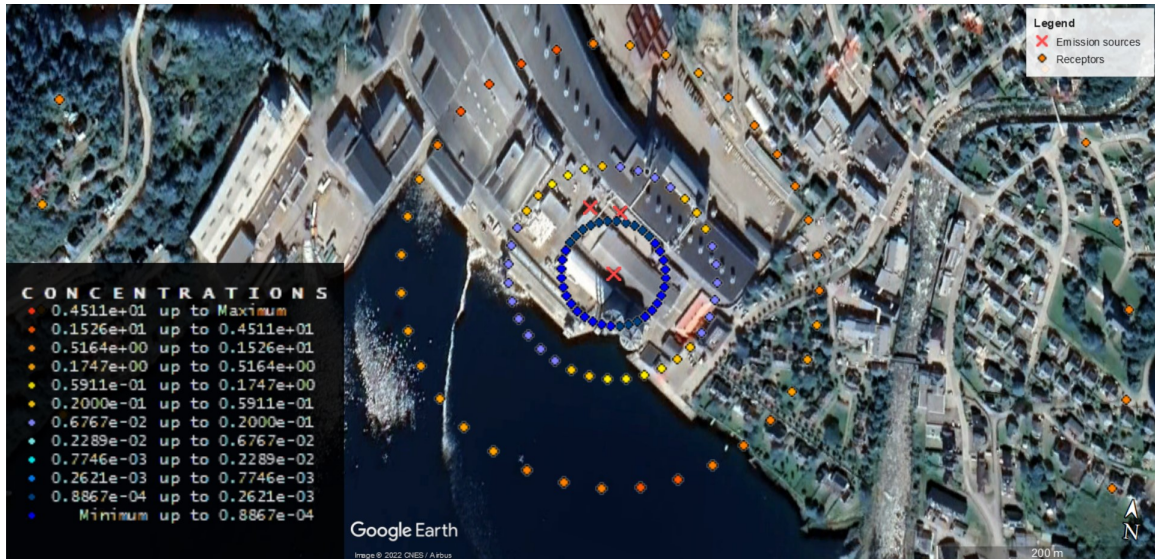
Figure 3.4.1: Close-up view of plotted results of average concentrations throughout 2021 for SO_2. Concentrations are given in $\mu g/\text{m}^3$.
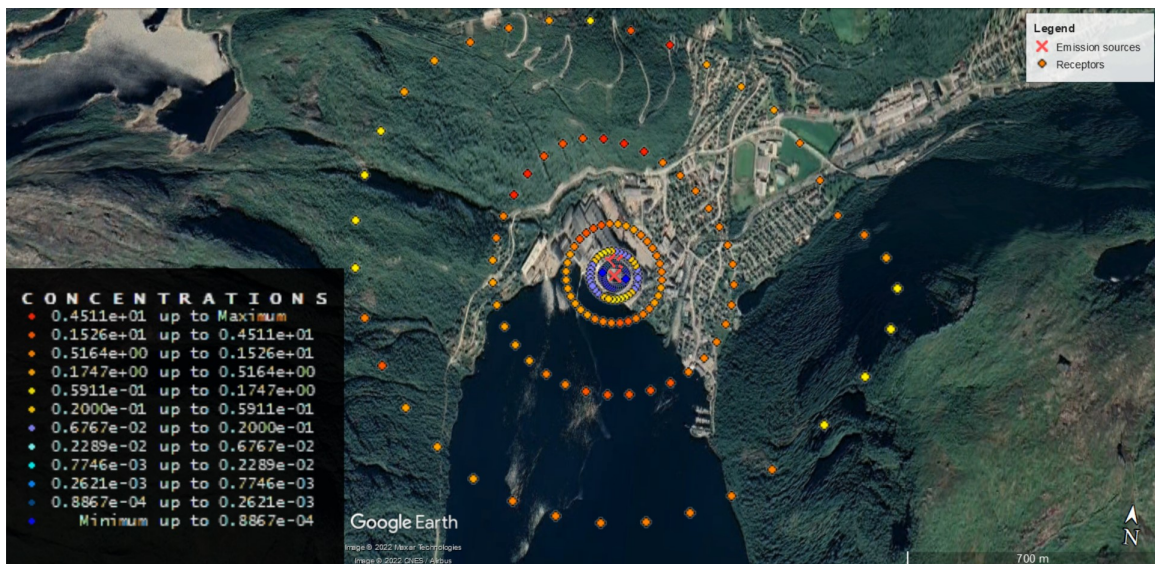
Figure 3.4.2: All plotted results of average concentrations throughout 2021 for SO_2. Concentrations are given in $\mu g/\text{m}^3$.
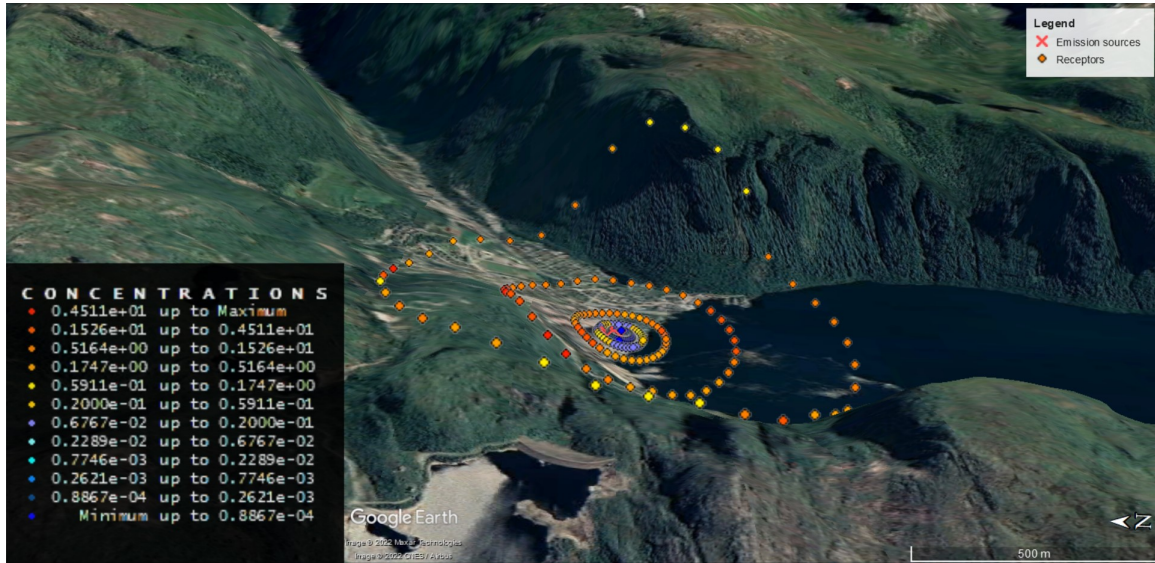
Figure 3.4.3: Side-view of plotted results of average concentrations throughout 2021 for SO$_2$. Concentrations are given in $\mu g/\text{m}^3$.

The following figure shows the receptor with the highest average concentration of SO$_2$:
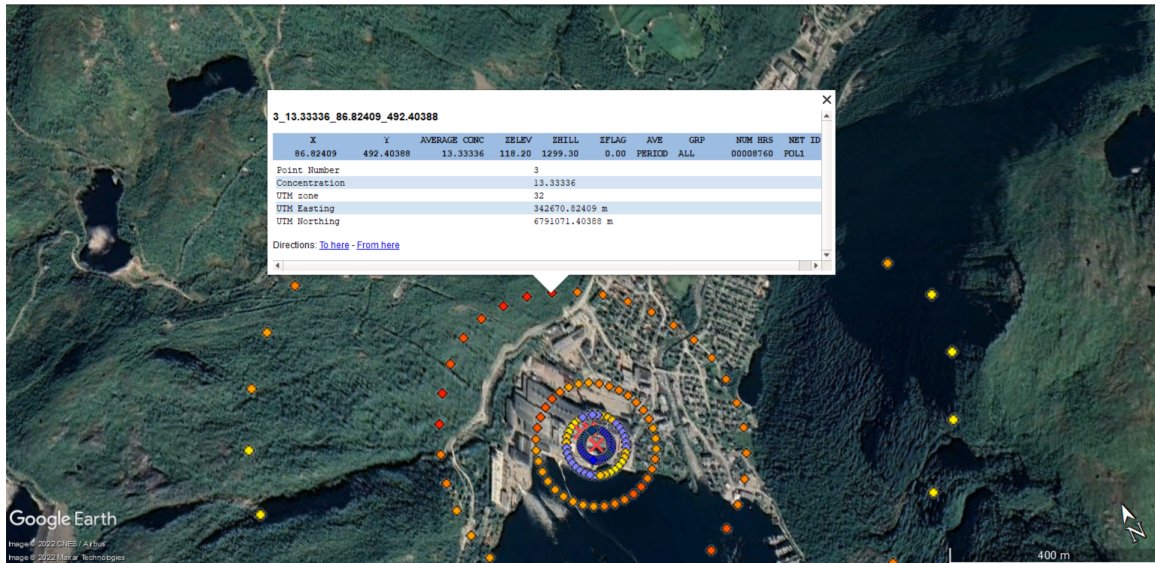
Figure 3.4.4: The highest valued receptor for the regulatory run of SO$_2$. The receptor shows an average value of 13.333 $\mu g/m^3$ for the whole modeling period.

The results from the regulatory run of HF are shown in the figures below.
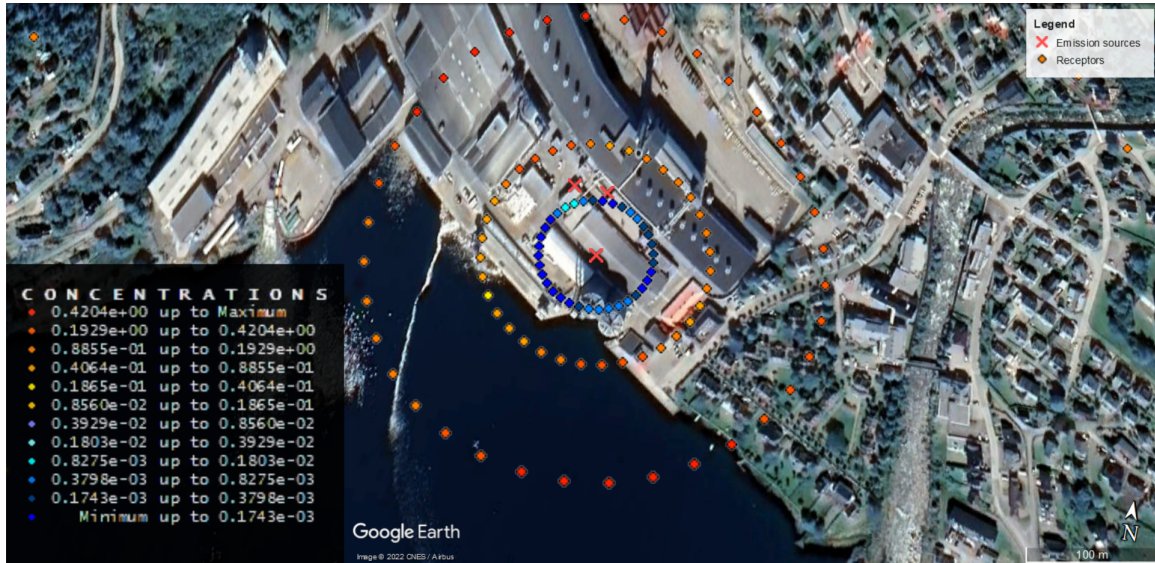
Figure 3.4.5: Close-up view of plotted results of average concentrations throughout 2021 for HF. Concentrations are given in $\mu g/\text{m}^3$.
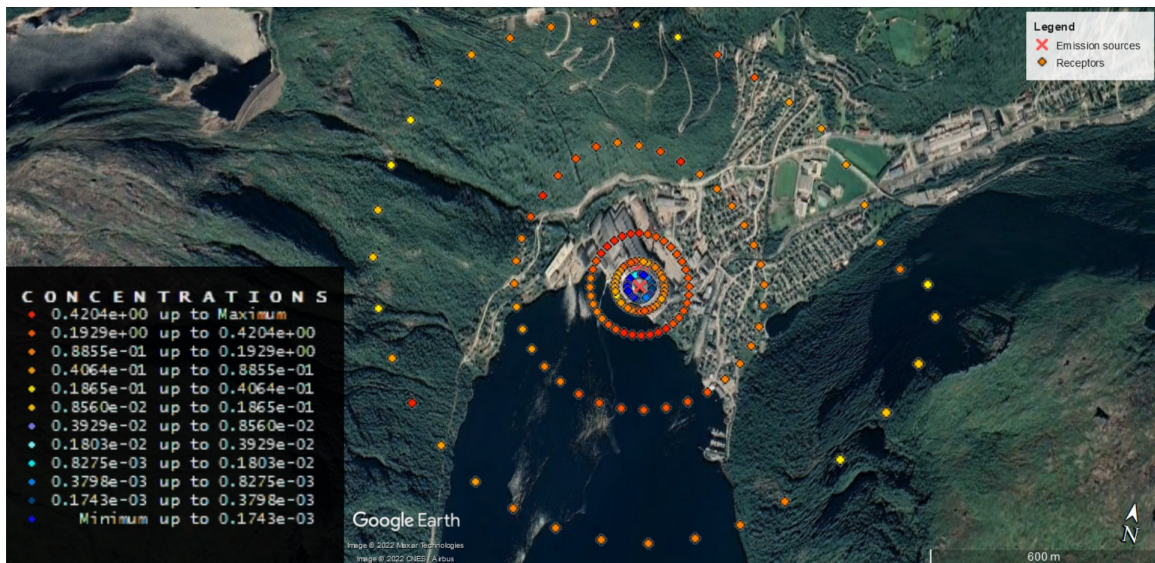
Figure 3.4.6: All plotted results of average concentrations throughout 2021 for HF. Concentrations are given in $\mu g/\text{m}^3$.
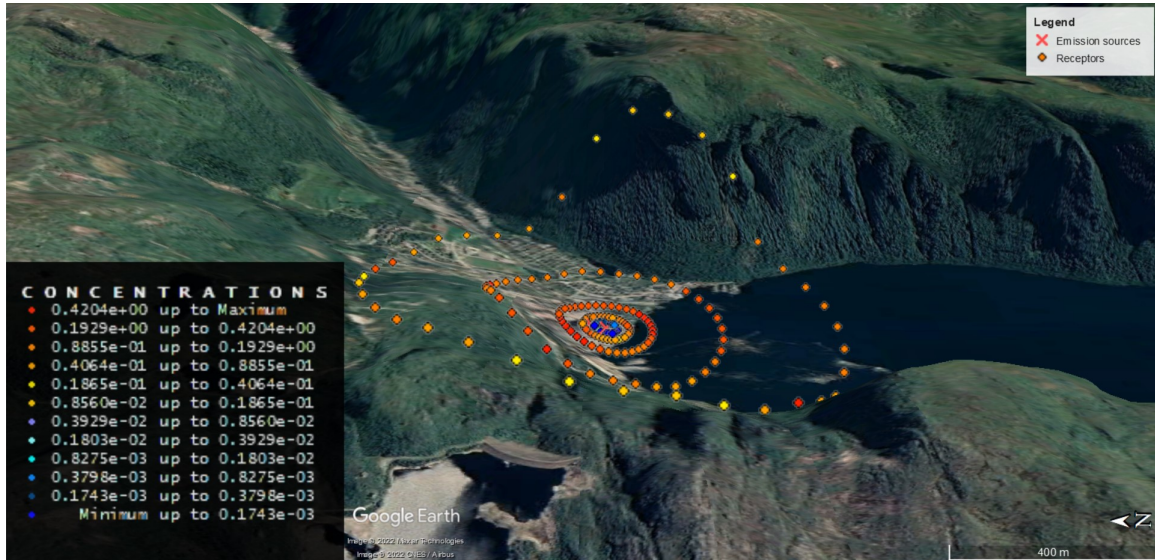
Figure 3.4.7: Side-view of plotted results of average concentrations throughout 2021 for HF. Concentrations are given in $\mu g/\text{m}^3$.

The following figure shows the receptor with the highest average concentration of HF:
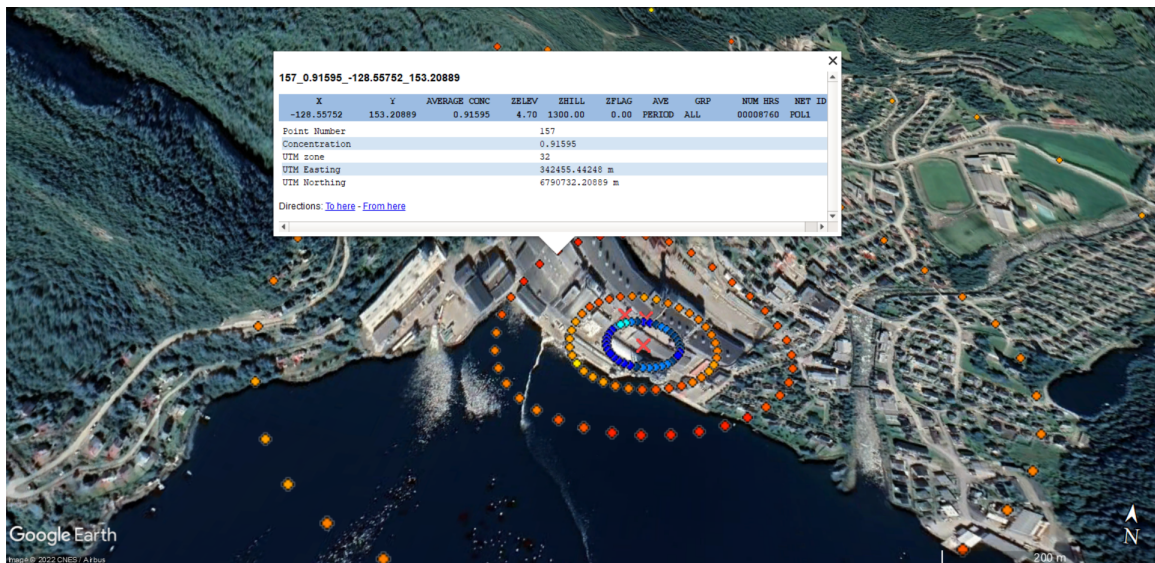
Figure 3.4.8: The highest valued receptor for the regulatory run of HF. The receptor shows an average value of 0.916 $\mu g/m^3$ for the whole modeling period.

The results from the regulatory run of particulate matter are shown in the figures below.
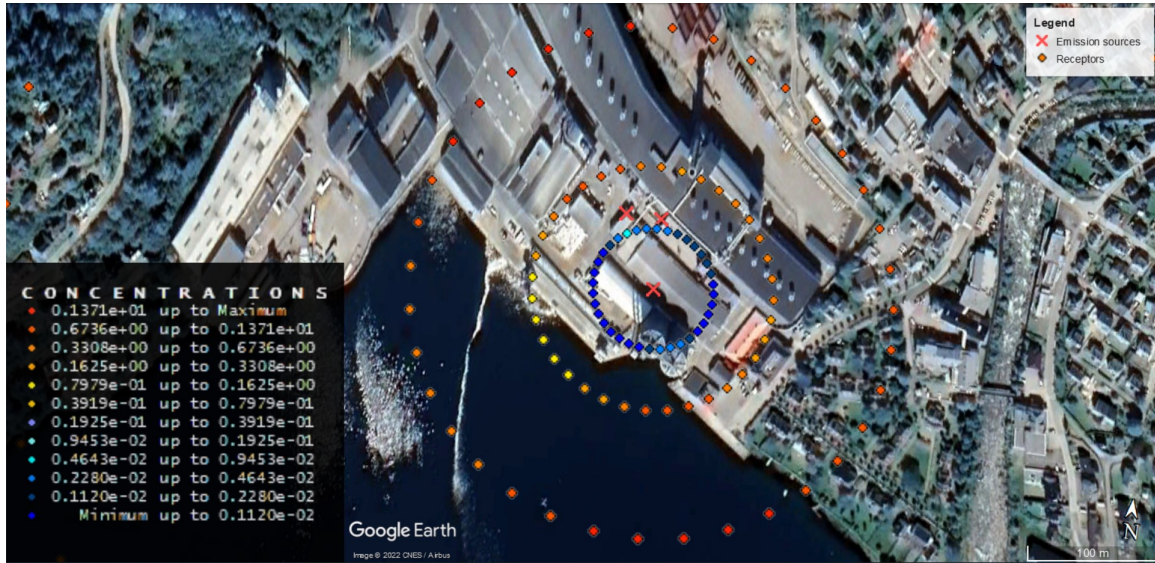
Figure 3.4.9: Close-up view of plotted results of average concentrations throughout 2021 for particulate matter. Concentrations are given in $\mu g/\text{m}^3$.
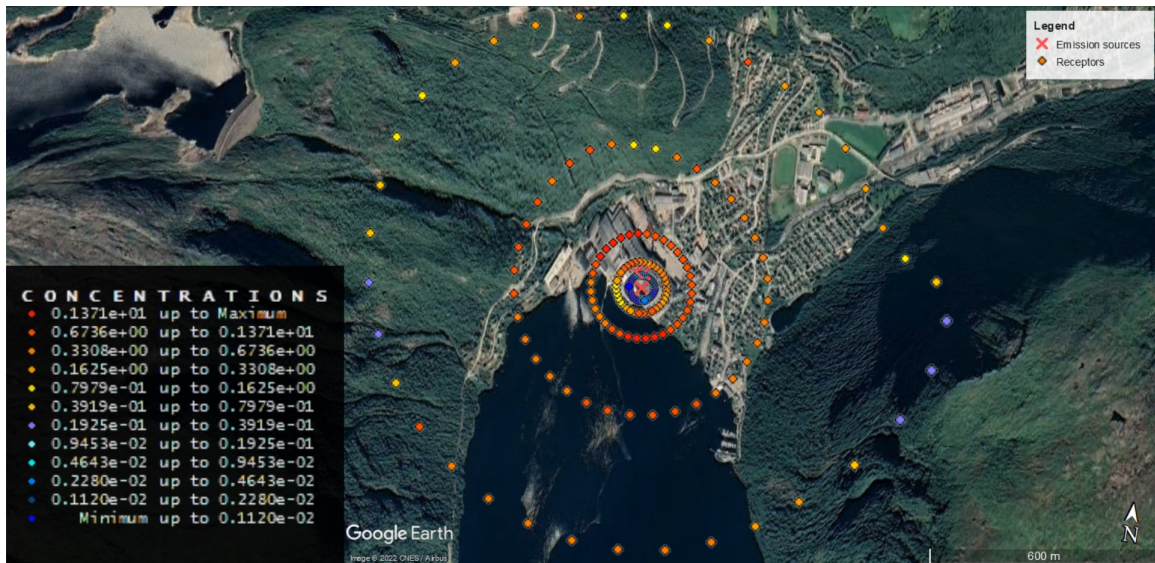
Figure 3.4.10: All plotted results of average concentrations throughout 2021 for particulate matter. Concentrations are given in $\mu g/\text{m}^3$.

Figure 3.4.11: Side-view of plotted results of average concentrations throughout 2021 for particulate matter. Concentrations are given in $\mu g/\text{m}^3$.

The following figure shows the receptor with the highest average concentration of particulate matter:
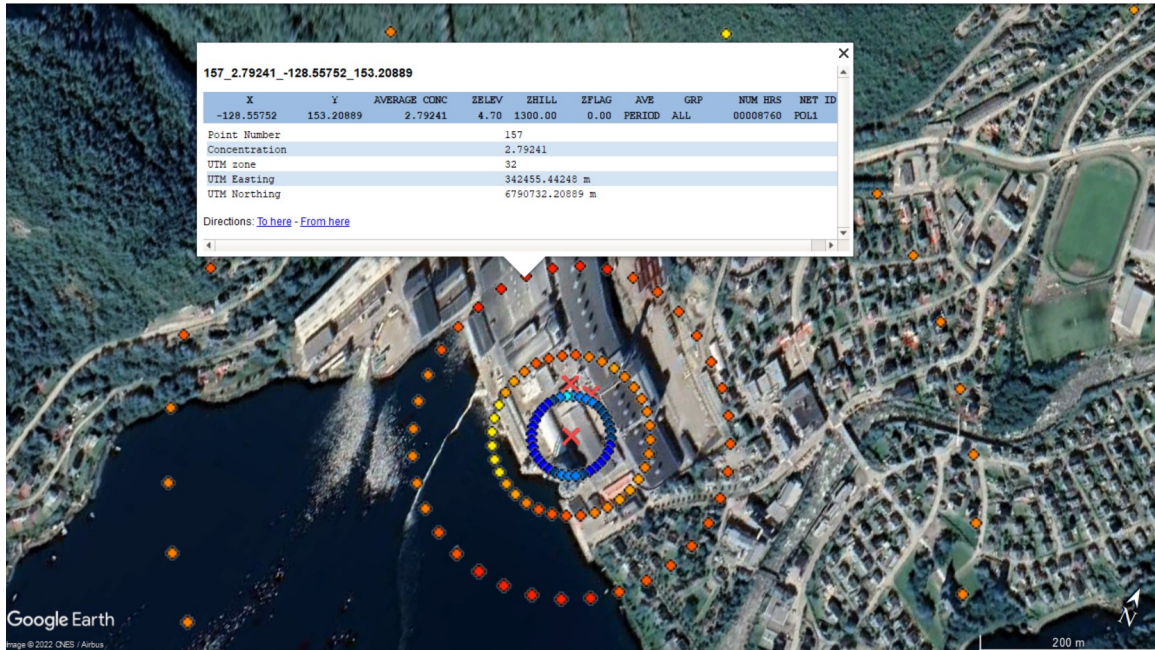
Figure 3.4.12: The highest valued receptor for the regulatory run of particulate matter. The receptor shows an average value of 2.792 $\mu g/m^3$ for the whole modeling period.

3.4.2 Factorial experiment results

The normalized results of SO_2, HF and particulate matter, respectively, are shown in the tables below. Note that y_i' denotes the result of the run when parameter i is turned to its non-standard value, not the quantified effect or interaction.

Table 3.4.1: Normalized results from the factorial experiment of SO_2.

Factorial experiment normalized data SO2	I	II	III	IV
-'	1.000	1.000	1.000	1.000
y'_A	1.000	1.000	1.000	1.000
y'_B	9.770	1.547	0.107	0.074
y'_C	0.617	0.503	0.657	0.859
y'_D	0.479	0.274	0.397	0.586
y'_{AB}	9.770	1.547	0.107	0.074
y'_{AC}	0.617	0.503	0.657	0.859
y'_{AD}	0.479	0.274	0.397	0.586
y'_{BC}	7.121	0.973	0.079	0.064
y'_{BD}	7.708	1.396	0.095	0.053
y'_{CD}	0.477	0.369	0.481	0.612
y'_{ABC}	7.121	0.973	0.079	0.064
y'_{ABD}	7.708	1.396	0.095	0.053
y'_{ACD}	1.198	0.119	0.229	0.495
y'_{BCD}	6.407	0.899	0.074	0.047
y'_{ABCD}	6.407	0.899	0.074	0.047

Table 3.4.2: Normalized results from the factorial experiment of HF.

Factorial experiment normalized data HF	I	II	III	IV
$\_$'	1.000	1.000	1.000	1.000
y'_A	1.000	0.995	0.995	0.990
y'_B	5.857	0.929	0.096	0.078
y'_C	0.659	0.522	0.707	0.881
y'_D	0.639	0.715	0.729	0.756
y'_{AB}	5.736	0.911	0.092	0.070
y'_{AC}	0.659	0.520	0.705	0.874
y'_{AD}	0.639	0.709	0.725	0.748
y'_{BC}	4.504	0.608	0.066	0.064
y'_{BD}	4.965	0.827	0.073	0.056
y'_{CD}	0.429	0.399	0.535	0.671
y'_{ABC}	4.444	0.602	0.064	0.059
y'_{ABD}	4.853	0.809	0.070	0.050
y'_{ACD}	0.429	0.397	0.533	0.665
y'_{BCD}	3.899	0.568	0.055	0.048
y'_{ABCD}	3.842	0.562	0.053	0.044

Table 3.4.3: Normalized results from the factorial experiment of particulate matter.

Factorial experiment normalized data particulate matter	I	II	III	IV
-'	1.000	1.000	1.000	1.000
y'_A	0.772	0.642	0.855	0.907
y'_B	4.749	0.701	0.128	0.200
y'_C	0.741	0.614	0.730	0.985
y'_D	0.670	0.729	0.688	0.851
y'_{AB}	4.214	0.548	0.078	0.069
y'_{AC}	0.521	0.348	0.633	0.842
y'_{AD}	0.487	0.436	0.605	0.676
y'_{BC}	3.949	0.505	0.087	0.214
y'_{BD}	3.925	0.579	0.086	0.196
y'_{CD}	0.479	0.530	0.540	0.765
y'_{ABC}	3.355	0.379	0.056	0.058
y'_{ABD}	3.511	0.464	0.054	0.046
y'_{ACD}	0.334	0.258	0.468	0.628
y'_{BCD}	3.288	0.448	0.077	0.174
y'_{ABCD}	2.875	0.345	0.045	0.041

The results of the factorial experiments for SO_2, HF and particulate matter are shown in the tables below. "-" denote the standard cases. The standard cases have values of 0.000 for all receptors, as these cases have no effects or interactions associated with them. A, B, C, and D are the individual effects of turning the parameters A, B, C and D, respectively, to their non-standard values. The remaining values denote the interactions between the parameters that are given (e.g., AB is the calculated interaction between effect A and B). Recall that the values are given in fractions relative to the standard case. For instance, a value of 0.9 indicates an increase of 90 % compared to the standard case. Correspondingly -0.9 indicates a 90 % decrease compared to the standard case. Values of 0 indicate that the given effect or interaction has no impact.

Table 3.4.4: Calculated effects and interactions from the factorial experiment of SO_2.

Calculated effects and interactions for SO_2	I	II	III	IV
-	0.000	0.000	0.000	0.000
A	0.000	0.000	0.000	0.000
B	8.770	0.547	-0.893	-0.926
C	-0.383	-0.497	-0.343	-0.141
D	-0.521	-0.726	-0.603	-0.414
AB	0.000	0.000	0.000	0.000
AC	0.000	0.000	0.000	0.000
AD	0.000	0.000	0.000	0.000
BC	-2.266	-0.077	0.314	0.130
BD	-1.540	0.575	0.590	0.393
CD	0.381	0.592	0.427	0.166
ABC	-2.266	-0.077	0.314	0.130
ABD	-1.540	0.575	0.590	0.393
ACD	1.102	0.342	0.175	0.050
BCD	-2.458	0.575	0.912	0.527
$ABCD$	-2.458	0.575	0.912	0.527

Table 3.4.5: Calculated effects and interactions from the factorial experiment of HF.

Calculated effects and interactions for HF	I	II	III	IV
-	0.000	0.000	0.000	0.000
A	0.000	-0.005	-0.005	-0.010
B	4.857	-0.071	-0.904	-0.922
C	-0.341	-0.478	-0.293	-0.119
D	-0.361	-0.285	-0.271	-0.244
AB	-0.121	-0.013	0.001	0.002
AC	0.000	0.003	0.003	0.003
AD	0.000	0.000	0.001	0.003
BC	-1.012	0.157	0.262	0.105
BD	-0.532	0.184	0.248	0.222
CD	0.131	0.162	0.098	0.033
ABC	-1.072	0.156	0.265	0.109
ABD	-0.643	0.171	0.249	0.226
ACD	0.131	0.166	0.101	0.038
BCD	-1.257	0.403	0.522	0.332
$ABCD$	-1.313	0.402	0.525	0.339

Table 3.4.6: Calculated effects and interactions from the factorial experiment of particulate matter.

Calculated effects and interactions for particulate matter	I	II	III	IV
-	0.000	0.000	0.000	0.000
A	-0.228	-0.358	-0.145	-0.093
B	3.749	-0.299	-0.872	-0.800
C	-0.259	-0.386	-0.270	-0.015
D	-0.330	-0.271	-0.312	-0.149
AB	-0.307	0.205	0.094	-0.038
AC	0.008	0.091	0.048	-0.050
AD	0.044	0.065	0.062	-0.081
BC	-0.541	0.190	0.229	0.029
BD	-0.494	0.149	0.271	0.145
CD	0.067	0.187	0.122	-0.070
ABC	-0.908	0.421	0.343	-0.034
ABD	-0.680	0.392	0.383	0.088
ACD	0.150	0.273	0.196	-0.115
BCD	-0.872	0.403	0.531	0.139
$ABCD$	-1.057	0.659	0.644	0.098

3.5 Discussion

3.5.1 Factorial design experiment

The effect of including dry deposition, A, can be seen in Table 3.4.4 and Table 3.4.5. The effect is very small, being negligible for SO_2 and minimal for HF. The real deposition effect is probably larger, as the deposition algorithms for AERMOD are fairly conservative due to not being a regulatory option. Additionally, the runs did not include the effects of wet deposition, which would enhance the deposition of the species. This is especially the case for Høyanger, as Høyanger has a high amount of precipitation. In all receptors, the inclusion of dry deposition gives smaller values for the average concentration. This implies that species deposited to the ground are not included in the receptor values, further implying that the receptors show the concentrations of pollutants in the air.

Upon closer inspection of the deposition results, it has been observed that the species deposit more efficiently for receptors III and IV. This is probably due to these receptors being located in the water, where the pollutants have a better affinity. This indicates that the surface characteristics are accounted for in the deposition calculations.

The effect of finer particle sizes of particulate matter, A in Table 3.4.6, shows lower

concentrations for all receptors. The effect ranges between 9.3-35.8 %, where the effects become lower for the far-away receptors. This indicates that finer particles give better dispersion, which is to be expected. Finer particles weigh less, and will therefore disperse more easily. In total, the results show that particle sizes are reasonably determining for the dispersion calculated by the model, which is in accordance with the real world.

The effect of evaluating the months of January-February, rather than April-May, B, has by far the largest impact for all pollutants. The weather is the fundamental factor for determining the dispersion of emissions, so this is no surprise. The table below compares the averaged values of surface weather characteristics for January-February and April-May:

Table 3.5.1: Average values of sky ceiling height, sky cover, temperature and wind speed for January-February and April-May for the surface data used in the factorial experiment. The bottom row shows the change from April-May to January-February.

Months	Cloud ceiling height [m]	Sky cover [%]	Temperature [° C]	Wind speed [m/s]
April-May	975.03	4.57	7.40	3.73
January-February	1103.04	4.59	-0.55	3.43
Change	13.13 %	0.004 %	-7.95° C	-8.04 %

The cloud ceiling height in combination with cloud cover are used to estimate the solar insolation, which then is used to determine the stability class of the atmosphere. The difference in cloud ceiling height is 13.13 %, which might have some influence on the solar insolation. The sky cover is practically identical for both time intervals, meaning any effect caused by difference in sky cover is negligible. Altogether these may cause a small difference in solar insolation between the months, but in regards to dispersion these parameters are not expected to cause any significant difference between the months. The temperature difference is at almost 8° C. Lower temperatures tend to give higher plume rise [13], thus providing an increase in pollutant dispersion. The wind speed, being the main mechanism for movement of pollutants, is detrimental for the dispersion. The wind speed is 8 % lower for January-February, making the dispersion contribution from wind speed a bit lower compared to April-May.

The lower temperatures of January-February and higher wind speeds of April-May, give no clear indication of when one would expect the best dispersion. The results of B, being the effect of changing the time interval to January-February instead of April-May, are also too sporadic to come to any substantiated conclusion. The reason for the discrepancies is most likely due to the difference in wind directions for the months, seen in the wind roses below.
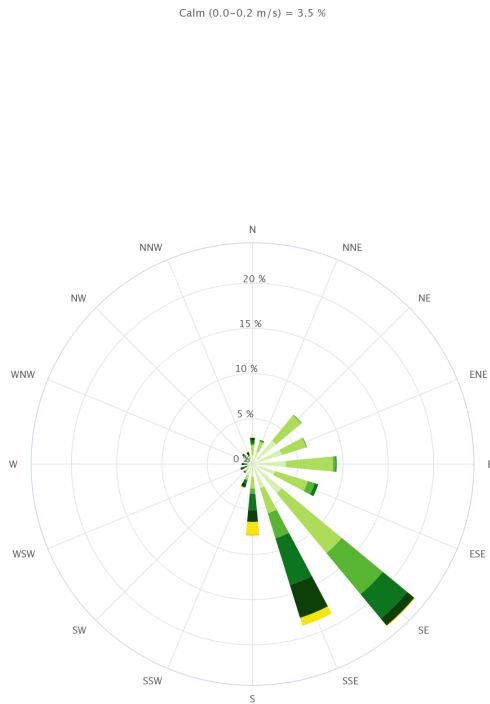
Figure 3.5.1: Wind rose for Flesland weather station from January-February [12].

Figure 3.5.2: Wind rose for Flesland weather station from April-May [12].

The figures show that the main wind direction is south-east for January-February and north/north-west for April-May. Comparing one receptor to another is therefore pointless without accounting for the wind directions. The pattern seems to be that the receptors in the direction of the wind contain the smallest concentrations. Receptor I, being at the north-west side of the plant, has substantially larger concentrations for all pollutants for January-February, while receptors III and IV has largest concentrations for April-May. This can seem counter-intuitive, as the wind governs which directions

80

the pollutants end up. This is true, but, as seen from the figures, a larger fraction of the stronger winds lie in the main wind directions. The strong winds will contribute to a larger dispersion in their respective directions, thus causing the receptors in these directions to achieve lower concentration values. Looking at e.g., the wind rose for January-February, the northwestern winds are calm compared to those in the southern directions. This gives high concentration values for north-western receptors whenever the winds blow this direction. The total concentration of the whole north-western direction, however, will be smaller than for the southern directions, as a bigger mass of emissions will be carried in this direction.

All in all, combining all the factors of varying between months makes the evaluation quite complicated. A more extensive illustration of the issue would be achieved if one were to include more receptors at far-away distances. Nevertheless, everything points to the wind directions being the most influential for the effect of varying between months, B.

The wind directions being the governing mechanism of B, mitigates the point of evaluating the interaction of B with other parameters. This is due to the nature of the calculation of interactions. The calculations of the effects are based on receptor point values, which are directionally dependent. Since the wind directions are different for the time intervals, this also makes the effect of B directionally dependent. This means that one can expect a different distribution of concentrations among the receptors for case B compared to the standard case. The difference in concentration distributions means that any effects (i.e., A, C and D) in April-May will be incomparable to the values these effects would have in January-February. All effects used to calculate interactions (see Equation 3.3.2) are found based on comparison with the standard case (Equation 3.3.1). Since the effects found from comparison with the standard case are not comparable to the effects they would have in case B, the resulting values of interactions will be misleading. For this reason, all evaluation of interactions containing B will be omitted from this thesis.

The effect of increased elevations, C, gives smaller emission concentrations for all receptors. The effect becomes less prominent for the far-away receptor, IV. This indicates that increased stack elevations contribute to a better dispersion. This is in accordance with real-life, as it gives the emissions more time to spread before they reach the surface-level. From Figure 2.3.2, one can see that the cone representing the concentration distribution becomes larger for higher stack elevations, thus achieving a better spread.

The effect of increased diameters, D, gives the same response. By increasing the

stack exit diameters of the source without decreasing the stack exit velocity, one will increase the volumetric flow rate of the plume (see Equation 3.2.2). Generally, this will increase the buoyancy- and momentum flux of the plume [13], causing an increase in plume rise. Hence, the effective height (Equation 2.3.2) of the plume will increase with increased diameters, essentially having the same effect as elevating the sources.

For the case with increased diameters, D, all source diameters were multiplied by 1.5. This causes a larger increase in diameter for the sources of higher standard diameters. From Table 3.3.1, one can see that the wet- and dry scrubber have the bigger standard diameters, and additionally have the highest stack exit velocities. The relation in Equation 3.2.2 then implicitly states that the increase in volumetric flow rate should be largest for the wet- and dry scrubber. This further implies that the effect of increased diameters, D, should be more prominent for these sources. This is in accordance with the results. SO_2 is the pollutant which has the most of its emissions originating from other sources than the rooftop pipes (see Table 3.3.2), and also has the biggest effect of D.

In real-life, increasing the diameter for increased dispersion can have varying effects. When increasing the diameter, one will also decrease the stack exit velocity of the emissions, thus negating the effect of increased diameters to some extent.

The results show that there is basically no interaction between dry deposition and increased stack elevations, AC, and dry deposition and increased diameters, AD. This is most likely due to the effects of dry deposition being negligible in the first place. For particulate matter, the effect of A is the effect of decreased particle sizes. For this pollutant, AC and AD are fairly small as well, even though the effects of A, C and D are large. This indicates that the effects of stack diameters and source elevations are fairly independent of the particle distribution.

The interactions between increased stack elevations and increased diameters, CD, are positive for HF and SO_2. This means that the dispersing effects of C and D decrease when coupled together. As both these effects in practice elevate the plume, it implies that dispersion based on plume elevation becomes less effective the more the plume rises. This may also explain why SO_2 has a more positive value of CD than HF, as SO_2 had a more dispersing effect of D. Particulate matter shows positive interactions for all receptors except IV. CD is smaller for particulate matter than for the gaseous species. Particulate matter is the pollutant that has the biggest share of its emissions coming from the rooftop pipes. The rooftop pipes are less elevated than the dry- and wet scrubber, meaning every contribution of plume elevation will be more efficient for the rooftop pipes. This might explain why CD is

smaller for particulate matter. Receptor IV for particulate matter has a negative value for CD. Since both C and D contribute negatively to concentration values, a negative interaction between these imply that their effects are amplified when together. Since both C and D are plume elevating effects, this further implies that any additional contributions to plume elevation is still exponentially efficient for this receptor.

ACD, being the interaction between dry deposition, increased stack elevations and increased diameters, has similar values as CD for the gaseous pollutants. This is once again due to the deposition having very small effects on the gas dispersion. For particulate matter, the interaction between decreased particle sizes, increased stack elevations and increased diameters, ACD, are basically scaled versions of CD. This is interesting, as AC and AD were fairly small. Seemingly, the effect of A generally scales with plume elevation. For receptors I, II and III, the results imply that further enhancements of plume dispersing mechanisms will have smaller dispersing effects. For receptor IV, having a negative value, such effects will still be efficient.

3.5.2 Regulatory runs

The biggest uncertainty of the modeling cases is definitely the weather data being acquired from a weather station 112 km away from Høyanger. As surface weather is one of the most influential factors of the dispersion of emissions, dictating the PBL characteristics to a large extent, the results cannot be deemed representative. Additionally, the weather data are lacking various parameters, like station pressure, which can be important for calculating PBL parameters. Additionally, precipitation code- and amount is omitted, which is important for calculating the wet deposition of particulate matter. The upper air station, being located at Svalbard, is also very far away from the modeling domain. Although there is a bigger tolerance on distance regarding upper air data, the distance is more than large enough to question the representativeness of the data. The upper air station also lacks all data for June, July and August, and is additionally lacking some data for certain time-intervals at certain elevations.

The plume characteristics, being the stack exit velocities, stack exit temperatures and emission rates, are all implemented as their averaged values for the whole modeling period, rather than feeding the model individual data by the hour. This is done to remedy with irregularities in measurements, which can cause values not being representative of the plume to be overrepresented. Using hourly data for plume characteristics can achieve different results. Since weather data is also time-dependent, certain combinations of plume characteristics and weather data can in theory give visible contributions to the results. Adding to this, aluminum plants generally experience

higher emission rates during the summer [74], something that is not accounted for when averaging the emission rates for the whole year. Thus, if one were to measure hourly, daily or maybe even monthly maximums, one could expect significant differences between the two approaches. However, as the results are the average concentrations through a whole year, these kinds of discrepancies are probably mitigated to a degree where they are be negligible. Conclusively, averaging the plume characteristics for the whole modeling period is not deemed to be detrimental for the representativeness of the results, as the results are given as the average concentration through a whole year.

The emission data given by the industry are not thoroughly validated in regards of what the data actually mean. Depending on the measurement methods, it is not given that the data given to the model are representative of the real situation. All parameters fed to the model are assumed to be representative for the stack exits. Reports showing measurement routines at Høyanger, seem to indicate that most parameters are measured at measuring points in pipes on the way to the stack exits. Depending on the nature of the pollutants, and the distance these have to travel before reaching the end of the pipes, this can lead to values not representative for the stack exits. This uncertainty is most prominent for the stack exit temperatures, as these tend to decrease upon reaching the atmosphere. Turbulent conditions in the pipes can cause unrepresentative values for emission rates and stack exit velocities as well.

It is also not given that the size distributions for particulate matter are representative. The distributions fed to the model are assumed to be particulate matter which is emitted to air. Analyses of particulate matter are often based on particles caught by filters somewhere on the way to the stack exits. The large particle sizes given by the industry begs to question if these would have had the same sizes when emitted to air, as they tend to split up into smaller particles on their way out of the stacks.

Many of the emission rates in Table 3.2.1 show high standard deviations, ranging between 5.6-320 %. In the provided data for emission rates, two types of measurements were found. These were "routine measurement", being most of the provided data, and "extra measurement" being a few data points per pollutant. Upon closer inspection of the extra measurement values, these were found to generally have much higher values than the routine measurements. These measurements seem to be the reason for the high standard deviations. In contact with Hydro, it was found that these measurements were taken during extraordinary circumstances, which may not be representative for typical operation. The addition of these values have had significant contribution to some of the emission rates, generally making the concentration values higher than what they would be if only routine measurements were used. The standard deviations of the normal flow rates and temperatures range between 0.89% and

7.55%, indicating that these parameters are quite stable throughout the year. The measurement uncertainties of the stack exit velocity and temperature of the rooftop pipes are $\pm$ 3.96 % and $\pm$ 1° K, respectively. These are quite low, but they are based on measurements taken from 2011. Since these measurements were taken 10 years prior to the modeling case, they may not be representative. The uncertainty of the temperature is only a measurement uncertainty, thus not accounting for the variation of temperatures which can occur throughout the year.

For the calculations of the stack exit velocities of the wet- and dry scrubber, the normal volumetric flow rate was assumed to be equal to the actual volumetric flow rate. From Equation 3.2.1, one can see that the difference between these rates depend on the difference between the standard conditions and the real conditions. Assuming the flow rate is measured at the stack exit, the pressure of the plume should be close to 1 atm, as it is just beneath the atmosphere. The difference in the real pressure and standard pressure is therefore deemed to be small, only having a minor impact on the flow rate. The impact of the temperature can be found by applying the temperatures in Table 3.3.1 into Equation 3.2.1. From this, one can see that the temperatures alone can potentially contribute to a 8 % and 31 % increase in flow rate for the wet scrubber and dry scrubber, respectively. As mentioned in the discussion of the factorial experiment, the flow rate is one of the main factors in determining the plume rise of the pollutants. Increased plume rise increases the effective height of the plume, enhancing the dispersion of the pollutants. This means that the real pollutants will achieve a better dispersion contribution from the volumetric flow rates than the modeled pollutants. However, as mentioned earlier, the temperatures obtained from the industry are often measured inside the pipes, and not at the stack exits. Therefore, the real stack exit temperatures may be lower than those from Table 3.3.1, mitigating the uncertainty. The potential effect of estimating the normal volumetric flow rate to be equal to the volumetric flow rate is largest for the pollutants coming from the dry scrubber, which is mainly SO_2. HF is also affected somewhat, having a 22 % share of its pollutants coming from the dry scrubber. Particulate matter will largely be unaffected, as most of its emissions come from the rooftop pipes.

The height above sea level and the height of the dry- and wet scrubber were estimated based on pictures. The results of the elevated sources' effect, C, from Table 3.4.4, Table 3.4.5 and Table 3.4.6 can give an indication of the impact of wrongful estimates. For receptors I, II and III, being close to the emission sources, increasing the elevation by 10 meters has impactful results. These give deviances ranging between around 20-45 %. For receptor IV, being far away from the sources, the effect of increasing the height of receptors are less significant. All in all, wrongful estimates can have a significant impact on receptor concentrations close to the sources. This

naturally depends on the difference between the estimated heights and the real heights.

The diameter of the dry scrubber is also estimated. As the calculated stack exit velocity is based on this diameter, any wrongful estimate of the diameter will propagate to the stack exit velocity. Again, one can look at the results of the factorial experiment to evaluate the significance of a wrongful estimate. The effect of increasing the stack diameter by 1.5 times is represented by D in Table 3.4.4, Table 3.4.5 and Table 3.4.6. The results show that the size of the diameter has significant effects on all receptors. However, these results do not account for the accompanying decrease in stack exit velocity when increasing the diameters. Since the volumetric flow rate is known, and found from Equation 3.2.2, the volumetric flow rate will be the same no matter how wrongful the estimated diameter is. On the whole, the volumetric flow rate is the most influential factor in regards of atmospheric dispersion [75]. Hence, a wrongful estimate will not be as crucial as indicated by the effect D.

Only the diameter of the dry scrubber is estimated, meaning a wrongful estimate will mostly affect pollutants having significant emissions from the dry scrubber. From Table 3.3.2 one can see that only a small amount of HF and particulate matter emissions come from the dry scrubber. For SO_2 however, more than 80 % of the emissions stem from the dry scrubber. Conclusively, wrongful estimates of the dry scrubber diameter can have an impact on SO_2. This impact will be smaller for HF and insignificant for particulate matter.

The regulatory runs did not include building downwash effects. The most prominent buildings close to the sources are the silos, the dry scrubber and the wet scrubber. The dry scrubber and the wet scrubber can cause some building downwash effects on the pollutants coming from the rooftop pipes, as these are at higher elevations. These effects will however be very small for the dry- and wet scrubber's emissions, as their building downwash effects will not affect their own emissions. As these additionally are not very large dimension wise, their building downwash effects are in this case deemed to be small. The silos, albeit being large, are placed at a lower elevation than the emission sources, mitigating their building downwash effects somewhat. Still, they would probably cause some building downwash effects. Høyanger includes other buildings as well, like houses, stores, hotels, etc. These are for the most part placed at lower elevations, and are less prominent than the structures already mentioned. Their individual impacts are therefore deemed small, but they may have an impact altogether. All in all, including building downwash effects for all buildings will probably give more representative results, but only to a small extent. The inclusion of building downwash effects would mostly affect the emissions coming from the lower elevated sources. HF and particulate matter have most of their emissions coming from the rooftop pipes,

which are the lowest sources. Thus, HF and particulate matter will be most affected by the inclusion of building downwash effects.

All sources were treated as point sources. For the dry- and wet scrubber, this is probably the most representative source type. All the 18 rooftop pipes were treated as a single point source, located at the middle of the roof of the plant. The 18 rooftop pipes are in reality somewhat evenly distributed across the long side of the hall, which is about 300 meters long. Treating all the rooftop pipes as individual sources would give a different distribution of emissions for the receptors close to the plant, being the three inner circles seen in the results. The far-away receptors are mostly unaffected, as the distances between the rooftop pipes eventually become negligible compared to the overall distance from the plant. Hence, this treatment can have some effect on the representativeness of the receptors close to the plant, but will be insignificant for the far-away receptors. The eventual deviance this treatment represents is relevant for HF and particulate matter, as most of their emissions stem from the rooftop pipes.

The urban option, accounting for the urban heat island effect, was omitted from the modeling case. AERMOD accounts for urban heat island effects by using the population size as input. As the town only has around 4000 inhabitants, the contribution of this option is deemed to be small. Høyanger is however quite industrial for its size, meaning that there could be some urban heat island effects. Thus, inclusion of this option could achieve more representative results.

Despite the number of uncertainties making the modeling case unrepresentative of real-life, several observations, relevant to the real-life dispersion of emissions, can be made. The results show a correlation between decreased dispersion of emissions and elevated terrain, which is to be expected. This can be seen as the elevated receptors far away from the sources have lower concentration values than the non-elevated sources far away from the sources. This indicates that the model accounts for the topography of the area. All results of the regulatory studies show that the emissions are significantly higher at the foot of the mountains at the north-side of the plant, compared to other receptors at the same distance. This makes sense, as pollutants tend to get trapped in highly elevated areas. The concentrations at these receptors may be lower in reality, as the wind directions input to the model do not account for the influences the fjords have on the real wind directions.

Interestingly, the lowest concentrations for all pollutants are at the receptors closest to the emission sources. Generally, contributions to these sources will come from a combination of calm winds and low plume rises. As the diameters and stack exit velocities for all sources were averaged throughout the whole year, the plume rise

caused by these parameters will be the same throughout the modeling case. Therefore, the plume rise will be relatively stable, and hence not become significantly low. Closer inspection of the wind speeds show that about 5 % of the wind speeds are between 0-1 knots (0-0.514 m/s). The low amount of calm winds in combination with the relatively steady effective heights of the plumes may explain the low concentrations of the receptors close to the plant.

The results show general differences in the dispersion of the gaseous species, even though deposition is not included. The results show a better dispersion of SO_2 than HF, which can be seen as SO_2 has a lower share of its emissions close to the plant. The most plausible explanation for this, is that the majority of HF-emissions stem from the pipes, while the SO_2 mainly comes from the more highly elevated-, and bigger diameter wet- and dry scrubber. The factorial experiment shows that higher elevations and bigger diameters lead to better dispersion, which makes this the most likely reason for the difference in the dispersion between the gaseous pollutants.

Comparison between the gaseous species and particulate matter shows that the particulate matter does not disperse as well as the gases. This is as expected, as the particulate matter is heavier than the gaseous species, and will then deposit faster. This indicates that the deposition algorithms for particulate matter are active. The deposition algorithms' accuracy is hard to determine. Another contribution to low dispersion is that most of the pollution of particulate matter originate from the pipes.

Comparing the highest valued receptors (Figure 3.4.8, Figure 3.4.4 and Figure 3.4.12), one can see that the highest valued receptor is the same for HF and particulate matter, but not for SO_2. This is most likely due to the origins of the emissions. Both particulate matter and HF mainly come from the rooftop pipes, explaining why they have the same highest valued receptor. Note that deposition is included for particulate matter, meaning the general dispersion of particulate matter is expected to be different than for HF. This means that it is not given that these pollutants have the same highest valued receptors, even if they come from the same source.

4 Conclusion and further recommendations

In this thesis, the AERMOD dispersion model was used to measure the dispersion of SO_2, HF and particulate matter, coming from an aluminum plant located in Høyanger. The modeling cases included three regulatory runs and a factorial design experiment. The regulatory runs were given to provide a qualitative representation of how the pollutants disperse around the aluminum plant. The factorial design experiment was

given to test the influence of changing different parameters, both individually, and when coupled together.

The factorial design experiment tested for the effects of including dry deposition/decreasing particle sizes, varying months of weather, increased elevations and increased diameters. Including dry deposition had low impact on the results, which may in part be due to conservative calculations by the model. Decreasing particle sizes gave better dispersion, which is in accordance with theory, as smaller particles disperse better than bigger particles. Varying between months had the biggest impact, which is explained by the months having very different wind directions. The wind directions being the governing mechanism for the effect of varying between months was found to make any interaction with this parameter irrelevant to evaluate. Increased diameters and increased elevations were both found to increase dispersion of the pollutants. In essence, both of the parameters increase the effective height of the plume, thus leading to increased dispersion. The interaction between elevated sources and increased diameters indicated that the dispersing effect of increasing the effective height became less effective the more the effective height was increased.

The interactions between dry deposition and other parameters were negligible, most likely due to the low effect of dry deposition in the first place. For decreased particle sizes, the interactions were small when coupled with increased diameters and increased elevations individually, but seemed to scale the interactions between increased diameters and elevations when all were coupled together.

The biggest uncertainty of the modeling case was the applied weather data. The surface weather data and the upper air data were acquired from stations 112 km and 1915 km away from the plant, respectively. This is too far away for the data to be deemed representative. Additionally, both the radiosonde data and surface weather data were lacking some data which may be important for a representative run. These uncertainties alone, are enough to make the case unrepresentative for the real world emissions. Other uncertainties that possibly impacted the validity of the run, in decreasing order of significance, were:

- Inclusion of likely unrepresentative emission rate data ("extra measurement"), causing high standard deviations for the emission rate data. Affected all pollutants to varying degrees.

- Assuming the normal volumetric flow rate to be equal to the actual volumetric flow rate. This mostly affected SO_2.

- Potentially wrongful estimations of heights for the dry- and wet scrubber. This

mostly affected SO_2.

- Assuming data of emission properties given by the industry to be representative for the conditions at the stack exits. Affected all pollutants.

- Potentially wrongful estimates of the dry scrubber diameter. This mostly affected SO_2.

- Treating the rooftop pipes as a single point source. This mostly affected HF and particulate matter.

- Averaging the plume characteristics for the whole year rather than using data by the hour. Affected all pollutants.

- No inclusion of building downwash effects. Mostly affected particulate matter and HF.

- No inclusion of urban heat island effects. Affected all pollutants.

Most of the adverse uncertainties mainly affected the dispersion of SO_2, indicating that the results of SO_2 are likely to be the least representative.

Despite the number of uncertainties for the regulatory runs, several relevant observations were made. The results showed that the dispersion was better for SO_2 than HF, most likely due to SO_2 coming from more elevated sources. The dispersion was worst for particulate matter, indicating that the model accounted for the deposition mechanisms of this pollutant. The results also showed that several of the general mechanisms concerning emission dispersion were accounted for, implying that the tool can be used for qualitative measurements of emission dispersion.

The biggest challenge of performing the modeling case was acquiring applicable and representative data. Acquiring correct weather data required data acquisition skills which may go beyond the scope of the thesis. For more accurate modeling results, one should include surface weather data that are representative for the conditions of the plant. This can be done by acquiring modeled data from Thredds.met.no, or by setting up an on-site weather station at the plant. Preferably, the data should include station pressure, precipitation amount and precipitation code, in addition to the data used in this thesis. The upper air data should be acquired from a station closer to the plant, and these data may be found at The Norwegian Meteorological Institute's database [66].

Reformatting raw data before implementation was done by using of Excel, Python and

QGIS, and was a time consuming process. This process should be streamlined if one wants to implement dispersion models on a regular basis. With the wide availability of technological tools that exist, this should be fully possible.

Wrongful values of emission rates propagate when implemented into the model. Therefore there should be strict demands in measurement routines if one wants to achieve accurate results from the dispersion model. Additionally, one should make sure that the source characteristics are accurate and representative of the conditions for the stack exits.

A powerful approach which should be investigated, is to couple AERMOD with more advanced models, like CFD. In such an approach, CFD can be used for close range dispersion, while AERMOD takes over for longer ranges. This kind of approach is more demanding in computational requirements and modeling expertise.

All in all, if one is to overcome the mentioned uncertainties and challenges accompanied by AERMOD, there seems to be potential for the model to be used to qualitatively estimate how pollutants disperse from the plants. For more quantitative evaluations, one should be cautious. The modeling conditions of aluminum plants in Norway can be quite complex, and the results of this thesis do not verify the quantitative capabilities of AERMOD in these kinds of conditions. For such purposes, an evaluation of the tool by comparison with more advanced tools and physical measurements, should be performed.

References

[1] Turner, B.D.: *Workbook of atmospheric dispersion estimates*, volume 999-AP-26 of *Public Health Service publication.* U.S. Department of Health, Education, and Welfare, Public Health Service, Bureau of Disease Prevention and Environmental Control, National Center for Air Pollution Control, Cincinnati, Ohio, 1967.

[2] Briggs, G.A: *Diffusion estimation for small emissions. Preliminary report.* National Oceanic and Atmospheric Administration, Oak Ridge, Tenn. (USA). Atmospheric Turbulence and Diffusion Lab, 1973.

[3] Larson, T.V.: *Atmospheric Dispersion Modeling.* University of Washington, civil and environmental engineering, 2012.

[4] Hydro: *Partikkelstørrelsesfordeling*, July 2010.

[5] Slade, D.H. (ed.): *METEOROLOGY AND ATOMIC ENERGY, 1968.* Environmental Science Services Administration, Silver Spring, Md. Air Resources Labs, 1968.

[6] EPA: *Air Quality Dispersion Modeling - Preferred and Recommended Models*, Last visited: December 2021. https://www.epa.gov/scram/air-quality-dispersion-modeling-preferred-and-recommended-models.

[7] EPA: *User's Guide for the AERMOD Meteorological Preprocessor (AERMET).* EPA, 2021. https://gaftp.epa.gov/Air/aqmg/SCRAM/models/met/aermet/aermet_userguide.pdf.

[8] Google: *Google Maps*, Last visited: May 2022. https://www.google.com/maps.

[9] Hydro: *Hydro Aluminium Metal Høyanger*, Last visited: November 2021. https://www.hydro.com/en-GB/about-hydro/hydro-worldwide/europe/norway/hoyanger/hydro-aluminium-as-hoyanger/.

[10] Skistad, H.: *LUFTMENGDER I ELEKTROLYSEHALL, HYDRO ALUMINIUM HØYANGER.* Technical report, Siv.ing. Håkon skistad, May 2011.

[11] Kartverket: *Norgeskart*, Last visited: May 2022. https://www.norgeskart.no.

[12] Norwegian Centre For Climate Services: *Observations and weather statistics*, Last visited: May 2022. https://seklima.met.no/.

[13] Beychok, M. R: *Fundamentals of stack gas dispersion.* Milton R. Beychok, Irvine, Calif., 1979.

[14] Indresand, H.: *Airborne dust at Knarrdalstranda*. Technical report, NORCE, May 2020.

[15] Hagen, L.O. and Tønnesen, D.: *Grovvurdering av luftkvaliteten i Norge i henhold til foreløpig utkast til EU-direktiv om tungmetaller og BaP i luft*. Technical report, NILU, 2002.

[16] Leelőssy, Á., Lagzi, I., Kovács, A. and Mészáros, R.: *A review of numerical models to predict the atmospheric dispersion of radionuclides*. Journal of environmental radioactivity, 182:20–33, 2018, ISSN 0265-931X.

[17] EPA: *Revisions to the Guideline on Air Quality Models: Enhancements to the AERMOD Dispersion Modeling System and Incorporation of Approaches To Address Ozone and Fine Particulate Matter*. Federal register, 2017, ISSN 0097-6326.

[18] Bailly, C.: *Turbulence*, 2015, ISBN 3-319-16160-1.

[19] Leelossy, A., Mona T., Mészáros R., Lagzi I., and Havasi Á.: *Eulerian and Lagrangian Approaches for Modelling of Air Quality*, volume 24, pages 73–85. January 2016, ISBN 978-3-319-40155-3.

[20] Obukhov, A.M: *Turbulence in an atmosphere with a non-uniform temperature*. Boundary-layer meteorology, 2(1):7–29, 1971, ISSN 0006-8314.

[21] Nilsen, M.: *Predictive models for emissions from aluminum industry*. Project assignment, NTNU: Institutt for materialteknologi, 2021.

[22] Demeal, E. and Carissimo B.: *Comparative Evaluation of an Eulerian CFD and Gaussian Plume Models Based on Prairie Grass Dispersion Experiment*. Journal of applied meteorology and climatology, 47(3):888–900, 2008, ISSN 1558-8424.

[23] Briggs, G.A.: *Plume Rise Predictions*, pages 59–111. American Meteorological Society, Boston, MA, 1982, ISBN 978-1-935704-23-2. https://doi.org/10.1007/978-1-935704-23-2_3.

[24] Briggs, G.A: *Chimney plumes in neutral and stable surroundings*. Atmospheric environment, 6(7):507–510, 1972, ISSN 0004-6981.

[25] Briggs, G.A.: *Plume rise*, volume 25075 of *AEC critical review series*. The Laboratory, Oak Ridge, Tenn, 1969.

[26] Bluet, J. and Gimson N.: *Good Practice Guide for Atmospheric Dispersion Modelling*. Ministry for the environment, 2004. https://environment.govt.nz/publications/good-practice-guide-for-atmospheric-dispersion-modelling/.

[27] AERMIC: *Current Progress in the AERMIC Model Development Program*, March 1996.

[28] EPA: *AERMOD Modeling System Development*, Last visited: March 2022. https://www.epa.gov/scram/aermod-modeling-system-development.

[29] EPA: *AERMOD Model Formulation and Evaluation*, April 2021. https://gaftp.epa.gov/Air/aqmg/SCRAM/models/preferred/aermod/aermod_mfed.pdf.

[30] EPA: *AERMOD Implementation Guide*, July 2021. https://gaftp.epa.gov/Air/aqmg/SCRAM/models/preferred/aermod/aermod_implementation_guide.pdf.

[31] EPA: *AERMINUTE User's Guide*, October 2015. https://gaftp.epa.gov/Air/aqmg/SCRAM/models/met/aerminute/aerminute_userguide.pdf.

[32] EPA: *THE PRIME PLUME RISE AND BUILDING DOWNWASH MODEL*, November 1997. https://gaftp.epa.gov/Air/aqmg/SCRAM/models/other/iscprime/useguide.pdf.

[33] Google: *Download Google Earth Pro (Windows)*, Last visited: April 2022. https://www.google.no/earth/about/versions/#download-pro.

[34] EPA: *AERMOD: Latest Features and Evaluation Results.* EPA, 2003. https://nepis.epa.gov/Exe/ZyPDF.cgi/P1009S6X.PDF?Dockey=P1009S6X.PDF.

[35] EPA: *User's Guide for the AMS/EPA Regulatory Model (AERMOD).* EPA, 2021. https://gaftp.epa.gov/Air/aqmg/SCRAM/models/preferred/aermod/aermod_userguide.pdf.

[36] Hurley, P.J.: *An evaluation and inter-comparison of AUSPLUME, AERMOD and TAPM for seven field datasets of point source dispersion.* Clean Air and Environmental Quality, 40(1):45–50, 2006, ISSN 1444-2841. https://search.informit.org/doi/10.3316/informit.163971128686180.

[37] El Harbawi, M.: *Air quality modelling, simulation, and computational methods: a review.* Environmental reviews, 21(3):149–179, 2013, ISSN 1181-8700.

[38] Moreno-Silva, C., Calvo, D.C., Torres N., Ayala L., Gaitán M., González, L., Rincón, P., Rodríguez Susa, M.: *Hydrogen sulphide emissions and dispersion modelling from a wastewater reservoir using flux chamber measurements and AERMOD® simulations.* Atmospheric environment (1994), 224:117263, 2020, ISSN 1352-2310.

[39] Rood, A.S.: *Performance evaluation of AERMOD, CALPUFF, and legacy air dispersion models using the Winter Validation Tracer Study dataset.* Atmospheric environment (1994), 89:707–720, 2014, ISSN 1352-2310.

[40] Carruthers, D.J., Seaton, M.D., McHugh, C.A., Sheng, X., Solazzo, E., Vanvyve, E.: *Comparison of the Complex Terrain Algorithms Incorporated into Two Commonly Used Local-Scale Air Pollution Dispersion Models (ADMS and AERMOD) Using a Hybrid Model.* Journal of the Air Waste Management Association (1995), 61(11):1227–1235, 2011, ISSN 1096-2247.

[41] Heist, D., Isakov V., Perry S., Snyder M., Venkatram A., Hood C., Stocker J., Carruthers D., Arunachalam S., and Owen R.C.: *Estimating near-road pollutant dispersion: A model inter-comparison.* Transportation research. Part D, Transport and environment, 25:93–105, 2013, ISSN 1361-9209.

[42] Nattawut, J., Nattaporn P., and Sarawut T.: *Performance Evaluation of AERMOD and CALPUFF Air Dispersion Models in Industrial Complex Area.* Air, Soil and Water Research, 8(1), 2020. https://doi.org/10.1177/ASWR.S32781.

[43] EPA: *User's Guide for the AERMOD Terrain Preprocessor (AERMAP).* EPA, 2021. https://gaftp.epa.gov/Air/aqmg/SCRAM/models/related/aermap/aermap_userguide_v18081.pdf.

[44] Private communication: *SFI Metal Production meeting, NTNU Trondheim*, November 2021.

[45] EPA: *Meteorological Processors and Accessory Programs*, Last visited: April 2022. https://www.epa.gov/scram/meteorological-processors-and-accessory-programs.

[46] EPA: *Air Quality Dispersion Modeling - Related Model Support Programs*, Last visited: April 2022. https://www.epa.gov/scram/air-quality-dispersion-modeling-related-model-support-programs#aermap.

[47] Microsoft: *Visual Studio: IDE and Code Editor for Software Developers and Teams*, Last visited: April 2022. https://visualstudio.microsoft.com/.

[48] Britannica: *FORTRAN*, Last visited: April 2022. https://www.britannica.com/technology/COBOL.

[49] Fortran: *Learn Fortran*, Last visited: April 2022. https://fortran-lang.org/learn/.

[50] Straum G.A., Buer, F. and Strømsnes, L.M.: *Utslippsmålinger ved Hydro Høyanger, november 2018.* Technical report, Sintef, December 2018.

[51] Kartverket: *Høydedata*, Last visited: May 2022. https://hoydedata.no.

[52] Rizwan, A., Dennis L., and Liu C.: *A review on the generation, determination and mitigation of urban heat island.* Journal of Environmental Sciences, 20(1):120–128, 2008, ISSN 1001-0742. https://www.sciencedirect.com/science/article/pii/S1001074208600194.

[53] SSB: *Population*, Last visited: May 2022. https://www.ssb.no/en/statbank/table/11342/tableViewLayout1/.

[54] *Atmospheric transport and dispersion of air pollutants associated with vehicular emissions.* In *Air Pollution, the Automobile, and Public Health*, pages 77–98. National Academies Press, 2000, ISBN 0309086825.

[55] Povinec P., Hirose, K., Aoyama, M. and Tateda, Y.: *Chapter 5 - radioactivity impact on japan.* In Povinec P., Hirose K., Aoyama M. and Tateda Y. (editor): *Fukushima Accident (Second Edition)*, pages 245–384. Elsevier, second edition edition, 2021, ISBN 978-0-12-824496-8. https://www.sciencedirect.com/science/article/pii/B9780128244968000018.

[56] Cheng, M.D.: *Atmospheric chemistry of hydrogen fluoride.* Journal of atmospheric chemistry, 75(1):1–16, 2017, ISSN 0167-7764.

[57] Wesely, M.L., Doskey, P.V. and Shannon, J.D.: *Deposition parameterizations for the Industrial Source Complex (ISC3) model* . Technical report, Argonne National Lab, 2002.

[58] Walcek, C., Brost, R., Chang J. and Wesely, M.: *So2, sulfate and hno3 deposition velocities computed using regional landuse and meteorological data.* Atmospheric Environment, 20:949–964, 1986.

[59] Jain, R., Cui, Z. and Domen, J.: *Chapter 4 - environmental impacts of mining.* In Jain, R., Cui, Z. and Domen, J. (editor): *Environmental Impact of Mining and Mineral Processing*, pages 53–157. Butterworth-Heinemann, Boston, 2016, ISBN 978-0-12-804040-9. https://www.sciencedirect.com/science/article/pii/B9780128040409000048.

[60] EPA: *Sulfur Dioxide Basics*, Last visited: May 2022. https://www.epa.gov/so2-pollution/sulfur-dioxide-basics.

[61] Garland, J.A.: *On the Size Dependence of Particle Deposition.* Water, air soil pollution: Focus, 1(5):323–332, 2001, ISSN 1567-7230.

[62] Kjeller Vindteknikk: *Vindkart for Norge.* Technical report, NVE, 2009.

[63] STORM: *Høyanger*, Last visited: May 2022. https://www.storm.no/h\T1\ oyanger?tab=stormVsYr.

[64] The Weather Channel: *Monthly weather, Høyanger, Vestland, Norway*, Last visited: May 2022. https://weather.com/weather/monthly/l/ a88039e42042f561458f4f88bf44c48b9cf5e09d785e29d9cde076815687e528.

[65] QGIS: *Welcome to the QGIS project!*, Last visited: May 2022. https://qgis.org/ en/site/.

[66] Private communication: *Conversation with Norwegian Meteorological Institute*, May 2022.

[67] EPA: *PCRAMMET USER'S GUIDE*, Last visited: May 2022. https://gaftp.epa. gov/Air/aqmg/SCRAM/models/met/pcrammet/pcramtd.pdf.

[68] pandas: *pandas*, Last visited: May 2022. https://pandas.pydata.org/.

[69] NOAA, ESRL: *NOAA/ESRL Radiosonde Database*, Last visited: May 2022. https://ruc.noaa.gov/raobs/.

[70] NOAA, ESRL: *FSL Output Format Description*, Last visited: May 2022. https: //ruc.noaa.gov/raobs/fsl_format-new.html.

[71] Wong, D., Tjahyono, N. and Hyland, M.: *The nature of particles and fines in potroom dust*. In *Light Metals 2014*, volume 9781118889084, pages 553–558. John Wiley Sons, Inc, Hoboken, NJ, USA, 2014, ISBN 1118889088.

[72] Wulff, S.: *A first course in design and analysis of experiments*. The American Statistician, 57(1):66–67, 2003, ISSN 0003-1305.

[73] Cohen, J.: *Multiple regression as a general data-analytic system*. Psychological Bulletin, 70:426–443, 1968.

[74] Alcoa Mosjøen: *Conversation with Alcoa Mosjøen*, October 2021.

[75] Macdonald, R.: *Theory and objectives of air dispersion modelling*. Modelling Air Emissions for Compliance, pages 1–27, 2003.

Mads Urang Nilsen

Using AERMOD to predict the dispersion of emissions from the aluminum industry

NTNU
Kunnskap for en bedre verden